FAULT TOLERANT SLIDING MODE CONTROL ON COMMUNICATION SATELLITE USING CHEMICAL PROPULSION

KİMYASAL İTKİ SİSTEMİ KULLANAN HABERLEŞME UYDULARINDA ARIZA TOLERANSLI KAYAN KİP KONTROLÜ

YAVUZ ANDAÇ

ASSIST. PROF. DR. EMIR KUTLUAY

Supervisor

Submitted to

Graduate School of Science and Engineering of Hacettepe University

as a Partial Fulfillment to the Requirements

for the Award of the Degree of Master of Science

in Department of Mechanical Engineering

June 2024

ABSTRACT

FAULT TOLERANT SLIDING MODE CONTROL ON COMMUNICATION SATELLITE USING CHEMICAL PROPULSION

Yavuz ANDAÇ

Master of Science , Department of Mechanical Engineering

Supervisor: Assist. Prof. Dr. Emir KUTLUAY

June 2024, 117 pages

This thesis presents the design and implementation of a fault-tolerant sliding mode control (FTSMC) system for communication satellites using chemical propulsion. The research addresses the need for robust and reliable attitude control in geostationary orbit, where communication satellites play a crucial role. A novel FTSMC strategy is proposed, specifically tailored for this application, filling a gap in existing research. The study utilizes a realistic satellite model based on the TÜRKSAT 1B parameters, ensuring practical relevance and accurate performance evaluation. The proposed controller is rigorously tested under various scenarios, including normal operation, thruster performance degradation, and total thruster failure. This comprehensive analysis demonstrates the controller's ability to maintain stability and functionality even in the presence of uncertainties and faults. The research contributes to the advancement of satellite control systems by providing a robust and reliable FTSMC strategy for communication satellites with chemical propulsion.

Keywords: Satellite attitude control, Fault-tolerant sliding mode control, Chemical propulsion, Communication satellite

ÖZET

KİMYASAL İTKİ SİSTEMİ KULLANAN HABERLEŞME UYDULARINDA ARIZA TOLERANSLI KAYAN KİP KONTROLÜ

Yavuz ANDAÇ

Yüksek Lisans, Makine Mühendisliği Bölümü

Danışman: Dr. Öğr. Üyesi Emir KUTLUAY

Haziran 2024, 117 sayfa

Bu tez, kimyasal itki sistemi kullanan haberleşme uyduları için arıza toleranslı kayan kip kontrol (FTSMC) sisteminin tasarımını ve uygulamasını sunmaktadır. Araştırma, haberleşme uydularının kritik rol oynadığı jeosenkron yörüngede sağlam ve güvenilir bir kontrole olan ihtiyacı ele almaktadır. Bu uygulama için özel olarak uyarlanmış yeni bir FTSMC stratejisi önerilerek mevcut araştırmadaki bir boşluk doldurulmaktadır. Çalışmada, TÜRKSAT 1B parametrelerine dayanan gerçekçi bir uydu modeli kullanılarak, pratik durumlarda ve doğru performans değerlendirmesi sağlanmaktadır. Önerilen kontrolör, normal çalışma, itici performans düşmesi ve tam itici arızası dahil olmak üzere çeşitli senaryolar altında titizlikle test edilmektedir. Bu kapsamlı analiz, kontrolörün belirsizlikler ve arızalar mevcut olsa bile kararlılık ve işlevselliği koruma yeteneğini göstermektedir. Araştırma, kimyasal itki sistemi kullanan haberleşme uyduları için sağlam ve güvenilir bir FTSMC stratejisi sağlayarak uydu kontrol sistemlerinin ilerlemesine katkıda bulunmaktadır.

Anahtar Kelimeler: Uydu yönelim kontrolü, Hata toleranslı kayan kip kontrolü, Kimyasal itki, Haberleşme uydusu

ACKNOWLEDGEMENTS

I extend my heartfelt gratitude to my thesis supervisor, Assistant Professor Dr. Emir Kutluay, for his invaluable guidance and support throughout the entirety of this research endeavor. His expertise, patience, and insightful feedback have been instrumental in shaping the development of this Master's Thesis.

Furthermore, I am deeply indebted to my family for their unconditional love, encouragement, and understanding during the course of this academic pursuit. Their unwavering support provided the necessary strength and motivation to persevere through the challenges encountered in completing this thesis project.

Lastly, I am grateful to all those who contributed directly or indirectly to this work, whether through discussions, feedback, or encouragement. Your contributions have been immensely valuable and are greatly appreciated.

CONTENTS

Page

TABLES

FIGURES

ABBREVIATIONS

ACS	:	**A**ttitude **C**ontrol **S**ystem
ADCE	:	**A**ttitude **D**etermination and **C**ontrol textbfElectronics
ADCS	:	**A**ttitude **D**etermination and **C**ontrol **S**ystem
BoL	:	**B**eginning **o**f **L**ife
BoT	:	**B**eginning **o**f **T**ransfer
CoG	:	**C**enter **o**f **G**ravity
EoL	:	**E**nd **o**f **L**ife
EoM	:	**E**quation **o**f **M**otion
EoT	:	**E**nd **o**f **T**ransfer
FDIR	:	**F**ault **D**etection, **I**solation, and **R**ecovery
FMW	:	**F**lywheel **M**omentum **W**heel
FMWA	:	**F**lywheel **M**omentum **W**heel **A**ssembly
FTSMC	:	**F**ault-**T**olerant **S**liding **M**ode **C**ontrol
FTSMC-MST	:	**F**ast **T**erminal **S**liding **M**ode **C**ontrol with **M**odified **S**uper-**T**wisting
GO	:	**G**eostationary **O**rbit
GEO	:	**G**eosynchronous **E**quatorial **O**rbit
ILO	:	**I**terative **L**earning **O**bserver
IOT	:	**I**n **O**rbit **T**est
IRES	:	**I**nfra**R**ed **E**arth **S**ensor
ISMC	:	**I**ntegral **S**liding **M**ode **C**ontrol
LEO	:	**L**ow **E**arth **O**rbit
MEO	:	**M**edium **E**arth **O**rbit
MPC	:	**M**odel **P**redictive **C**ontrol
NAMC	:	**N**utation and **A**ngular **M**omentum **C**ontrol
NM	:	**N**ormal Operating **M**ode
PID	:	**P**roportional **I**ntegral **D**erivative

PWM	:	**P**ulse **W**idth **M**odulation
RIGA	:	**R**ate **I**ntegrated **G**yroscope **A**ssembly
SKM	:	**S**tation-**K**eeping **M**ode
SMC	:	**S**liding **M**ode **C**ontrol
SOM	:	**S**pecial **O**peration **M**ode
TO	:	**T**ransfer **O**rbit
WDE	:	**W**heel **D**rive **E**lectronic

1. INTRODUCTION

The need for reliable and robust attitude control systems in communication satellites has never been more critical due to the increasing complexity of satellite missions, the expanding demand for precise positioning to ensure effective communication, and the harsh conditions of space which can disrupt operational accuracy. These systems are essential for maintaining the proper orientation of satellites in orbit, which is crucial for effective communication, data transmission, and operational longevity. The reliance on chemical propulsion in geostationary communication satellites presents unique challenges, particularly in terms of the vulnerability of actuator systems to failures. Traditional control strategies often fall short in addressing total failure scenarios, leading to potential service interruptions and mission failures.

This thesis addresses these challenges by introducing a novel fault-tolerant sliding mode control (FTSMC) strategy designed to enhance the robustness and reliability of satellite attitude control systems against total actuator failures—an area that has received limited attention in current research. Through a combination of theoretical development and simulation-based validation, this work seeks to push the boundaries of current fault-tolerant control technologies and contribute to the safer, more efficient operation of communication satellites.

1.1. Scope of the Thesis

This thesis mainly focuses on the development and evaluation of a fault-tolerant sliding mode control (FTSMC) strategy for communication satellites equipped with chemical propulsion systems. The research specifically targets the robustness and reliability of attitude control mechanisms under conditions of total actuator failure. By implementing a comprehensive FTSMC system, this work aims to demonstrate improved fault tolerance over traditional control methods, ensuring satellite functionality despite severe actuator degradations or failures.

The scope extends to a detailed simulation study using a realistic satellite model based on the TÜRKSAT 1B satellite parameters. This model helps in accurately assessing the performance of the proposed control strategy under various fault scenarios, including both partial and total thruster failures. Furthermore, the thesis explores the theoretical underpinnings of sliding mode control techniques, tailored specifically for the challenges posed by the space environment and the operational demands of geostationary communication satellites.

1.2. Contributions

In this research, the deficiencies are addressed by proposing a novel, simple, and efficient approach. The main contributions of this thesis can be summarized as follows:

- This research proposes a fault-tolerant sliding mode control strategy that enhances the robustness of satellite attitude control against actuator faults and failures, ensuring sustained operation under varying conditions.
- Unlike most of the previous works, which primarily focus on handling partial failures, the approach robustly addresses both partial and total actuator failures, providing comprehensive fault management for communication satellites.
- For the first time, advanced fault-tolerant control techniques are applied to the specific domain of communication satellites using chemical propulsion. This study demonstrates their viability and effectiveness in a realistic simulation environment based on the TÜRKSAT 1B satellite model.
- The simulation results show that the proposed control strategy maintains stability and control accuracy even under scenarios of actuator failure, outperforming traditional control methods in terms of resilience and reliability.

1.3. Organization

The organization of the thesis is as follows:

- Chapter 1 introduces the motivation behind the research, outlines its contributions, and delineates the scope of the work, setting the foundation for the subsequent chapters.
- Chapter 2 furnishes a comprehensive background overview, delving into the various types of satellites, actuators, and control methodologies prevalent in the field. This chapter provides the necessary technical background to understand the complexities involved in satellite attitude control.
- Chapter 3 undertakes a thorough literature review, presenting an overview of similar works while summarizing their key findings. This review highlights the gaps in existing research that this thesis aims to fill, particularly in the area of fault tolerance under total failure conditions.
- Chapter 4 introduces the dynamic model utilized for analysis, providing insights into its formulation and significance. This chapter describes the mathematical and simulation models that form the basis for the proposed control strategies.
- Chapter 5 delves into the specific control strategies developed in this thesis, elucidating the principles and applications of Integral Plus State Variable Feedback Control and Integral Sliding Mode Control.
- Chapter 6 presents the nonlinear simulation results, conducts stability analyses, and compares the efficacy of the proposed control strategies. This chapter evaluates the performance of the control strategies through various simulated fault scenarios to demonstrate their effectiveness and robustness in maintaining satellite stability.
- Chapter 7 offers a succinct summary of the thesis, along with a discussion on potential future avenues for research.

2. BACKGROUND OVERVIEW

Satellites have become indispensable tools in modern society, playing a crucial role in various aspects of our lives, from communication and navigation to Earth observation and scientific research. To effectively fulfill their diverse missions, satellites require robust and reliable attitude control systems (ACS). This chapter provides a comprehensive overview of the key concepts and technologies relevant to satellite attitude control, setting the stage for the subsequent discussion on fault-tolerant sliding mode control strategies.

The research begins by exploring the different types of satellites, categorized by their orbit and mission objectives. This classification helps us understand the diverse operational environments and requirements that satellite ACS must cater to. Next, the discussion delves into the various actuators commonly employed in satellite attitude control, including reaction wheels, thrusters, and magneto-torquers. Understanding the principles and limitations of these actuators is essential for designing effective control strategies.

Furthermore, the research addresses the critical issue of actuator failure, which can significantly impact satellite performance and mission success. This discussion highlights the need for fault-tolerant control systems that can maintain stability and functionality even in the presence of actuator malfunctions. Finally, the research reviews different control methods used in satellite attitude control systems, ranging from classical techniques like PD and PID control to more advanced approaches such as sliding mode control, model predictive control, and adaptive control. This overview provides a foundation for understanding the rationale behind the choice of fault-tolerant sliding mode control as the focus of this research.

By providing a comprehensive background on satellite types, actuators, and control methods, this chapter establishes the context and theoretical framework for the subsequent investigation into fault-tolerant sliding mode control strategies for communication satellites using chemical propulsion.

2.1. Types of Satellites

Satellites orbiting Earth can be categorized based on two primary criteria: their orbit and their mission. This classification helps us understand the diverse operational environments and requirements that satellite attitude control systems must cater to.

2.1.1. Classification Based on Orbit

The altitude and inclination of a satellite's orbit significantly influence its coverage area, revisit time, and communication capabilities. Based on these orbital characteristics, satellites can be broadly classified into three categories.

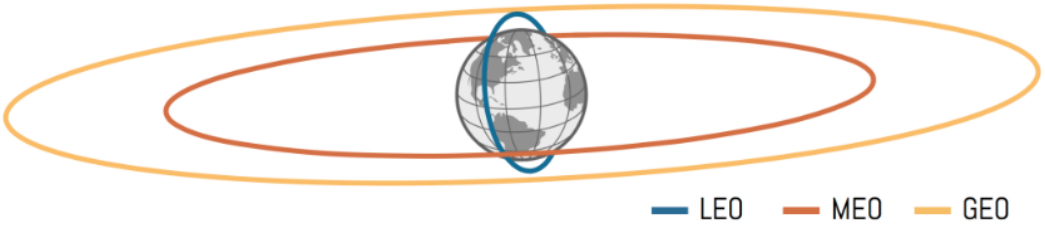

Figure 2.1 Orbit Regimes [3]

2.1.1.1. Geostationary Earth Orbit (GEO)

Satellites in GEO orbit maintain a fixed position relative to a specific point on Earth's surface. This is achieved by orbiting at an altitude of approximately 36,000 kilometers above the equator and matching the Earth's rotational speed. The key advantage of GEO satellites is their continuous coverage of a specific region, making them ideal for communication, broadcasting, and weather monitoring applications. However, their high altitude results in signal latency and requires powerful transmitters for effective communication.

2.1.1.2. Medium Earth Orbit (MEO)

MEO satellites occupy orbits at altitudes ranging from 2,000 to 36,000 kilometers. They have a wider coverage area than LEO satellites but are not stationary relative to Earth. MEO

satellites typically have orbital periods of several hours, offering a balance between coverage and latency. They are often used for navigation and communication purposes, providing global coverage with moderate signal delays.

2.1.1.3. Low Earth Orbit (LEO)

LEO satellites orbit at altitudes between 160 and 2,000 kilometers, resulting in relatively short orbital periods, typically ranging from 90 to 120 minutes. Their proximity to Earth allows for high-resolution imagery and data collection, making them suitable for Earth observation, remote sensing, and scientific research applications. However, LEO satellites have a limited coverage area and require frequent communication handovers as they move across the sky.

2.1.2. Classification Based on Mission

Beyond their orbital characteristics, satellites are further categorized based on their specific mission objectives.

2.1.2.1. Communication Satellites

These satellites serve as relay stations, facilitating communication by transmitting and receiving signals between different locations on Earth. They play a crucial role in various communication applications, including television broadcasting, internet connectivity, telephone communications, and maritime and aeronautical communications.

2.1.2.2. Earth Observation Satellites

Satellites designed for Earth observation are outfitted with various sensors and instruments that gather data and images of the Earth's surface and atmosphere. These data are employed in numerous applications such as predicting weather, monitoring the environment, managing disasters, exploring resources, and conducting mapping.

2.1.2.3. Navigation Satellites

Navigation satellites provide positioning and timing information for navigation systems such as the Global Positioning System (GPS) and Galileo. These satellites transmit signals that allow receivers on Earth to determine their precise location and time, enabling navigation, surveying, and other location-based services.

2.1.2.4. Scientific Research Satellites

Scientific research satellites carry specialized instruments to conduct research in various fields, such as astronomy, astrophysics, and Earth science. These satellites gather data and observations that contribute to the understanding of the universe, Earth's environment, and other scientific phenomena.

2.2. Actuators Used in Satellites

Satellite attitude control systems (ACS) rely on actuators to generate the necessary torques for maneuvering and maintaining desired orientations. These actuators play a crucial role in ensuring the satellite's proper functioning and mission success. The choice of actuators for a specific satellite mission depends on various factors, including the required torque levels, mission duration, and available resources. Often, a combination of different actuators is used to achieve optimal performance and redundancy.

Understanding the principles, advantages, and limitations of these actuators is essential for designing effective and robust attitude control strategies for satellites. The specific choice and configuration of actuators will depend on the unique requirements and constraints of each mission.

2.2.1. Reaction Wheel

Reaction wheels are momentum exchange devices that exploit the principle of conservation of angular momentum. They consist of spinning wheels mounted inside the satellite, typically arranged in a tetrahedral configuration to provide three-axis control. By accelerating or decelerating a reaction wheel, a torque is generated in the opposite direction, allowing the satellite to rotate.

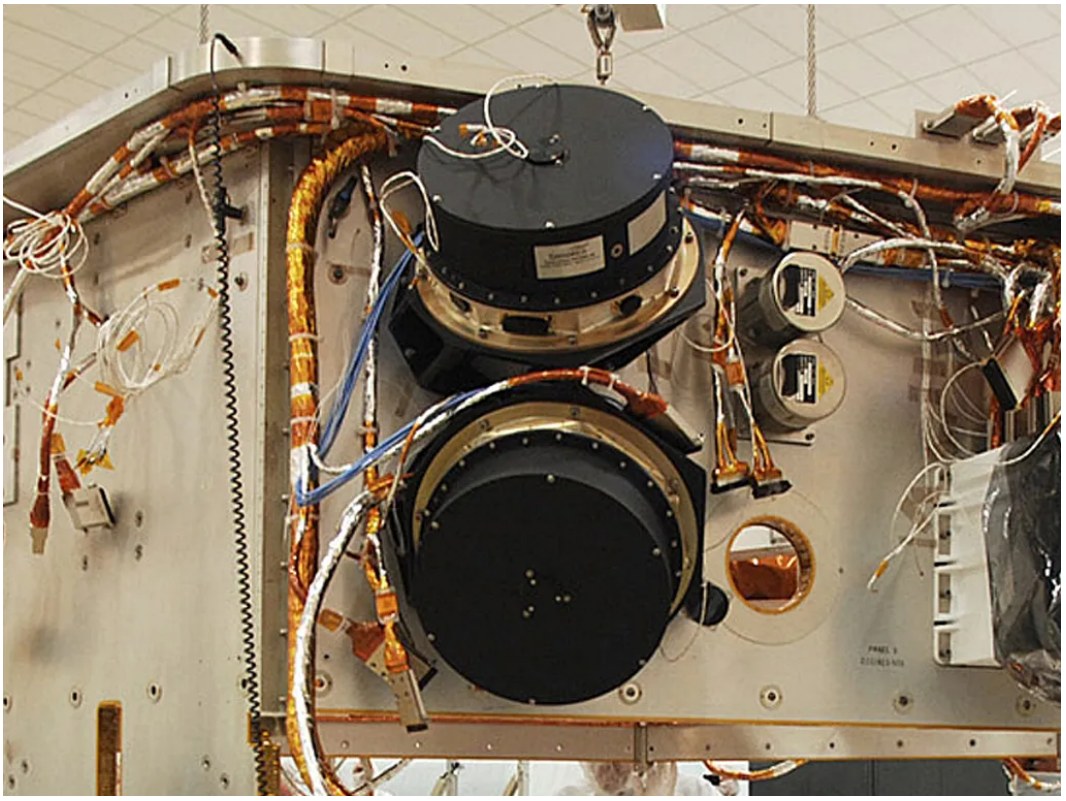

Figure 2.2 Reaction wheel on NASA's Kepler spacecraft [4]

Reaction wheels offer several advantages for satellite attitude control:

- **High Efficiency:** Reaction wheels are highly efficient, requiring minimal power to operate.
- **Precision:** They provide precise and accurate attitude control, making them suitable for fine pointing and stabilization maneuvers.

- **Cleanliness:** Unlike thrusters, reaction wheels do not expel propellant, eliminating the risk of contamination and plume impingement.

However, reaction wheels also have limitations:

- **Limited Torque Capability:** Their torque capability is relatively low compared to thrusters, making them less suitable for large attitude changes or rapid maneuvers.
- **Momentum Desaturation:** As reaction wheels absorb angular momentum from the satellite, they can eventually reach saturation. To prevent this, they require regular momentum desaturation, typically achieved by using thrusters or magnetic torquers.

2.2.2. Thrusters

Thrusters are small rockets that expel propellant to generate thrust. By strategically firing thrusters in different directions and for varying durations, torques can be created to maneuver the satellite. Thrusters are essential components of satellite attitude control systems, particularly for large attitude changes, orbital maneuvers, and momentum desaturation of reaction wheels. Thrusters offer several advantages:

- **High Torque Capability:** Thrusters can generate significantly higher torques than reaction wheels, making them suitable for large attitude changes, orbital maneuvers, and momentum desaturation.
- **Simplicity:** Thrusters are relatively simple devices with a long heritage in spacecraft applications.

However, thrusters also have limitations:

- **Propellant Consumption:** Thrusters consume propellant, which is a limited resource on satellites. This limits their operational lifetime and necessitates careful propellant management.

- **Disturbances:** Thruster plumes can impinge on satellite surfaces, introducing disturbances and potentially affecting sensitive instruments.

2.2.2.1. Types of Thrusters

Thrusters can be categorized based on the type of propellant they use:

- **Chemical Thrusters:** These thrusters use chemical reactions to generate hot exhaust gases, which are expelled through a nozzle to produce thrust. Chemical thrusters are further divided into monopropellant and bipropellant systems. Monopropellant thrusters use a single propellant, while bipropellant thrusters use two propellants that react with each other. Chemical thrusters offer high thrust-to-weight ratios but have lower specific impulse (fuel efficiency) compared to other types.

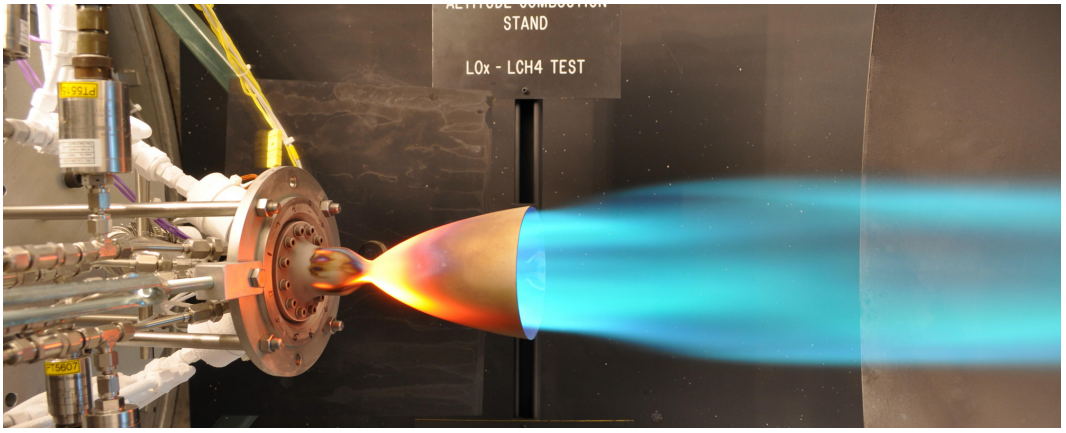

Figure 2.3 Chemical thruster [5]

- **Electric Thrusters:** Electric thrusters use electrical energy to accelerate propellant, typically an inert gas such as xenon. They offer significantly higher specific impulse than chemical thrusters but have lower thrust levels. Electric thrusters are well-suited for long-duration missions where fuel efficiency is critical.

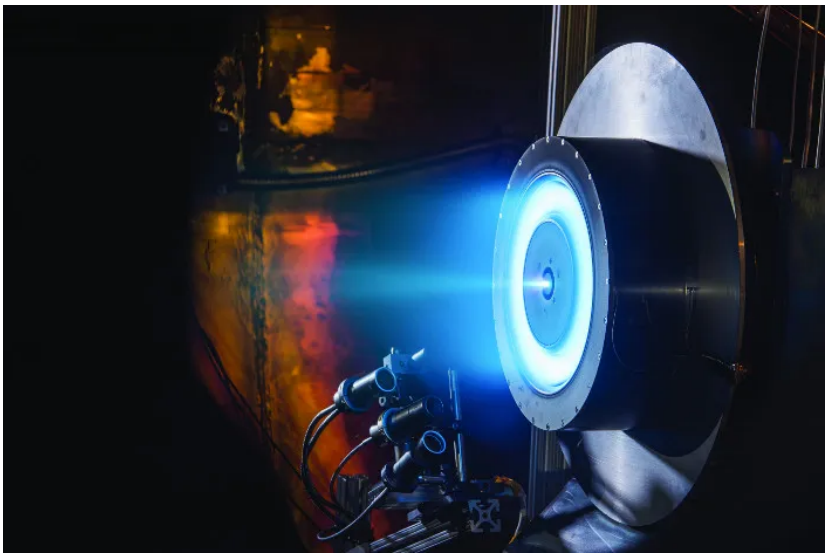

Figure 2.4 Hall effect thruster [6]

2.2.3. Magneto-Torquers

Magneto-torquers produce torques by taking advantage of the interaction between the magnetic dipole moment of the satellite and the Earth's magnetic field. By varying the current in coils or using electromagnets, the satellite's magnetic dipole moment can be adjusted, resulting in a torque due to the interaction with the Earth's magnetic field.

Figure 2.5 Magneto Torquer [7]

Magneto-torquers offer several advantages:

- **High Efficiency:** They are highly efficient, requiring minimal power to operate.

- **No Propellant Consumption:** Unlike thrusters, magneto-torquers do not require propellant, making them a sustainable option for attitude control.

However, magneto-torquers also have limitations:

- **Limited Torque Capability:** Their torque capability is generally lower than that of reaction wheels and thrusters, and it depends on the strength of the Earth's magnetic field. This makes them more suitable for low Earth orbit satellites where the magnetic field is stronger.
- **Environmental Dependence:** Their effectiveness is dependent on the Earth's magnetic field, which can vary in strength and direction.

2.3. Control Methods Used in Satellites

Satellite attitude control systems (ACS) employ various control methods to achieve and maintain desired orientations. The choice of control method depends on factors such as the satellite's mission requirements, the type of actuators available, and the level of robustness and precision required.

2.3.1. Classical Control Methods

Proportional-Derivative (PD) control, a classical technique that calculates the control signal based on the error between the desired attitude and the measured attitude, as well as the rate of change of the error. PD controllers are simple to implement and effective for stabilizing systems with linear dynamics. However, they may not be optimal for systems with significant nonlinearities or disturbances, as they can exhibit steady-state errors and be sensitive to parameter variations.

Proportional-Integral-Derivative (PID) control extends PD control by adding an integral term that accumulates the error over time, helping to eliminate steady-state errors and

improve the controller's accuracy. PID controllers find extensive application across diverse control scenarios, such as satellite attitude control, owing to their simplicity, efficacy, and capacity to manage a broad spectrum of system dynamics. However, tuning PID controllers can be challenging, and they may not be as robust as other control methods in the presence of significant disturbances or uncertainties.

2.3.2. Robust Control Methods

In the realm of satellite control, a variety of robust control methods such as Loop Shaping [14], Bode Integral Constraints [15], and Gain Scheduling [16] have traditionally played a central role in managing the complex dynamics and ensuring stability across different frequency ranges. These techniques, deeply rooted in frequency-domain analysis, have provided the means to design sophisticated control systems tailored to the unique challenges of satellite operations. However, as technology advances and the demands on satellite functionality increase, these established methods are gradually making way for newer, more advanced techniques. These emerging methods offer enhanced capabilities in handling higher dimensional systems, non-linearities, and uncertainties more effectively, thus promising to redefine the landscape of control systems in satellite technology.

H-infinity control (H∞ control) is a robust control methodology designed to optimize the worst-case performance of a control system subjected to model uncertainties and disturbances. It is particularly beneficial in scenarios like satellite attitude control, where precision and robustness are critical [17]. By minimizing the H∞ norm, which quantifies the maximum amplification of disturbances in the system, H∞ control ensures that performance degradation remains within acceptable bounds under all modeled disturbances. This method offers substantial advantages for controlling satellites with chemical propulsion, such as enhanced robustness to parameter variations and external influences, which are crucial for maintaining stable satellite operations [18]. However, the complexity of solving associated optimization problems poses challenges, often requiring sophisticated computational methods and a deep understanding of robust control theory.

Sliding mode control (SMC) is a robust control method that utilizes a sliding surface within the state space. The control strategy aims to steer the system towards this surface and maintain its position despite disturbances and uncertainties. Upon reaching the sliding surface, the system demonstrates advantageous traits, such as resistance to changes in parameters and external disturbances. SMC offers several advantages for satellite attitude control, including robustness against disturbances and uncertainties, fast response times, and relative insensitivity to changes in the satellite's parameters. However, SMC may lead to chattering, defined by rapid oscillations in the control signal, posing potential risks to actuators and possibly demanding additional filtering or alterations to the control methodology.

Integral sliding mode control (ISMC) is an extension of SMC that incorporates an integral term in the sliding surface definition. This integral term helps eliminate steady-state errors and improve the controller's accuracy. ISMC offers similar robustness and disturbance rejection capabilities as SMC while addressing the issue of steady-state errors, making it a suitable choice for satellite attitude control systems where high precision and robustness are required.

2.3.3. Advanced Control Methods

An sophisticated control method called **Model predictive control (MPC)** makes use of a system model to forecast future behavior and choose the best control signal. MPC optimizes the control signal over a finite horizon, taking into account constraints on the system's states and inputs. This makes it suitable for satellite attitude control with multiple objectives and limitations, such as actuator saturation and pointing accuracy requirements. MPC can handle complex, nonlinear systems and constraints, and it optimizes the control signal to achieve desired performance objectives while respecting limitations. However, MPC requires significant computational resources, which can be a challenge for onboard implementation on satellites with limited processing power, and its performance is dependent on the accuracy of the system model.

Adaptive control techniques adjust the controller parameters online based on the system's behavior, allowing the controller to adapt to changing conditions and uncertainties and improve performance and robustness. Adaptive control methods are particularly useful for satellite attitude control, where the system dynamics can vary due to factors such as fuel consumption, thermal effects, and actuator degradation. Adaptive controllers offer the advantage of adjusting to changing system dynamics and reducing dependence on accurate models. However, designing and implementing adaptive controllers can be complex, and ensuring their stability and convergence can be challenging.

2.3.4. Conclusion

Classical control methods have been effective for basic satellite attitude control applications, yet the growing requirements for fuel efficiency and enhanced pointing accuracy have necessitated the adoption of more sophisticated control strategies. Sophisticated control strategies, including H-infinity control, model predictive control and adaptive control, provide promising approaches to address these issues.

H-infinity control, a robust control method, optimizes the worst-case performance against disturbances and model uncertainties, enhancing the resilience and reliability of satellite control systems. While H-infinity control is highly effective in scenarios demanding high accuracy and robustness under uncertain conditions, it also involves complex computational processes and detailed design work.

MPC employs a system model to forecast future states and determine the best control actions within a limited timeframe, considering the limitations on the system's states and inputs. This allows for optimization of fuel consumption and precise pointing control. However, MPC requires significant computational resources, which can be a challenge for onboard implementation on satellites with limited processing power.

Adaptive control techniques adjust the controller parameters online based on the system's behavior, allowing the controller to adapt to changing conditions and uncertainties. This

improves fuel efficiency and pointing accuracy by compensating for variations in the satellite's dynamics. However, designing and implementing adaptive controllers can be complex, and ensuring their stability and convergence can be challenging.

While these advanced and robust control methods offer promising solutions on paper, their practical implementation on satellites faces challenges due to the limitations of current technology. Faster and smaller-sized chips, necessary for these advanced control algorithms, are more prone to radiation and failure in the harsh space environment. This poses a significant risk to mission success and necessitates a careful trade-off between performance and reliability. Given these constraints, sliding mode control emerges as a promising compromise for satellite attitude control. SMC provides robustness against disturbances and uncertainties, rapid response times, and a degree of insensitivity to variations in the satellite's parameters. Although SMC can introduce chattering, this issue can be mitigated through appropriate modifications to the control law. Additionally, SMC requires less computational power compared to other advanced methods, making it more feasible for onboard implementation with current technology. Therefore, sliding mode control represents a "sweet spot" for satellite attitude control, balancing performance, robustness, and technological feasibility. This motivates the focus of this thesis on designing and implementing a fault-tolerant sliding mode control system for communication satellites using chemical propulsion.

2.4. Robustness and Reliability in Satellite Operations

Robustness and reliability are paramount in the realm of satellite operations due to the substantial initial investments involved. Satellites represent significant financial commitments, often requiring several years to yield a return on investment. Typically, a satellite begins to generate profit after approximately ten years of operation. Beyond this point, the revenue produced contributes to financing future projects, thus sustaining and expanding the technological and operational capabilities of satellite operators.

For illustration, consider the Türksat 3A satellite. This satellite offers 1296 MHz of bandwidth in the Ku band. As depicted in Figure 2.6, the average capacity pricing for the Ku band is estimated to be around 3000 USD per MHz per month. Based on these figures, Türksat 3A generates an annual income exceeding 45 million USD. This substantial revenue underscores the importance of ensuring that satellites are designed and maintained to be highly reliable and robust, as any failure could jeopardize significant financial returns and future project funding.

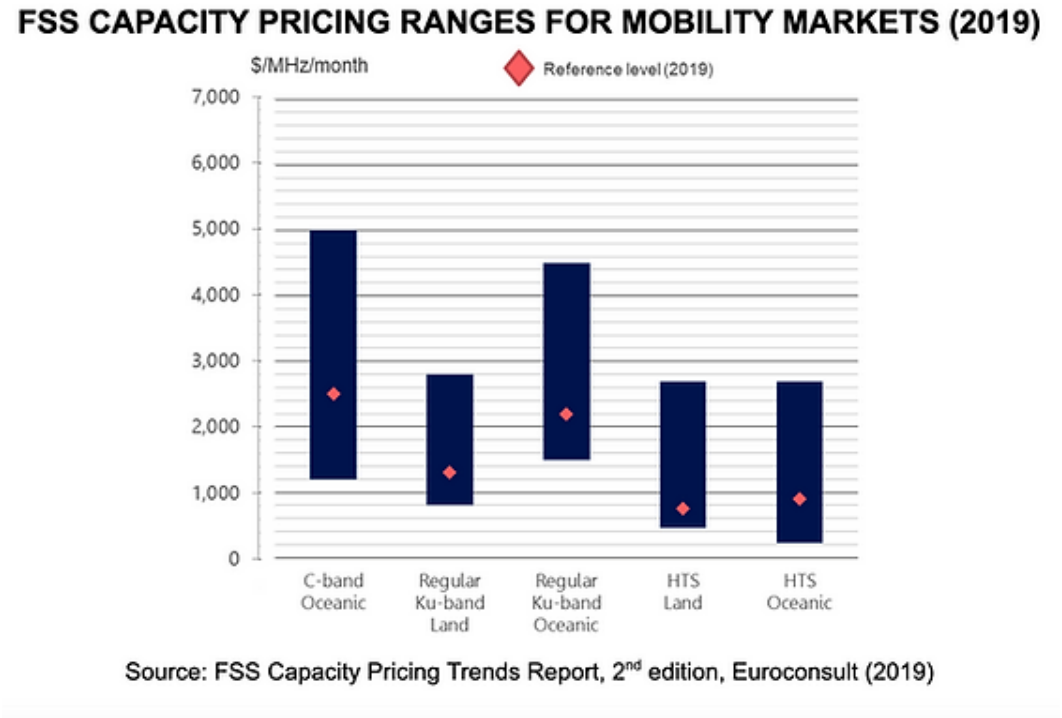

Figure 2.6 Capacity pricing [8]

3. LITERATURE REVIEW

This chapter aims to establish the theoretical framework and context in which research is conducted by identifying key themes, debates, and ideas that have shaped the current state of knowledge in the field. Through a critical analysis of the existing literature, this chapter will identify any gaps or inconsistencies in the research and suggest areas for further investigation.

In their work, Prabhat, Mukherjee, Giri, and Sinha [19] introduced an attitude control mechanism for satellites using magneto-Coulombic torquers, termed Fast Terminal Sliding Mode Control with Modified Super-Twisting (FTSMC-MST). This approach is utilized on a satellite in low-Earth orbit, exclusively employing magneto-Coulombic actuators to deliver the required torque. The resilience of this control method to failures in any single magneto-Coulombic torquer axis was examined. Additionally, the potential for online fault detection is slated for future exploration.

Jin, Ko, and Ryoo [20] presented a clear method for fault-tolerant control designed for a satellite with four reaction wheels, based on dynamic inversion and time-delay control theory. Unlike most studies that describe satellite attitude using Euler angles, direction cosines, or quaternions, this research utilizes modified Rodrigues parameters. The model incorporates both additive faults like bias faults and multiplicative faults such as decreased control torque. The effectiveness of this approach was evaluated against traditional PD control.

Boskovic, Li, and Mehra [21] devised a reliable method for estimating bias in attitude tracking. This method utilizes non-linear observers to identify bias and estimate states. It guarantees strong global tracking capabilities. The characteristics of this method are tested through simulations with a standard spacecraft model.

Another fault-tolerant control approach was proposed by Alwi and Edwards [22] based on on-line sliding mode control allocation scheme. A small fighter aircraft model named ADMIRE is used for the analysis. This study demonstrates that the on-line sliding mode control allocation scheme is capable of managing faults and complete actuator failures

without the need to reconfigure the controller. The model used is this paper is not a spacecraft but nevertheless effectiveness of the sliding mode to obtain a fault-tolerant control is proved.

The paper by Shen, Wang, and Poh [23] uses integral type sliding mode control to obtain a fault-tolerant design on a rigid spacecraft. The general non-linear spacecraft attitude dynamic with partial loss of actuator effectiveness model in Xiao, Hu, and Zhang's [24] article is used, and the usage of the model can also be seen in multiple papers. In this study, input saturation and actuator redundancy is not investigated.

Similar to the work of Shen, Wang [23], and Poh, Wenjie, Dayi, and Chengrui [25] also explored integral sliding mode fault-tolerant control. However, their research primarily concentrated on fault-tolerant control for over-actuated time-invariant linear systems that exhibit uncertainties and input saturation. The robustness of their approach was confirmed through the use of Lyapunov stability criteria. They conducted their analysis using a spacecraft model equipped with six momentum wheels.

Xiao, Hu, and Zhang [26] present an alternative fault-tolerant attitude tracking control method. Their approach integrates a neural network to manage system uncertainties and develops an adaptive sliding mode controller. This controller features an online updating mechanism designed to estimate the limits of actuator faults. To prevent saturation, they modify the control law accordingly. Simulations are conducted on a low Earth orbiting satellite equipped with a flexible solar array and reaction wheel actuators. The study focuses solely on partial loss of actuator effectiveness and actuator saturation, while significant external disturbances like gravitational, aerodynamic, solar, and magnetic effects are excluded from consideration.

Xiao, Hu, and Friswell [27] have introduced an innovative approach to active fault-tolerant attitude stabilization control. Their method tackles the fault detection issue through the incorporation of an observer-based mechanism for fault detection and diagnosis, aimed at reconstructing actuator faults. Subsequently, a restructured fault-tolerant control law based on backstepping is employed, leveraging the reconstructed fault information.

Chen and Saif [28] proposed a diagnostic approach for detecting faults in time-varying thrusters. In response to the difficulties in detecting these faults, they developed an iterative learning observer (ILO), presenting it as a substitute for adaptive observers. The proposed strategy for fault identification based on ILO incorporates a learning mechanism for fault estimation. The ILO, depicted in equation (1), involves gain matrices K_1 and K_2, update interval τ, a positive definite matrix Λ, input $v(t)$ to the ILO, and angular velocity ω. Utilizing this ILO design, the study demonstrated accurate estimation of various time-varying thruster faults, including constant, periodic, and aperiodic faults.

$$\begin{aligned} J\dot{\hat{w}} &= -\hat{w}^x J\hat{w} + \Lambda(w - \hat{w}) + Bu + B_f v(t) \\ v(t) &= K_1 v(t-\tau) + K_2[w(t) - \hat{w}(t)] \end{aligned} \tag{1}$$

Hu [9] developed a robust adaptive fault-tolerant control approach utilizing a sliding-mode control scheme to address reaction wheel failures, external disturbances, and uncertainties in time-varying inertia parameters. The stability and performance of this method are analyzed on a flexible spacecraft, where the spacecraft dynamics are determined by calculating the kinetic and potential energies and applying the Lagrange equations under the assumption of small elastic displacements. The arrangement for four reaction wheels is depicted in Figure 3.1. This control scheme is demonstrated to be effective in scenarios of complete failure or reduced efficiency of one or several reaction wheels.

Maganti and Singh [29] propose an adaptive controller for the attitude system of a spacecraft with flexible appendages, which operates based on feedback from the output error and the states of the reference model. This method is distinct in requiring only four adaptively tunable parameters for output regulation. Notably, the controller's functionality is independent of the state space dimension of the spacecraft model. Additionally, this design effectively eliminates issues related to observation and control spillover.

Cao, Gong, and Han [10] presented an active fault tolerant sliding mode control scheme for the attitude control system of a spacecraft with external disturbance and actuator faults. For actuators four reaction flywheels are selected. The fault diagnosis is performed by a

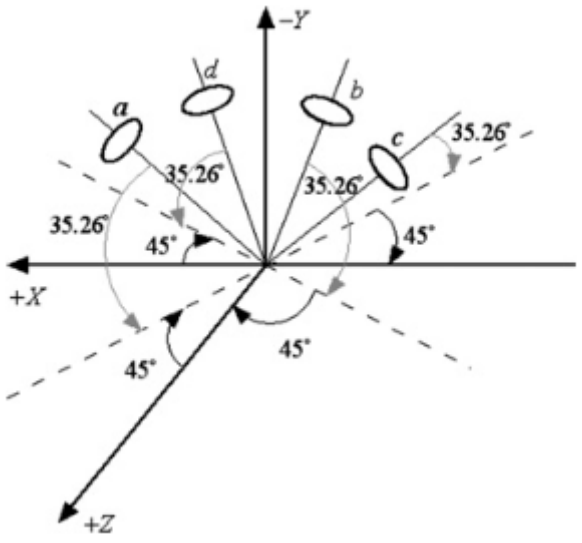

Figure 3.1 Configuration of four reaction wheel used by Hu [9]

nonlinear observer. The proposed structure of the fault-tolerant attitude control system is shown in Figure 3.2. The stability of the closed-loop system is evaluated with Lyapunov theory.

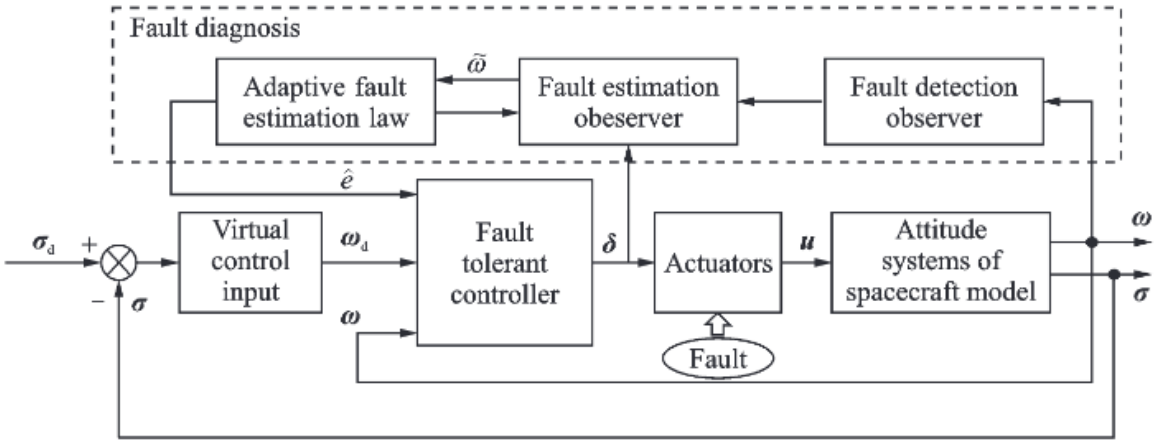

Figure 3.2 The structure of fault tolerant attitude control system used by Cao, Gong, and Han [10]

3.1. Conclusion

In conclusion, this literature review has provided a comprehensive analysis of existing studies in the field of satellite control systems. While the majority of research has concentrated on satellites in low Earth orbit, this review has identified a critical gap in the literature pertaining to communication satellites in geostationary orbit, particularly concerning sliding mode control for chemical propulsion systems.

The prevailing research has predominantly focused on reaction wheels, magnetic torquers, and magneto-Coulombic torquers in low Earth orbit scenarios. Notably absent are studies on chemical propulsion systems in geostationary orbit, presenting a distinct research niche that this study aims to address. The comparative analysis of existing methodologies has underscored the need for a tailored approach in the face of chemical propulsion systems, a facet not explored in current literature.

The highlighted gaps, particularly the absence of investigations into total loss scenarios in redundant systems, provide a clear rationale for the significance of the upcoming research. By introducing fault-tolerant sliding mode control for chemical propulsion systems in geostationary orbit, this study aims to not only contribute to existing knowledge but also to fill these critical voids in the literature.

In essence, this literature review positions the forthcoming research as a pioneering endeavor, extending the boundaries of fault-tolerant control strategies in satellite systems. The synthesized insights from prior studies serve as a foundation for this novel exploration into geostationary orbits, emphasizing the unique challenges posed by chemical propulsion systems. As the research progresses, it is poised to make a substantial contribution to the advancement of satellite control systems.

4. DYNAMIC MODEL OF THE SATELLITE

Obtaining a dependable attitude model for spacecraft is of paramount importance for simulation purposes. Given the inherent risks associated with testing software on operational satellites, intricate models are meticulously constructed for each satellite to mitigate any potential risks. It is worth noting that satellite manufacturers employ unique designs and incorporate various payloads, resulting in the creation of distinct models for each satellite.

Simulation plays a crucial role in expediting the development process, minimizing costs, and providing a safe platform for experimentation with new concepts and technologies. By leveraging simulations, researchers and engineers can simulate various scenarios, assess system performance, and validate proposed solutions before implementation, thereby enhancing overall mission readiness and success.

To develop a realistic model, the TÜRKSAT 1B communication satellite, positioned in geostationary orbit, serves as the chosen reference. Building upon Uslu's thesis [11] as a primary reference , Derman [2] further refined and constructed a similar satellite attitude dynamic model resembling TÜRKSAT 1B. This study is grounded on the utilization of the aforementioned model, and the comparison will be conducted with the control methods proposed in Derman's thesis [2].

In this chapter, the initial focus is on introducing the assumptions made and outlining the mass properties of the system. Subsequently, the derivation of the equation of motion using Newtonian mechanics is presented. Following this, the actuator dynamics are incorporated into the model. Finally, environmental disturbances are integrated to develop a comprehensive model of non-linear attitude dynamics.

4.1. Description of TÜRKSAT 1B Satellite

The TÜRKSAT 1B satellite is a significant milestone as the first communication satellite of Türkiye. It succeeded the TÜRKSAT 1A satellite, which unfortunately was lost due to

launcher failure. The basic descriptions of the satellite are provided below:

- **Launcher:** Ariane 44LP H10+
- **Predecessor:** TÜRKSAT 1A
- **Longitude:** 42°E
- **Payload:** 16 Ku Band transponder
- **Manufacturer:** Aérospatiale
- **Mission Duration:** August 1994 - October 2006 (13 years)

4.1.1. Attitude Determination and Control Subsystem

The Attitude Determination and Control System (ADCS) of the TÜRKSAT 1B satellite features a strategic integration of critical hardware—most elements are paired with backups—and specialized software designed for both automated and manual control operations. The primary goal of the ADCS is to consistently maintain the spacecraft's orientation within its predefined limits.

Essential to this system are the Sun and Earth sensor assemblies and the Rate Integrated Gyroscope Assembly, which are crucial in providing accurate measurements of the spacecraft's current orientation. The ADCS then manages the operation of various actuators, such as hydrazine thrusters and momentum wheels. These components are precisely coordinated by the ADCS to adjust the satellite's positioning according to mission requirements.

4.1.1.1. Sensors

In the TÜRKSAT 1B satellite's Attitude Determination and Control System, Sun Sensors and Earth Sensors are used. Each type of Sun Sensor is duplicated for redundancy, with each

pair featuring four heads that monitor either the pitch or the roll/yaw axis. For detecting the spacecraft's pitch and roll attitudes, two Earth Sensor units are deployed, which are also referred to as Infrared Earth Sensors (IRES).

When the primary sensors—the Sun and Earth sensors—are not operational, the system switches to a backup attitude measurement approach. This is accomplished through the use of Rate Integrated Gyroscope Assembly (RIGA), which consists of two duplicate sets of gyroscopes. These gyroscopes act as a secondary means to maintain accurate attitude measurements under conditions where the primary sensors cannot be relied upon.

4.1.1.2. Actuators

The actuator system consists of two redundant Flywheel Momentum Wheels (FMWs), with one designated as the nominal unit and the other as backup. Additionally, each FMW is paired with two redundant Wheel Drive Electronics (WDE), collectively forming the Flywheel Momentum Wheel Assembly (FMWA).

The FMWA is primarily responsible for two key functions: [1]

- It manages the satellite's pitch attitude by modulating the speed of the reaction wheel, which involves either speeding up or slowing down its rotation. This control mechanism effectively adjusts the spacecraft's orientation in its pitch axis. [30]
- For roll and yaw movements, the FMWA utilizes the gyroscopic properties of a rapidly spinning disc. This disc is carefully positioned within the spacecraft's architecture to ensure its movements are tightly controlled and contribute to overall stability.

The ADCS system engages twelve thrusters, each nominally rated at 10N, to ensure the satellite remains within its operational attitude range while orbiting. These thrusters, fueled by Hydrazine—a highly toxic chemical also used in several aircraft power systems—exhibit variability in their thrust output. This variability arises due to the unique plume impingement

characteristics of each thruster, influenced by their specific orientations and placements on the spacecraft.

As the satellite orbits, its solar panels continuously adjust to face the sun directly, influencing the spatial dynamics of the satellite. These adjustments modify the areas impacted by the thruster emissions, periodically altering the resulting forces and torques due to thruster plume dynamics.

The distribution of the attitude thrusters on the satellite is carefully planned for optimal control: [1]

- Four Roll thrusters are installed on the South panel,
- Two Pitch thrusters and Two Yaw thrusters are strategically placed on the East and West panels respectively.

A diagram in Figure 4.1 provides a clear schematic of the thruster placements relative to the spacecraft's coordinate system. Specifically, thrusters 6A/B and 7A/B are categorized as South thrusters; 2B, 3B, 4A, and 5A as East thrusters; and the remaining as West thrusters.

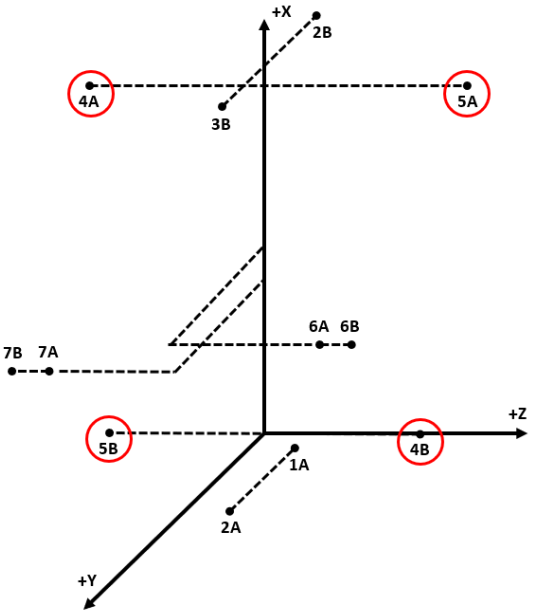

Figure 4.1 Thruster Schematic Locations [2]

4.1.2. ADCS Modes

There are several mission phases, each with distinct responsibilities assigned to the Attitude Determination and Control System (ADCS). The main phases include:

- Transfer Orbit (TO) Phase
- Geostationary Orbit (GO) Phase
- In Orbit Test (IOT) Phase
- De-Orbiting Phase

For this study, the Geostationary Orbit (GO) phase is selected as the focus because the satellite will primarily operate in this phase for the majority of its operational lifespan. During the Geostationary Orbit (GO) phase, there are three operational modes:

4.1.2.1. Normal Operating Mode (NM)

This mode is executed through fully automated commands governing the Attitude Determination and Control System (ADCS), rendering ground telecommand unnecessary. The NM comprises three fundamental control loops: [31]

1. Automatic Regulation of Pitch via Flywheel Unloading:
   In Normal Mode (NM), the control of the spacecraft's pitch attitude is managed by finely adjusting the acceleration and deceleration rates of the Flywheel Momentum Wheel (FMW), which functions in torque mode. The rotational inertia of the FMW disk generates reaction torque, effectively regulating the satellite's pitch rate and position. As the FMW operates within its designated operational range, it oscillates between its upper and lower speed thresholds, effectively counteracting the cumulative angular momentum resulting from external disturbances. When this equilibrium is disturbed, an automatic logic signal triggers the activation of preset pitch thruster

firings in pulse form, facilitating wheel unloading. To prevent premature or repeated thruster firings, a pre-programmed time-limited algorithm inhibits subsequent firing until the wheel dynamics have sufficiently responded. Thruster firing for wheel unloading is activated in two distinct scenarios:

(a) When transitioning from the NM to the Station-keeping Mode (SKM).

(b) When the wheel approaches or exceeds its operational limits, defined within a ±10% range of its nominal rotation speed, specifically between 4140 and 5060 rpm.

2. Roll / Yaw Control Loop:

   The approach to controlling the roll and yaw attitudes in NM utilizes the capabilities of both the roll thrusters and the Flywheel Momentum Wheel Assembly (FMWA) located on the satellite's southern side. This coordinated approach utilizes the distinct functionalities of each component to regulate the satellite's orientation within specified parameters.

   The roll thrusters are strategically positioned in a vectorial alignment relative to the satellite's coordinate system. This setup includes a deliberate offset designed to create a compensatory torque component in the yaw direction. This configuration enables precise control over both roll and yaw axes, facilitating the maintenance of desired attitude configurations.

   Meanwhile, the FMWA contributes to overall stability by providing gyroscopic stiffness, essential for implementing the wheel control principle. This principle dictates the coordinated utilization of reaction wheels and thrusters for attitude control.

   Upon detecting a deviation of approximately ±0.05° in the roll attitude relative to the reference information from the Inertial Reference System (IRES), the Attitude Determination and Control Electronics (ADCE) initiates corrective action. This involves activating the roll thrusters for a precise duration of 8 milliseconds, calibrated to counteract the detected error and restore the satellite to its intended orientation.

By integrating the FMWA and roll thrusters within the control architecture, the NM mode ensures robust and responsive attitude control capabilities, safeguarding the satellite's operational integrity and facilitating precise positioning in alignment with mission objectives.

In the system, yaw motion is not directly controlled. Instead, a gyro-compassing effect produced by the pitch reaction wheel transforms errors in yaw attitude into roll discrepancies, with these transformations occurring every six hours. Identified as roll error signals, these variances indirectly affect yaw motion via a phenomenon called roll coupling, which facilitates passive yaw attitude control within the inertial frame. Moreover, the torque produced by the roll thrusters incorporates a yaw offset, accounting for approximately 15% of this coupling effect. Both the alignment of this thruster bias and the FMWA are leveraged for the passive control of yaw attitude, eliminating the need for direct yaw attitude measurements. Subsequently, the roll bias signal undergoes processing to trigger the activation of the south thrusters within their designated deadband range.

3. Nutation and Angular Momentum Control Mode (NAMC):

   Nutation refers to the oscillatory motion observed in a satellite's rotation around its main axis, typically induced by external forces or uneven mass distribution, which can impact the satellite's stability and orientation precision. Beyond the basic wheel control mode, this advanced setting enhances the ADCS's pointing accuracy. While the roll bias continues to be ascertained via the Inertial Reference System (IRES), the yaw error is now dynamically calculated on-board, utilizing data from the Satellite Sensor Head Assembly (SSHA). Decoupling of these signals is efficiently managed through the IRES.

   In this mode, primary actuation is provided by roll and yaw thrusters instead of utilizing the Flywheel Momentum Wheel. During Normal Mode, ground commands are required no more than once daily, unless the Inertial Reference Earth Sensors (IRES) need to be deactivated due to interference from the sun or moon.

The Attitude Determination and Control System (ADCS) maintains spacecraft attitude within strict tolerances: ±0.5° for roll and ±1.5° for pitch, with an impressive accuracy of 0.01°. [1]

4.1.2.2. Station-keeping Mode (SKM)

During the Geostationary Orbit (GO) phase, it's imperative to maintain the satellite within a predetermined contact window to ensure accurate communication between the satellite and ground stations, thereby ensuring optimal coverage of the transmission area.

Station-keeping Mode (SKM) serves multiple purposes during this phase. The system not only secures the satellite's final placement in the drift orbit but also manages its descent from orbit when it reaches the end of its operational lifespan.

Within these control loops, the Attitude Determination and Control System (ADCS) is essential for maintaining the satellite's stability across all three axes during corrective maneuvers in both North/South (N/S) and East/West (E/W) directions. This ensures precise positioning and maneuverability of the satellite as needed throughout the GO phase [1].

4.1.2.3. Special Operation Mode (SOM)

This mode is utilized for specific mission-related tasks or activities that deviate from the standard operating procedures. It may involve temporary adjustments to the satellite's attitude or configuration to facilitate specialized operations or experiments.

4.2. Mass Properties

The satellite's mass undergoes variations throughout its operational lifespan. Table 9.1 provides a summary of the evolution of TÜRKSAT 1B, including changes in mass.

The upcoming control system is specifically tailored for managing the attitude in Geostationary Orbit (GO). This design will incorporate specific mass and inertia values

that reflect the initial (Beginning of Life) and final (End of Life) operational stages of the TÜRKSAT 1B satellite. Notably, there is a reduction of approximately 250 kg in mass from BOL to EOL. This significant change influences the satellite's center of gravity (CoG), resulting in movements of approximately 37 mm in the X direction and 1 mm each in the Y and Z directions of the body coordinate system.

The developed model relies on the assumption of a Rigid Body representation for the satellite structure, deemed suitable for the objectives. The model simplifies satellite dynamics by eliminating considerations of body elasticity, working under the assumption that the separations between any pair of points on the satellite structure are invariant.

Observations of the Center of Gravity (CoG) shifts in TÜRKSAT 1B suggest that, for the Geostationary Orbit (GO) phase model, it is reasonable to maintain that the CoG is static within the satellite's structure. With a mass around 2000 kg, minor CoG shifts of a few millimeters are inconsequential for the Equations of Motion (EOM) development and controller design. Therefore, the attitude dynamics of the system can be envisioned as rotational kinematics centered on the CoG. This thesis employs a simplified design strategy by assuming constant moments of inertia. However, subsequent research will investigate the controller's adaptability to changes in mass, CoG positions, and additional inertial variables.

4.3. Inertial Properties

In Derman's thesis [2], the following inertia tensor is proposed:

$$I = \begin{bmatrix} I_{xx} & -I_{xy} & -I_{xz} \\ -I_{yx} & I_{yy} & -I_{yz} \\ -I_{zx} & -I_{zy} & I_{zz} \end{bmatrix} = \begin{bmatrix} 3770 & 0 & 0 \\ 0 & 730 & 0 \\ 0 & 0 & 4020 \end{bmatrix} kg.m^2 \tag{2}$$

The analysis reveals that a principal axis frame was adopted, in which the Product Mass Moment of Inertia (PMMOI) values are effectively negligible. This approach is justified

given that, within the designated spacecraft coordinate frame of TÜRKSAT 1B, PMMOI values are minuscule when contrasted with Principal Moment of Inertia (PMOI) values.

4.4. Derivation of Rigid Body Equation of Motion

Newtonian mechanics serves as the foundation for deriving the Equation of Motion (EoM) governing the rigid body dynamics of satellites. To establish these equations, a reference frame that adheres to the principles of Newtonian mechanics is necessary. According to the established definition, an inertial frame should ideally remain stationary or exhibit uniform rectilinear motion in relation to distant celestial bodies.

For the purposes of this thesis, the geostationary reference frame is selected as the basis for inertial calculations. This decision is supported because the model, mirroring TÜRKSAT 1B, remains geostationary at a fixed longitude (42° East) and maintains a direct alignment with the equatorial plane of the Earth. It orbits in a pattern that is in synchronous rotation with Earth, ensuring a consistent geographical location relative to the planet's surface.

The motion as perceived from within the satellite is articulated using a body-fixed reference frame, initially set up as a principal axes system. This framework aids in the straightforward representation of body rates, moments, and forces, all centralized at the satellite's Center of Gravity (CoG).

In this reference frame, the x-axis (roll) aligns tangentially to the circular orbit in the direction of satellite motion. The y-axis (pitch) is perpendicular to the orbit plane and points southward, while the z-axis (yaw) lies within the orbit plane and points toward the center of the Earth.

Figure 4.2 illustrates the configuration of the body-fixed and terrestrial reference coordinate frames, each defined as right-handed and orthogonal.

Both the terrestrial reference frame and the satellite's body-fixed frame rotate relative to an inertial frame at an orbital frequency of one full revolution per day, equating to an angular velocity of $\omega_0 = 7.272 \times 10^{-5}$ radians per second.

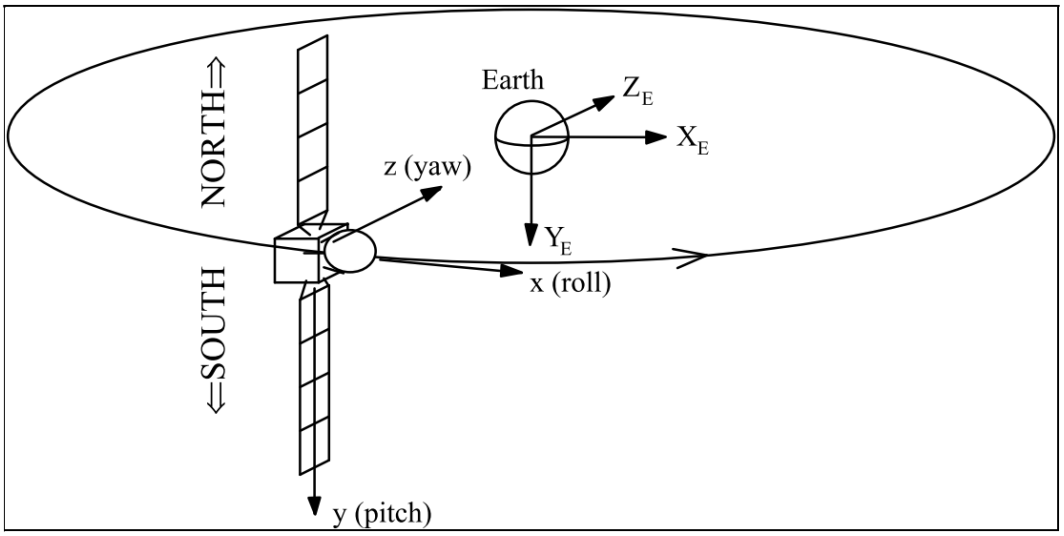

Figure 4.2 Reference frame definition [11]

The dynamic system equations are derived using the Earth-centered inertial reference frame. Angular velocity components and attitude variables are commonly selected as the set of states to define the rotational equations of motion with 3-DoF.

Assuming that the rigid body is aligned with the center of gravity, the following equation determines the angular momentum around the center of gravity:

$$\overrightarrow{H} = \int \overrightarrow{r} \times (\overrightarrow{r} \times \overrightarrow{\omega}) dm \tag{3}$$

$\overrightarrow{r}$ (or "r") represents the position vector of an element inside the body in the formula that is given. Likewise, $\overrightarrow{\omega}$ (or just ω) relates to the body's angular velocity vector, denoted by "B".

By evaluating and decomposing the stated vectorial integral, the angular momentum for body B is derived. The equations obtained from this derivation are as follows:

$$\begin{aligned} h_x &= I_x\omega_x - I_{xy}\omega_y - I_{xz}\omega_z \\ h_y &= -I_{xy}\omega_x + I_y\omega_y - I_{yz}\omega_z \\ h_z &= -I_{xz}\omega_x - I_{yz}\omega_y + I_z\omega_z \end{aligned} \tag{4}$$

In this context, ω denotes the angular rates of the body across the x, y, and z axes. By adopting principal axes, the inertia tensor is markedly simplified. This adjustment leads to the elimination of Product Mass Moment of Inertia (PMMOI) components from the inertia matrix, thereby streamlining the formula for the angular momentum vector to:

$$\begin{aligned} h_x &= 3770 \times \omega_x \\ h_y &= 730 \times \omega_y \\ h_z &= 4020 \times \omega_z \end{aligned} \tag{5}$$

The torque exerted on the system about its CoG can be represented as:

$$T = \frac{dH}{dt}_{body} + \omega \times H \tag{6}$$

The Euler equations, without considering the effect of the momentum wheel, result in:

$$\begin{aligned} T_x &= I_x\dot{\omega}_x + (I_z - I_y)\omega_y\omega_z \\ T_y &= I_y\dot{\omega}_y + (I_x - I_z)\omega_x\omega_z \\ T_z &= I_z\dot{\omega}_z + (I_y - I_x)\omega_x\omega_y \end{aligned} \tag{7}$$

Following the configuration used in TÜRKSAT 1B, a momentum wheel is selected such that its total torque is oriented along the negative y-axis. The equation for angular momentum is modified in a vector format as shown below in Cartesian coordinates, where i, j, k denote the unit vectors in the x, y, and z directions, respectively:

$$H = I_x\omega_x\mathbf{i} + (I_y\omega_y - h_w)\mathbf{j} + I_z\omega_z\mathbf{k} \tag{8}$$

Here, h_w denotes the standard torque for the momentum wheel, with $h_w = 60\,\text{Nm}$. Then, by applying the Euler angular momentum law as detailed in Equation 6 and incorporating the inertia values, the following result is obtained:

$$\begin{aligned} T_x &= 3770\dot{\omega}_x + 3290\omega_y\omega_z + 60\omega_z \\ T_y &= 730\dot{\omega}_y - 250\omega_x\omega_z - \dot{h}_w \\ T_z &= 4020\dot{\omega}_z - 3040\omega_x\omega_y - 60\omega_x \end{aligned} \tag{9}$$

$\dot{h}_w$ represents the rate of change in the wheel's angular momentum, crucial for establishing the pitch control law. In the absence of pitch control, this rate drops to zero ($\dot{h}_w = 0$).

The simulated momentum equations in Simulink, as illustrated in Figure 9.1, provide a comprehensive view of the modeled dynamics that govern the rotational motion of the satellite.

4.5. Euler Angle Transformation

The use of Euler angle transformation enables the evaluation of the satellite's orientation from the perspective of an observer stationed on Earth. By performing rotations in a predetermined order starting from Earth's coordinate system, one can determine the orientation of the satellite relative to its own axes. The notation employed is ϕ for roll angle, θ for pitch angle, and ψ for yaw angle.

Because the transformation is non-commutative, the sequence of operations carries substantial importance. Varying the order yields distinct resultant matrices. In the model, Derman [2] adopts a rotation sequence comprising yaw (ψ), followed by roll (ϕ), and finally pitch (θ).

The rotation sequence can be depicted as shown in Figures 4.3 and 4.4 below:

The obtained rotation matrices are defined in Equation 10.

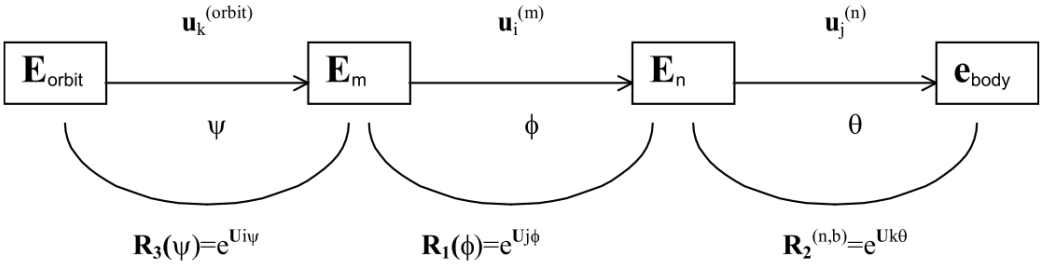

Figure 4.3 Transformation sequence [2]

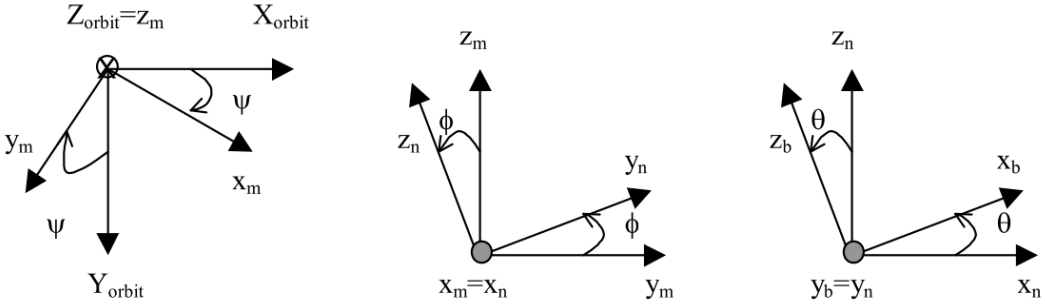

Figure 4.4 Sequence of rotations from the orbit-fixed to the body-fixed frame [2]

$$
\begin{aligned}
R_3(\psi) &= \begin{bmatrix} cos(\psi) & -sin(\psi) & 0 \\ sin(\psi) & cos(\psi) & 0 \\ 0 & 0 & 1 \end{bmatrix} \\
R_1(\phi) &= \begin{bmatrix} 1 & 0 & 0 \\ 0 & cos(\phi) & -sin(\phi) \\ 0 & sin(\phi) & cos(\phi) \end{bmatrix} \\
R_2(\theta) &= \begin{bmatrix} cos(\theta) & 0 & sin(\theta) \\ 0 & 1 & 0 \\ -sin(\theta) & 0 & cos(\theta) \end{bmatrix}
\end{aligned}
\tag{10}
$$

The individual rotations can be expressed as follows:

$$\begin{bmatrix} X \\ Y \\ Z \end{bmatrix}_{orbit} = R_3(\psi) \begin{bmatrix} x \\ y \\ z \end{bmatrix}_m \rightarrow \begin{bmatrix} x \\ y \\ z \end{bmatrix}_m = R_1(\phi) \begin{bmatrix} x \\ y \\ z \end{bmatrix}_n \rightarrow \begin{bmatrix} x \\ y \\ z \end{bmatrix}_n = R_2(\theta) \begin{bmatrix} x \\ y \\ z \end{bmatrix}_b \tag{11}$$

The angular velocity components $\omega_1, \omega_2, \omega_3$ in the spacecraft's principal body-fixed reference frame are described by:

$$\begin{bmatrix} \omega_1 \\ \omega_2 \\ \omega_3 \end{bmatrix} = \begin{bmatrix} 0 \\ 0 \\ \dot{\psi} \end{bmatrix} + R_3(\psi) \begin{bmatrix} \dot{\phi} \\ 0 \\ 0 \end{bmatrix} + R_3(\psi)R_1(\phi) \begin{bmatrix} 0 \\ \dot{\theta} \\ 0 \end{bmatrix} + R_3(\psi)R_1(\phi)R_2(\theta) \begin{bmatrix} 0 \\ \omega_0 \\ 0 \end{bmatrix} \tag{12}$$

Following the relevant matrix multiplication, the body rates yield the subsequent outcome, with ω_0 denoting the Earth's rotation rate:

$$\begin{bmatrix} \omega_1 \\ \omega_2 \\ \omega_3 \end{bmatrix}_{body} = \begin{bmatrix} \omega_x \\ \omega_y \\ \omega_z \end{bmatrix} = \begin{bmatrix} \dot{\phi}cos(\psi) + (\dot{\theta} + \omega_0)sin(\psi)cos(\phi) \\ -\dot{\phi}sin(\psi) + (\dot{\theta} + \omega_0)cos(\psi)cos(\phi) \\ \dot{\psi} - (\dot{\theta} + \omega_0)sin(\phi) \end{bmatrix} \tag{13}$$

If $(\dot{\theta} + \omega_0) = \dot{\theta}_1$ is defined to compute the inverse left part, and then $(\dot{\theta}_1 - \omega_0) = \dot{\theta}$ is substituted, the resulting equation becomes:

$$\begin{bmatrix} \dot{\phi} \\ \dot{\theta} \\ \dot{\psi} \end{bmatrix} = \begin{bmatrix} \omega_x cos(\psi) - \omega_y sin(\psi) \\ \omega_x \frac{sin(\psi)}{cos(\phi)} + \omega_y \frac{cos(\psi)}{cos(\phi)} - \omega_0 \\ \omega_x sin(\psi)tan(\phi) + \omega_y cos(\psi)tan(\phi) + \omega_z \end{bmatrix} \tag{14}$$

Equation 14 describes the Euler rates in body coordinates. The system exhibits singularity at a roll angle of 90° (ϕ=90°), where 1 / cos(90°) becomes infinity. Various rotation sequences may lead to singularities in different angles, but the chosen sequence avoids singularity specifically at the pitch angle. Angle limitations do not hinder the satellite, which offsets maximum ±6°. Throughout Normal Operating Mode, pitch and roll attitudes are upheld within a ±0.05° bias, thereby indicating that substantial alterations in roll/pitch attitude over the satellite's service orbit life are unlikely. The Euler angle transformation implemented in Simulink is depicted in Figure 9.2, offering a visual representation of the transformation process applied to the satellite's attitude representation.

An alternative method for expressing orientations is through the use of quaternions. This technique presents advantages such as avoiding singularities in coordinate transformations and enhancing onboard computation speed, both crucial for navigation and strapdown systems. However, visualizing actual angles using quaternions proves challenging. In contrast, Euler representation remains dependable, straightforward, and sufficiently accurate for the intended applications.

4.6. Internal and External Disturbance Model

The main environmental factors that disturb spacecraft attitude include aerodynamic forces, gravity gradients, solar radiation pressure and magnetic torques on the satellite. Such external disturbances are accompanied by internal perturbations, which typically involve movements within the hardware, misaligned thrust, leakage or sloshing of propellant, among other issues.

Solar radiation pressure significantly influences the attitude and trajectory deviations of satellites at altitudes exceeding 1000 km, marking it as a pivotal environmental disturbance. The extended dimensions of geostationary satellites give rise to gravity gradient disturbance torques. Magnetic disturbances primarily affect satellites below 1000 km altitude, resulting from interactions between the satellite's magnetic components and Earth's magnetic field. Conversely, aerodynamic disturbances are crucial below 500 km but become insignificant above 1000 km. These effects are represented in Figure 4.5, as cited in [30] and [32].

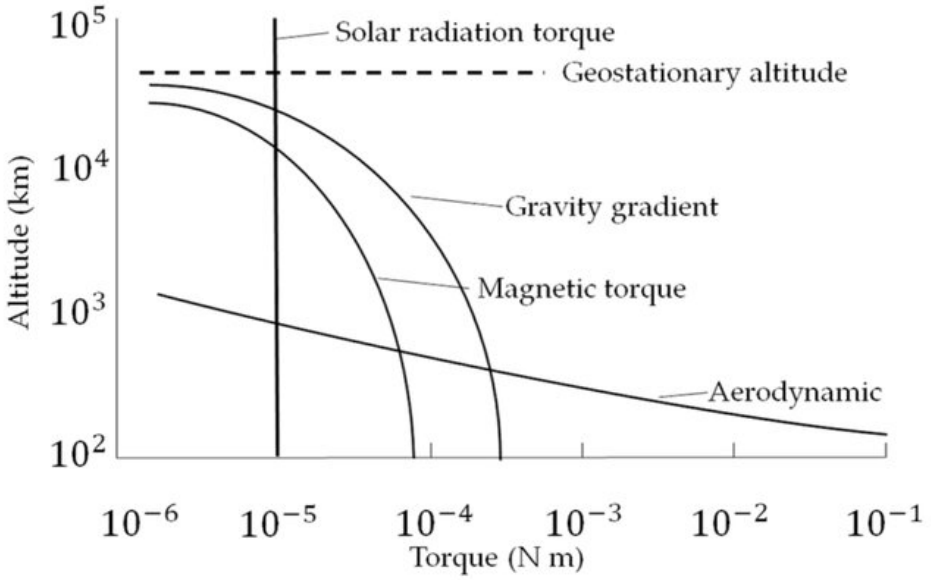

Figure 4.5 Approximations of the magnitudes of external environmental torques affecting spacecraft, categorized by altitude, attribution to Peter Yao [12]

Concerning the group of internal perturbation torques, the torques produced by internal dynamics—such as fluid circulation, scanning devices and rotating wheels —need to be integrated into the satellite's overall equations of motion for attitude. Leakage, propellant slosh and misalignment of devices that exchange momentum, such as momentum wheels and thrusters, can lead to shifts in the distribution of kinetic energy and momentum inside the satellite, thereby influencing its attitude [30].

4.6.1. Internal Disturbance Torques

Set to be outlined shortly, internal torques demonstrate entirely random characteristics. Due to this randomness, creating precise mathematical models for them, as is possible for environmental effects, is not feasible. Furthermore, their perturbative magnitudes are minimal when compared to external torques, leading to their exclusion from simulations.

4.6.1.1. Mass Expulsion Torque

Such torques originate from the discharge of propellant or additional masses from the satellite. They are divisible into two categories, distinguished by their origins: [11]

1. **Incidental Control System Torques:** This category encompasses issues such as fuel leaks, misalignments in thrust vectors, irregularities in the timing of thruster operations, and reaction forces from plume impacts.
2. **Torques from Intentional Mass Expulsion:** This category includes activities such as the discharge of leftover propellant, separation and ejection of payloads, jettisoning of equipment, and the effects from executing orbital maneuvers.

For plume impingement, it is significant to mention that with TÜRKSAT 1B, observations show that the maximum from the roll thrusters constitutes approximately 1% of the standard control torque.

4.6.1.2. Sloshing Effect Torque

The satellite's rotation or translation causes fluid to swirl around within, mostly in the partially full fuel tanks and pipelines. Numerous factors, including the propellant's properties, the layout of the tanks and pipelines, the fluid level, and the acceleration field's characteristics, affect the amount and severity of this sloshing [33], [11].

4.6.1.3. Dynamic Component Torques

Movement in specific satellite components, including solar array wings, antennas and microcomputer hard disks, also leads to the production of disturbance torques.

4.6.2. External Disturbance Torques

In this section, the mathematical models addressing the environmental torques that disturb satellite attitude are outlined. Within the simulation framework, the primary impactful forces are solar radiation and gravity gradient torques, given TÜRKSAT 1B's substantial altitude of 36,000 km in its geostationary orbit.

4.6.2.1. Solar Radiation Pressure Torque

Sun-emitted photons create a net torque upon impacting the diverse surfaces of the satellite's structure. The attitude of the satellite relative to the sun and its geometric shape determine the resultant net forces exerted on each unique satellite segment. These forces coalesce into an overall perturbing torque, centered around the satellite's center of gravity. The main factors influencing this disturbance torque include ([30] and [33]):

1. **Satellite Geometric Configuration:** The satellite's configuration affects the level of shading and force distance relative to the center of gravity of the satellite.
2. **Shading Effect:** Some parts of the satellite structure are inevitably shielded from sunlight due to the shading caused by other components. Satellites featuring prominently extended parts tend to experience marked shading effects.
3. **Optical Reflection Properties of the Satellite Surface:** The reflective characteristics of the satellite's surface influence how solar radiation is either absorbed or reflected.
4. **Satellite-Sun Vector Orientation:** The shading and total solar radiation received or reflected are determined by the satellite's orbital location, inclination with respect to the sun, and its past route.

The torque exerted by solar radiation takes the following form [30]:

$$\overrightarrow{T}^{(solar)} = \int_{e,s} \overrightarrow{r} \, \overrightarrow{df} \tag{15}$$

In this context, $\overrightarrow{r}$ represents the vector extending from the center of gravity of the satellite to the area element dA_i of the i-th surface, while e_s indicates the surface exposed to the sun.

Chobotov [30] details a standard equation for geosynchronous satellites applicable to a specified season. He identifies the essential Fourier elements of solar torque relative to the satellite's body axes in this way:

$$\begin{aligned} T_1^{(s)} &= A + Bcos(\omega_0 t) + Gsin(\omega_0 t) \\ T_2^{(s)} &= E + Fcos(\omega_0 t) + Isin(\omega_0 t) \\ T_3^{(s)} &= C + Dsin(\omega_0 t) + Hcos(\omega_0 t) \end{aligned} \tag{16}$$

where A through H represent constants. Equation 17 provides a full description of a periodic method for a three-axis stabilized satellite design, which is provided by Kaplan [11]. This model closely resembles the equations proposed by Chobotov, as shown in Equation 16.

$$\begin{aligned} T_x &= 2 \times 10^{-5}[1 - 2sin(\omega_0 t)] \\ T_y &= 10^{-4}cos(\omega_0 t) \\ T_z &= -5 \times 10^{-5}cos(\omega_0 t) \end{aligned} \tag{17}$$

The Simulink diagram corresponding to Equation 17 is depicted in Figure 9.3.

4.6.2.2. Gravity Gradient Torque

The disturbance in torque originates from subtle differences in the gravitational pull of the Earth affecting various parts of the satellite's framework.

Chobotov[30] offers an advanced model featuring primary body axes, where the gravity gradient torque is outlined in terms of its components as follows:

$$
\begin{aligned}
T_1^{(g)} &= K(I_{33} - I_{22})a_{21}a_{31} \\
T_2^{(g)} &= K(I_{11} - I_{33})a_{11}a_{31} \\
T_3^{(g)} &= K(I_{22} - I_{11})a_{11}a_{21}
\end{aligned}
\tag{18}
$$

where $K = \frac{3\mu}{R^3}$ and a_{ij} (for $i\&j = 1, 2, 3$) correspond to the elements of the transformation matrix, specifically the direction cosines. Here, $\mu = GM$ represents the gravitational constant of the Earth.

The generic formulae previously mentioned are reduced by Kaplan [11] to get a set of linearized equations that are given in component format:

$$
\begin{aligned}
T_x^{(g)} &= -3\omega_0^2(I_y - I_z)\phi \\
T_y^{(g)} &= -3\omega_0^2(I_x - I_z)\theta \\
T_z^{(g)} &= 0
\end{aligned}
\tag{19}
$$

Using a simplified version of the motion equation, $\frac{d\mathbf{G}}{dt} = \mathbf{h}$, Kaplan formulates these equations, where $\mathbf{G}$ denotes the net torque vector due to gravity gradients, and $\mathbf{h}$ is the total angular momentum vector.

After factoring in the model's inertia values, the subsequent equations characterizing the perturbing torque due to gravity gradients are deduced.

$$
\begin{bmatrix} G_x \\ G_y \\ G_z \end{bmatrix} = \begin{bmatrix} 5.21975 \times 10^{-5}\phi \\ 3.96637 \times 10^{-6}\theta \\ 0 \end{bmatrix}
\tag{20}
$$

4.6.2.3. Aerodynamic Disturbance Torque

At altitudes below approximately 400-500 km, this perturbation force significantly increases in influence.It is caused by a significant net torque around the satellite's center of gravity, which is the outcome of interactions between air molecules and the satellite body. The aerodynamic drag force F_a arises as the satellite moves, and its magnitude is determined by the density ρ of the surrounding atmosphere and the velocity vector v.

For satellites orbiting at low altitudes below approximately 400-500 km, this perturbation force becomes significantly more influential. The drag force is generated by the net torque around the satellite's center of gravity as a result of interactions between the air molecules and the satellite body. With a velocity vector v, the satellite travels through an atmosphere with a density ρ. The aerodynamic drag force F_a is calculated as follows:

$$F^{(a)} = \frac{1}{2}\rho v^2 C_d A \tag{21}$$

where C_d is the drag coefficient and A is the satellite's reference area, or the cross-section along v). Consequently, the total torque is expressed as:

$$T^{(a)} = \frac{1}{2}\rho v^2 l S C_d \tag{22}$$

where l signifies the distance from the satellite's center of gravity to the line of action of the force. Given the elevated orbit of the TÜRKSAT 1B geostationary satellite, positioned approximately 36,000 km above Earth, this perturbing torque can be confidently dismissed.

4.6.2.4. Magnetic Disturbance Torque

The interaction between the residual magnetic field of the spacecraft and the geomagnetic field gives rise to magnetic disturbance torques. Let M be the total magnetic moments in the satellite, which causes torque to be applied to it.

$$T^{(m)} = MxB \tag{23}$$

Here, B stands for the geomagnetic field vector, also referred to as the Earth's magnetic field intensity. Typically, M originates from a combination of permanent and induced magnets, as well as current loops generated within the satellite itself.

As emphasized by Derman[2], this disturbance is deemed insignificant for a geostationary satellite in a high-altitude orbit.

4.7. Actuator Models

4.7.1. Thruster Model

Derman [2] calculated the precise torque components of TÜRKSAT 1B, taking into account impingement forces. The contribution from the impingement characteristics was found to be negligible, amounting to less than 1% of the maximum component.

The model integrates canted roll thrusters positioned and aligned similarly to those on TÜRKSAT 1B. It specifically employs roll thrusters (Thruster 4A, 4B, 5A, and 5B) in accordance with the nominal setup during Normal Operating Mode (NM) in the Geostationary Orbit (GO) phase. In this configuration, Thruster 5A is designated for positive roll movement, while Thruster 5B is assigned for negative roll movement. To ensure redundancy, Thruster 4A serves as a backup for Thruster 5A, and Thruster 4B acts as a backup for Thruster 5B. However, for simplicity, only Thrusters 4A, 5A, and 5B are modeled in this thesis, omitting the backup for negative roll movement.

The optimal choice for thruster selection is the bang-bang or on-off type. These thrusters operate by either fully opening or closing valves for a controlled duration [30]. They often employ large springs to keep valves closed, minimizing leakage. The abrupt closing action ("bang") helps dislodge any ice or dirt particles that may accumulate [32].

On-off valves are dependable even after over a million activations and may be set to remain open for as little as a few milliseconds. They introduce discrete angular velocity changes with each firing as they stay open for a finite duration. To ensure that gas jets do not counteract one another, it is essential to establish a deadband—a specific period during which the jets remain off. Implementing this not only prevents interference but also promotes better fuel efficiency.

The Pulse Width Modulation (PWM) method was employed to mimic the operations of the actuator. The integral of the sampled control signal corresponds to the product of the actuator's firing strength and its operational duration. As a result, each control signal input to the actuator results in the generation of distinct pulse patterns. Each thruster is individually modeled with the thrust values outlined in Table 9.2. The model for Thruster 5A is illustrated in Figure 9.4.

To enhance fuel efficiency, Derman [2] conducted several experiments. His research illuminated an effective approach for reducing fuel consumption. However, to accommodate this reduced sampling period, it's crucial to adjust the pole locations to meet transient constraints adequately. He opted for a minimum sampling period of 0.1 seconds to avoid saturation risks. Interestingly, his investigations demonstrated that thrusters can be activated for durations as brief as a few milliseconds. Nonetheless, due to the considerable magnitude of thruster output compared to the proportional thruster model, he advised against activation periods shorter than 0.1 seconds. Such short "on" times would cause thrusters to generate excessive torque, leading to unnecessary fuel expenditure.

4.7.2. Momentum Wheel Model

Derman [2] utilized a second-order DC motor representation to achieve precise torque control. Due to the unavailability of physical parameters for the DC motor used in TÜRKSAT 1B, an assumed actuator model was employed. Stabilizing parameters were determined through root locus analysis, although many necessitated exceedingly high gains for the PD

controller. The designed Simulink model can be seen in Figure 9.6 and the parameters are given in Appendix 9.1.

5. ATTITUDE CONTROL SYSTEM DESIGN

This chapter delves into the design of the attitude control system (ACS) for the communication satellite. The ACS is responsible for maintaining the satellite's desired orientation in space, ensuring proper communication with ground stations and optimal coverage of the transmission area. The chapter begins by addressing the pitch control design, leveraging the existing PD controller proposed by Derman [2]. Subsequently, the focus shifts to the roll/yaw control design, where two distinct control strategies are explored:

- **Integral Plus State Variable Feedback Control:** This classical control approach utilizes feedback from the system's states and an integral term to achieve desired performance.
- **Integral Sliding Mode Control:** This robust control strategy employs a sliding surface and a discontinuous control law to ensure stability and mitigate the effects of disturbances and uncertainties.

The chapter concludes with a discussion on the Fault Detection, Isolation, and Recovery (FDIR) system, which plays a crucial role in identifying and compensating for potential thruster failures. By integrating FDIR capabilities, the ACS ensures uninterrupted functionality and mission continuity even in the face of adverse conditions. Through a comprehensive exploration of these control strategies and the incorporation of FDIR mechanisms, this chapter aims to design a robust and reliable ACS that effectively maintains the satellite's desired attitude throughout its operational lifespan.

5.1. Pitch Control Design

To facilitate the conversion of the governing equations into a state space representation, the first step in this inquiry is to isolate the pitch motion from the yaw and roll dynamics. This approach enables a more comprehensive understanding of the complex dynamic interactions

involved. As outlined by Derman [2], linearization of the nonlinear governing motion equations is a crucial step in this process, resulting in a decoupled pitch attitude equation that can be expressed as follows:

$$T_y + \theta \times 3.8722 \times 10^{-7} = \ddot{\theta} \times 730 + \dot{h} \tag{24}$$

In Equation 24, T_y exclusively denotes the perturbation torque attributed to solar pressure, whereas $\dot{h}$ denotes the control law dictating the operation of the momentum wheel—essentially, controlling its acceleration or deceleration. The absence of this control law renders the pitch motion unstable

To allow more efficient representation in the Simulink program, the pitch motion equation is converted into a state-space formulation.

$$\begin{bmatrix} \dot{\theta} \\ \ddot{\theta} \end{bmatrix} = \begin{bmatrix} 0 & 1 \\ 5.3043 \times 10^{-10} & 0 \end{bmatrix} \begin{bmatrix} \theta \\ \dot{\theta} \end{bmatrix} + \begin{bmatrix} 0 \\ 1.369863 \times 10^{-3} \end{bmatrix} u \tag{25}$$

$$y = \begin{bmatrix} 1 & 0 \\ 0 & 1 \end{bmatrix} \begin{bmatrix} \theta \\ \dot{\theta} \end{bmatrix} \tag{26}$$

Note that rate (dθ/dt) and attitude (θ) information are assumed to be measured for the proposed controller; rate information is derived from rate gyros, while attitude information is derived from optical earth sensor and sun sensor. This approach differs from the control configuration of TÜRKSAT 1B, which necessitates the measurement of attitude alone.

Derman [2] found that, even in the presence of disturbances, a combination of $K_p = 50$ and $K_d = 2.5$ offers adequate control to keep the satellite's pitch attitude within the predicted range of 0.8336 ± 0.05 degrees.

5.1.1. Conclusion

The chosen values of K_p and K_d effectively mitigate the effects of solar radiation pressure disturbances. The control system promptly responds to deviations from the desired angle and ensures stability against solar radiation perturbations over an extended period.

As a result, the PD controller with gains $K_p = 50$ and $K_d = 2.5$ efficiently mitigates deviations of up to ±0.1° from the desired attitude without displaying overshoot or risky oscillations. Moreover, this configuration adequately suppresses cyclic disturbances caused by solar radiation and is capable of rejecting random measurement errors of approximately ±0.00005° and ±0.00001 °/s. The performance of these gains has been tested and found to be satisfactory.

For this thesis, there's no necessity to develop a new pitch control system since Derman's design [2] adequately serves the overall system requirements. Instead, the comparison is conducted with the sliding mode control method for Roll/Yaw Control.

5.2. Roll/Yaw Control Design

In this section, the design of the roll/yaw control system for the communication satellite is delved into. The exploration begins with the integral plus state variable feedback control approach, a classical control technique that utilizes feedback from the system's states and an integral term to achieve desired performance. This method involves linearizing the coupled roll/yaw equations of motion and transforming them into a state-space representation. Subsequently, Ackermann's formula for pole placement is employed to determine the state feedback and integral control gain, ensuring stability and desired closed-loop performance.

However, classical control methods may not always be optimal for systems with significant nonlinearities or disturbances. To address this, attention is turned to sliding mode control (SMC), a robust control technique known for its ability to handle uncertainties and disturbances effectively. Within the realm of SMC, various types exist, each with its unique characteristics and advantages. For this application, integral sliding mode control

(ISMC) has been selected due to its inherent benefits. ISMC incorporates an integral term in the sliding surface definition, which helps eliminate steady-state errors and improve the controller's accuracy. This feature is particularly advantageous for satellite attitude control, where precise pointing and minimal steady-state errors are crucial for mission success. Additionally, ISMC retains the robustness and disturbance rejection capabilities of conventional SMC, making it a highly suitable choice for the satellite control system.

In the following subsections, the design and implementation of both the integral plus state variable feedback control and the integral sliding mode control strategies will be elaborated on.

5.2.1. Integral Plus State Variable Feedback Control

The design of the controller relies on the linearized Roll/Yaw coupled equations of motion. It's noted that the uncontrolled system is marginally stable. The eigenvalues for roll/yaw dynamics are:

$$\begin{aligned} \lambda_{(3,4)} &= 0 \pm 1.5422 \times 10^{-2} i \\ \lambda_{(5,6)} &= 0 \pm 2.2764 \times 10^{-5} i \end{aligned} \tag{27}$$

The thruster simulation incorporates nonlinearity through on-off type modulation. The linearized attitude dynamics for roll and yaw coupling can be represented as follows:

$$0 = \begin{bmatrix} 3770 & 0 \\ 0 & 4020 \end{bmatrix} \begin{bmatrix} \ddot{\theta} \\ \ddot{\psi} \end{bmatrix} + \begin{bmatrix} 0 & 60.1604 \\ -60.0091 & 0 \end{bmatrix} \begin{bmatrix} \dot{\theta} \\ \dot{\psi} \end{bmatrix} + \begin{bmatrix} -1.37 \times 10^{-3} & 0 \\ 0 & -1.36 \times 10^{-3} \end{bmatrix} \begin{bmatrix} \theta \\ \psi \end{bmatrix} \tag{28}$$

The state space representations is as follows:

$$A = \begin{bmatrix} 0 & 0 & 1 & 0 \\ 0 & 0 & 0 & 1 \\ 3.6342 \times 10^{-7} & 0 & 0 & -1.5958 \times 10^{-2} \\ 0 & 3.3911 \times 10^{-7} & 1.4928 \times 10^{-2} & 0 \end{bmatrix} \tag{29}$$

$$B = \begin{bmatrix} 0 \\ 0 \\ 2.6525 \times 10^{-4} \\ 0.3 \times 2.4876 \times 10^{-4} \end{bmatrix}, C = \begin{bmatrix} 1 & 0 & 0 & 0 \end{bmatrix}, D = \begin{bmatrix} 0 \end{bmatrix} \tag{30}$$

The B matrix is represented by a 1x4 vector. The selection of thrusters mirrors those found on TÜRKSAT 1B, which utilize a canted configuration for their roll and yaw thrusters. This means that activating the roll thruster also induces a yaw torque, as it is aligned in a certain way with respect to the satellite frames.

The procedure for designing servo systems is detailed in various feedback control literature. A typical representation of a state feedback system incorporating integral control is often illustrated as follows:

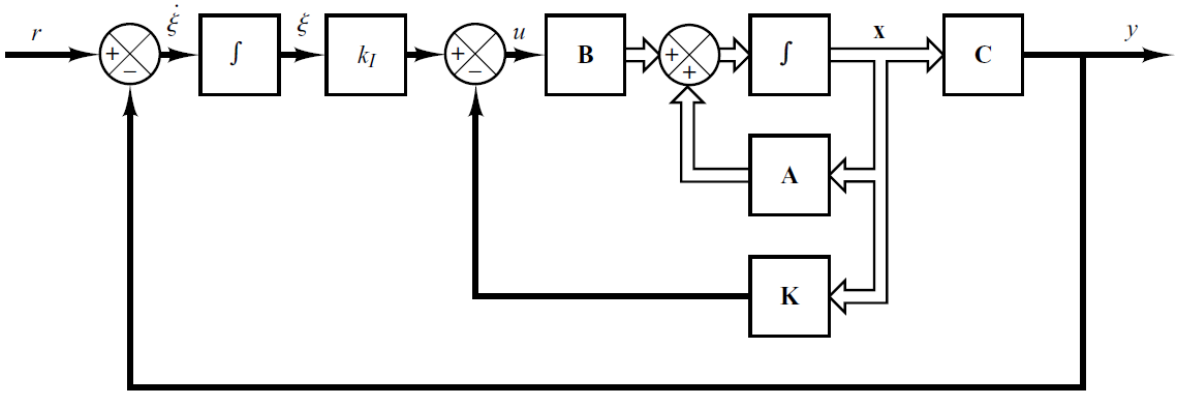

Figure 5.1 Generic integral plus state variable feedback attitude control block diagram [13]

From the block diagram, the following is obtained:

$$\begin{aligned} \dot{\mathbf{x}} &= \mathbf{A}\mathbf{x} + \mathbf{B}u \\ y &= \mathbf{C}\mathbf{x} \\ u &= -\mathbf{K}\mathbf{x} + k_I\xi \\ \dot{\xi} &= r - y = r - \mathbf{C}\mathbf{x} \end{aligned} \tag{31}$$

The notation $u = T_x$ and ξ signify the integrator's output, which represents a scalar state variable of the system. The state feedback gain matrix is denoted by K, the integral gain is indicated by k_I, the reference input signal (usually set to zero for regulation) is denoted by r, and the previously defined matrices are **A**, **B**, **C**, and **D**.

The dynamics of the system are captured by an equation that incorporates Equation 31:

$$\begin{bmatrix} \dot{\mathbf{x}}(t) \\ \dot{\xi}(t) \end{bmatrix} = \begin{bmatrix} \mathbf{A} & \mathbf{0} \\ -\mathbf{C} & 0 \end{bmatrix} \begin{bmatrix} \mathbf{x}(t) \\ \xi(t) \end{bmatrix} + \begin{bmatrix} \mathbf{B} \\ 0 \end{bmatrix} u(t) + \begin{bmatrix} \mathbf{0} \\ 1 \end{bmatrix} r(t) \tag{32}$$

Equation 32 can be written as:

$$\begin{bmatrix} \dot{\mathbf{x}}_e(t) \\ \dot{\xi}_e(t) \end{bmatrix} = \begin{bmatrix} \mathbf{A} & \mathbf{0} \\ -\mathbf{C} & 0 \end{bmatrix} \begin{bmatrix} \mathbf{x}_e(t) \\ \xi_e(t) \end{bmatrix} + \begin{bmatrix} \mathbf{B} \\ 0 \end{bmatrix} u_e(t) \tag{33}$$

where

$$u_e(t) = -\mathbf{K}\mathbf{x}_e(t) + k_I\xi_e(t) \tag{34}$$

Define a new (n+1)th-order error vector e(t) by:

$$\mathbf{e}(t) = \begin{bmatrix} \mathbf{x}_e(t) \\ \xi_e(t) \end{bmatrix} \tag{35}$$

Then Equation 33 becomes:

$$\dot{\mathbf{e}}(t) = \hat{\mathbf{A}}\mathbf{e} + \hat{\mathbf{B}}u_e \tag{36}$$

where

$$\hat{\mathbf{A}} = \begin{bmatrix} \mathbf{A} & \mathbf{0} \\ -\mathbf{C} & 0 \end{bmatrix}, \qquad \hat{\mathbf{B}} = \begin{bmatrix} \mathbf{B} \\ 0 \end{bmatrix}$$

and Equation 34 becomes:

$$u_e = -\hat{\mathbf{K}}\mathbf{e} \tag{37}$$

where

$$\hat{\mathbf{K}} = \left[\begin{array}{c|c} \mathbf{K} & -k_I \end{array} \right]$$

The main concept behind developing a servo controller is to push the new error vector $e(t)$ towards zero by building a (n+1)th order regulator system which is stable.

Using Ackermann's pole placement method, a MATLAB script is first created to compute the gains of integral control and state feedback [13]. The sequence commences with the definition of state equations, succeeded by an evaluation of system controllability. Subsequently, precise pole positions for the closed-loop system are assigned, culminating in the derivation of control gains through Ackermann's formulation.

With a controllability matrix rank of 5, the system is fully controllable. After numerous simulations employing various thruster sets, the closed-loop poles are selected to ensure optimal performance without overshoot and long-term stability.

$$\lambda_{closed} = \begin{bmatrix} -0.004 - 0.0015i \\ -0.004 + 0.0015i \\ -0.0001 - (1e-5)i \\ -0.0001 + (1e-5)i \\ -4.5 \end{bmatrix} \tag{38}$$

Utilizing Ackermann's formula, the state feedback gain matrix along with the integral gain constant can be derived as follows:

$$\hat{\mathbf{K}} = \begin{bmatrix} -65.7101 & 3.8203 & 1.2144 \times 10^4 & 1.7247 \times 10^4 & 0.0092 \end{bmatrix} \tag{39}$$

5.2.2. Integral Sliding Mode Control

Sliding Mode Control (SMC) stands out as a formidable method for managing systems prone to sudden and significant changes in their dynamics, finding utility in diverse applications such as vehicle stability, aerospace control, industrial process management, and energy systems [34]. The core principle of SMC revolves around the concept of the sliding surface—a predefined trajectory in the system's state space on which the system is constrained to operate. Once the system states are guided onto this surface, they are largely unaffected by certain types of disturbances, specifically those that directly influence the system's input pathways. This capability not only enhances the predictability of the system's behavior but also solidifies its stability and reliability under varying operational conditions.

Despite these strengths, traditional SMC is not without its drawbacks, particularly during the initial phase before the system reaches the sliding surface. During this initial reaching phase, the system remains susceptible to disturbances, which can affect the system's performance and stability. To address this issue, the development of Integral Sliding Mode Control (ISMC) marks a significant improvement. ISMC modifies the traditional approach by integrating the initial conditions into the sliding surface from the very start of the system's

response. This modification effectively eliminates the reaching phase, allowing the sliding mode to be active immediately, thus providing continuous robustness against disturbances from the moment the system starts operating.

To ensure uninterrupted operation and high reliability in mission-critical applications such as fault-tolerant sliding mode control for communication satellites using chemical propulsion, the adoption of Integral Sliding Mode Control presents a particularly advantageous strategy. The unique challenges faced by communication satellites, which include external disturbances from cosmic conditions and internal variances due to fuel burn and component wear, necessitate a control method that can offer immediate and unwavering robustness. ISMC, with its elimination of the reaching phase, directly addresses these requirements by maintaining control efficacy from the start, enhancing fault tolerance capabilities. This approach not only simplifies the control architecture but also significantly increases the system's resilience to faults and anomalies, which is crucial for maintaining the operational integrity and precise orientation of communication satellites throughout their missions. This enhanced stability and fault tolerance is imperative when employing chemical propulsion systems, where precise control over thrust and trajectory adjustments are vital for successful satellite maneuvering and station keeping.

For systems with reduced order, the selected control law for Integral sliding control applications is as follows:

$$u(t) = u_0(t) + u_1(t) \tag{40}$$

where $u_0(t) \in \mathbb{R}$ represents the nominal control, and $u_1(t) \in \mathbb{R}$ signifies the discontinuous control aimed at rejecting the perturbation term $h(x, t)$.

For the nominal control, various methods like Pole Placement or LQR can be employed. However, for this thesis, the controller designed in Section 5.2.1. is utilized. This choice facilitates a comprehensive comparison, shedding light on the advantages and disadvantages of Integral Sliding Control.

Based on the equivalent control method [35], the integral sliding variable can be formulated in the following manner:

$$s(t) = s_0(e) + z(t) \tag{41}$$

where $z(t) \in \mathbb{R}$ is an integral term given by

$$\dot{z} = -\frac{\partial s_0}{\partial e}\begin{bmatrix} \bar{e}_1 \\ [f_0(x) - x_d^{(n)}] + g_0(x)u_0 \end{bmatrix} \tag{42}$$

where $\bar{e}_1 := [e_2, e_3, ..., e_n]^T$ and $z(0) = -s_0(e(0))$ such that $s(0) = 0$.

The conventional sliding variable $s_0 \in \mathbb{R}$ is expressed as $s_0(e) = d/dt + \lambda)^{n-1}e_1$, where $\lambda \in \mathbb{R}^+$ is a design parameter defining the performance during the sliding phase. From the definitions of $e_1(t)$ and e, it follows that:

$$s_0(e) = \begin{bmatrix} \Lambda^T & 1 \end{bmatrix} e \tag{43}$$

where $\Lambda := [\lambda^{(n-1)}, (n-1)\lambda^{(n-2)}, \ldots, (n-1)\lambda]^T$. Taking the time derivative of s_0, one obtains:

$$\dot{s}_0 = [f_0(x) + v(x,t)] + g_0(x)u + h(x,t) \tag{44}$$

where $v(x,t) := [0, \Lambda^T]e(t) - x_d^{(n)}(t)$. By setting $h = 0$ and $u = u_0$ in equation 44, and choosing

$$u_0 = -\frac{k_c s_0 + f_0(x) + v(x,t)}{g_0(x)} \tag{45}$$

leads to the ideal closed-loop dynamics

$$\dot{s}_0 + k_c s_0 = 0 \tag{46}$$

where $k_c \in \mathbb{R}^+$ is a control gain parameter.

Substituting the expressions of s_0 from Equation 43, u_0 from Equation 45, and v under Equation 44 into Equation 42, one obtains:

$$\dot{z} = -\begin{bmatrix} \Lambda^T & 1 \end{bmatrix} \begin{bmatrix} \bar{e}_1 \\ -k_c s_0 - \begin{bmatrix} 0 & \Lambda^T \end{bmatrix} e \end{bmatrix} = k_c s_0 \tag{47}$$

Hence, the integral sliding variable s in Equation 41 is given by:

$$s(t) = s_0(e(t)) - s_0(e(0)) + kc \int_0^t s_0(e(\tau)) d\tau \tag{48}$$

The selected discontinuous control function is:

$$u_1 = -\alpha \text{sgn}(s), \quad \alpha \geq \frac{\bar{f} + \bar{d} + \eta}{g_0} \tag{49}$$

The Simulink diagram illustrated in Figure 9.7, created based on Equations 43, 48, and 49, showcases the implementation of the integral sliding mode control discontinuous control strategy. This diagram integrates the selected design parameters to achieve robust and effective control of the system dynamics.

In the controller design, extensive simulations were conducted to carefully evaluate the parameter α, leading to the selection of 3.5×10^{-2} as the optimal value. Figures 5.2 and 5.3 showcase some of these simulations. The parameter α significantly influences the control effort exerted by the system. Higher values of α, such as 10^{-1}, resulted in challenges in achieving zero error, leading to steady-state errors. Conversely, lower values, like 10^{-5}, did not offer substantial improvements in system performance. Thus, the chosen value

of α strikes a balance between effective control and preventing excessive oscillations or instability. This meticulous parameter selection process underscores the critical role of fine-tuning controller parameters to achieve the desired system behavior.

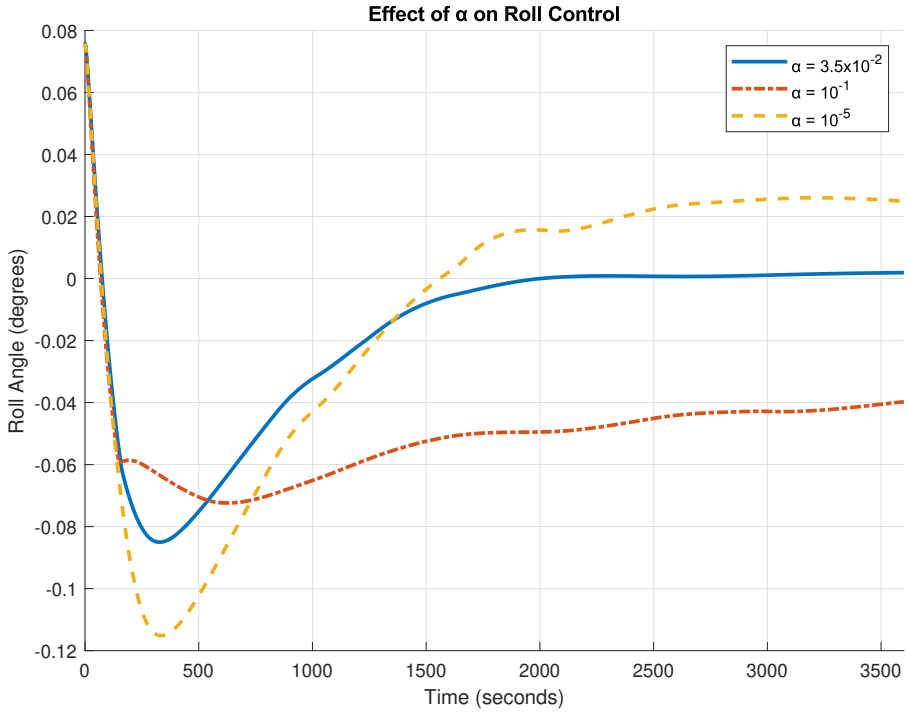

Figure 5.2 Effect of α on Roll

The evaluation of the total control effort is performed using the following equation:

$$u_{total} = \int u(t)^2 dt \tag{50}$$

In Table 5.1, it can be observed that for $\alpha = 10^{-1}$, the control effort is minimal due to the system exhibiting a steady-state error and being unable to reach zero error. On the other hand, for $\alpha = 10^{-5}$, the control effort is 164.5% higher compared to 3.5×10^{-2}, indicating a slower convergence without significant improvement in system performance.

The design parameter λ, which determines the performance during the sliding phase, is chosen as 25 for the system. This selection is based on careful consideration of the desired system behavior and performance requirements.

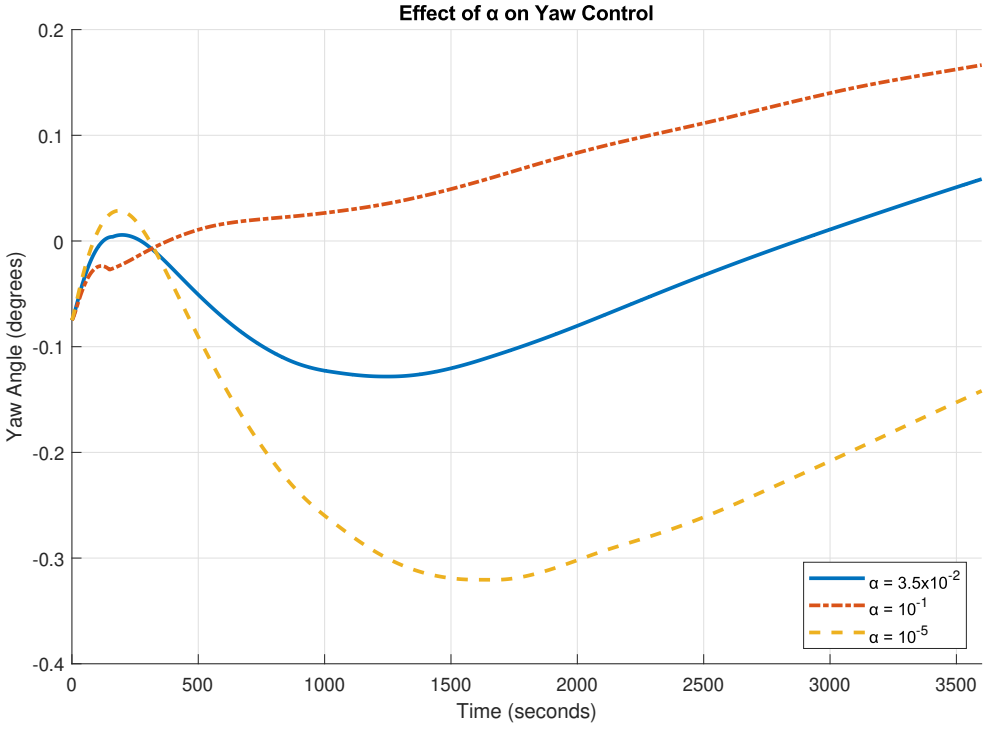

Figure 5.3 Effect of α on Yaw

α **Value**	**Total Control Effort**
3.5×10^{-2}	664.0
10^{-1}	483.8
10^{-5}	1756.8

Table 5.1 Effect of α on total control effort

By setting λ to 25, a balance between the speed of response and the stability of the system during the sliding phase is aimed to be achieved. This value ensures that the system effectively tracks the reference trajectory while maintaining robustness against disturbances and uncertainties.

5.3. Fault Detection, Isolation, and Recovery System Design

The Flywheel Momentum Wheel utilized for pitch control consists of one primary unit and one redundant unit. Likewise, the Wheel Drive Electronic system includes one primary unit and one backup unit. However, in the design, the backup system is not integrated as the primary focus is on roll/yaw control rather than pitch control.

For Roll/Yaw control, Thruster 5A is designated for positive roll control, while Thruster 5B is assigned for negative roll control. Thruster 4A serves as a backup for Thruster 5A, and Thruster 4B acts as a backup for Thruster 5B. To keep system simple, the backup for Thruster 5B is not integrated. Thus, only Thrusters 4A, 5A, and 5B are included in the model. This design ensures redundancy and reliability in the event of thruster failure, enhancing the overall operational resilience of the satellite system.

The Fault Detection and Identification (FDIR) system is a critical component of satellite operations, tasked with ensuring the integrity and reliability of onboard systems. It operates by continuously monitoring the thruster torque values and comparing them against the expected values computed by an optimal model. In the event that the error between the measured and expected values exceeds a predefined threshold, typically set around 20%, the FDIR system triggers a switchover from the main thruster to the backup thruster.

However, the role of FDIR systems extends beyond mere fault detection; they are integral to maintaining the overall safety and functionality of the satellite. When anomalies or out-of-range values are detected, these systems raise alerts at ground stations, prompting technical teams to conduct thorough analyses. These analyses involve evaluating the trends observed and identifying the root causes of the discrepancies. Based on their findings, appropriate precautionary measures are taken to mitigate any potential risks or failures.

In the context of this study, the aim is to demonstrate the robustness and effectiveness of the proposed controller under various scenarios, including performance losses or changes in thrusters. Designing a comprehensive FDIR system is a complex undertaking, often involving sophisticated algorithms and extensive testing. However, for the purpose of this

study, a simplified Fault Detection, Isolation, and Recovery (FDIR) mechanism has been integrated to demonstrate the controller's ability to maintain optimal performance even in the face of thruster changes or degradations. By subjecting the controller to such conditions, the study seeks to validate its ability to adapt and perform optimally in the face of challenges, thereby enhancing the overall reliability and resilience of satellite systems.

6. NONLINEAR SIMULATION RESULTS

For simulation and comparison purposes, the satellite's operational mode is selected as the Normal Operating Mode (NM), ensuring precise station pointing throughout its operational lifespan.

To ensure a comprehensive comparison, the focus is directed specifically towards the Roll/Yaw control loop. The evaluation encompasses three distinct cases, each illuminating different scenarios to assess the robustness and reliability of the system. In the nominal case, the system operates under standard conditions utilizing the nominal thruster set, representing an ideal operational scenario.

In the second case, a simulated performance degradation of 15% is introduced into the thrusters, simulating real-world conditions where thruster performance may diminish over time or due to environmental factors. This scenario allows for the examination of the system's response and adaptability to suboptimal conditions, shedding light on its resilience and ability to maintain operational efficacy despite performance losses.

Finally, the third case introduces a more critical failure scenario where one of the thrusters experiences either a significant performance loss exceeding the predetermined threshold or a total failure. In such instances, the Fault Detection, Isolation, and Recovery (FDIR) system is activated, swiftly identifying the malfunctioning thruster and initiating a seamless transition to the backup thruster. This scenario tests the efficacy and reliability of the FDIR system in promptly detecting and mitigating critical failures, ensuring uninterrupted functionality and mission continuity.

By systematically evaluating the system's performance across these diverse scenarios, a comprehensive understanding of its robustness, resilience, and fault tolerance capabilities is attained. This multifaceted evaluation approach facilitates informed decision-making and optimization efforts aimed at enhancing the overall reliability and effectiveness of the system in real-world operational environments.

6.1. Nominal Condition

In this study, pitch control and roll/yaw control are separately investigated under nominal conditions to elucidate the distinct dynamics and control strategies applicable to each axis. Specifically, for roll/yaw control, the analysis focuses on the operational roles of Thruster 5A and Thruster 5B. Thruster 5A is utilized for generating positive thrust, while Thruster 5B is employed for negative thrust.

6.1.1. ±0.1° Error in Pitch

In this section, the performance of the satellite's pitch control system under normal operating conditions is analyzed, focusing on a maximum allowable error of ±0.1°. This specific error margin is chosen based on the observation that, under normal circumstances, the satellite's pitch error rarely exceeds this threshold. By focusing on this realistic range, valuable insights can be gained into the controller's effectiveness in maintaining accurate pitch control during typical operations.

To ensure a comprehensive evaluation, simulations incorporate not only the effects of cyclic disturbances caused by solar radiation pressure but also random measurement errors. These measurement errors, introduced to both the attitude and angular rate sensors, are modeled with magnitudes of approximately ±0.00005° and ±0.00001 °/s, respectively. This approach allows us to assess the controller's robustness and ability to handle real-world uncertainties and noise in sensor measurements.

The desired pitch angle is set to 0.8336°, and the simulation duration is 10 minutes. This duration is chosen based on the observation that the system typically stabilizes within 3 minutes, allowing us to observe the controller's response and performance over a sufficient period. For longer-term stability analysis, please refer to Section 6.1.5..

The first analysis focuses on an initial pitch error of -0.1°. Figure 6.1 presents the simulation results for this scenario.

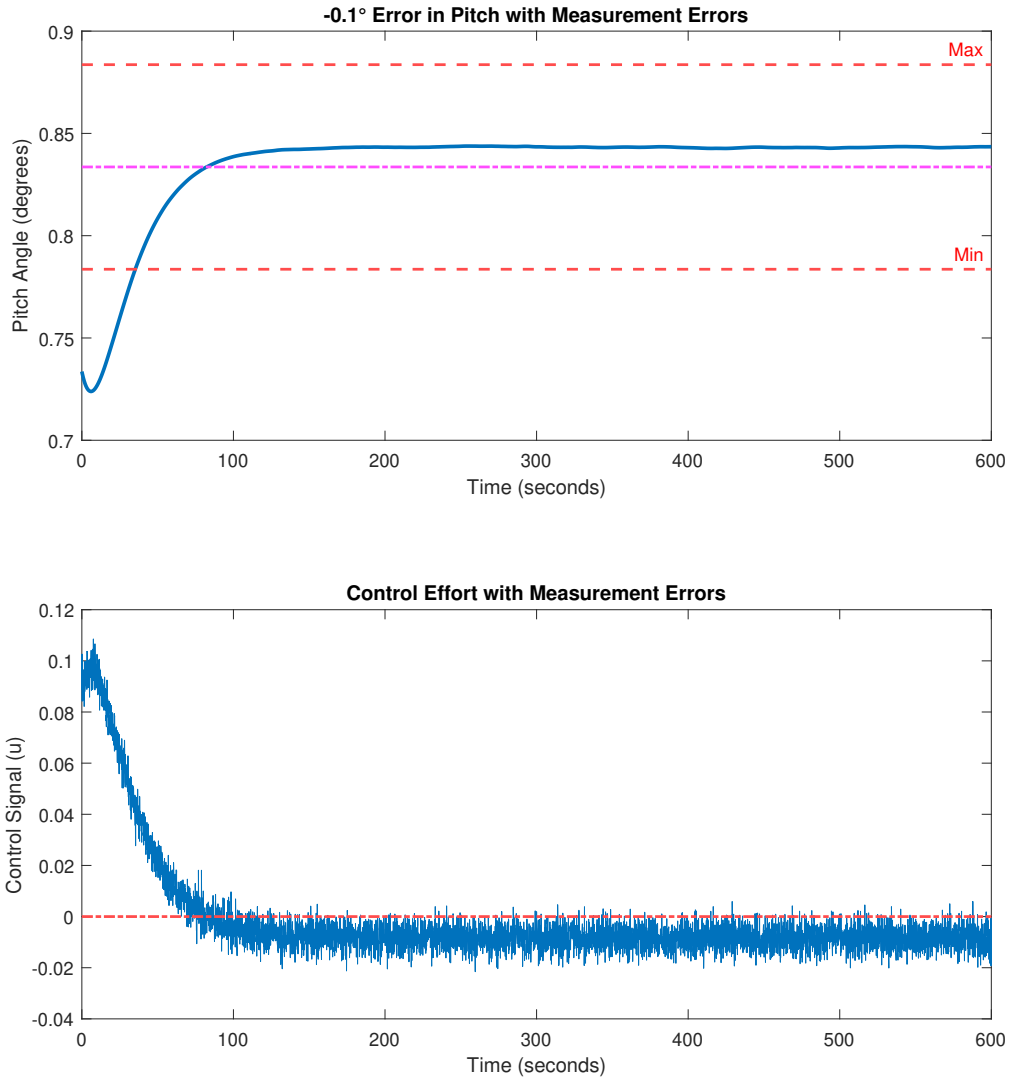

Figure 6.1 Pitch error of -0.1° with measurement errors

The pitch angle converges to the desired value of 0.8336° within approximately 100 seconds. The system exhibits minimal overshoot during the transient response. The pitch angle briefly exceeds the desired value by a small margin before settling, but this overshoot is negligible and does not pose any risk to the system's stability. The control effort, represented by the control signal sent to the momentum wheel, shows an initial spike as the controller corrects the initial pitch error. However, the control effort quickly settles to a relatively low level, indicating efficient control action.

The second analysis focuses on an initial pitch error of 0.1°. Figure 6.2 presents the simulation results for this scenario.

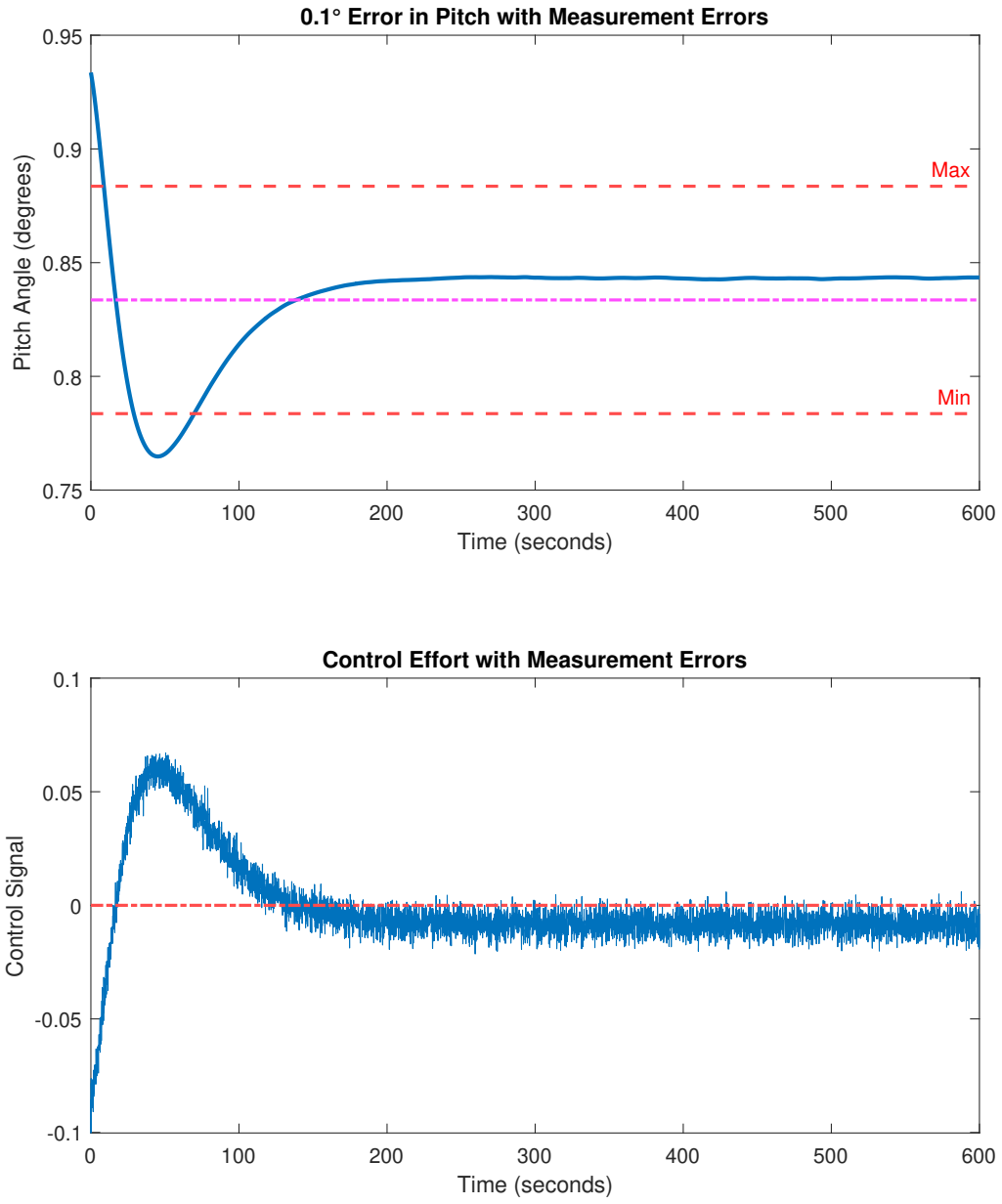

Figure 6.2 Pitch error of 0.1° with measurement errors

The pitch angle gradually approaches the target value of 0.8336° over a period of roughly 150 seconds, exhibiting behavior akin to that observed in the negative case. Despite momentarily

surpassing the minimum required angle, the system swiftly corrects course and returns to the desired value without undue delay. A comparable level of control effort is also evident in this scenario.

The steady-state error remains minimal for both scenarios, as depicted in Table 6.1, indicating that the pitch angle consistently tracks the desired value throughout the simulation.

Position Difference	**Minimum**	**Maximum**	**Error**
-0.1°	0.7238°	0.8438°	1.17%
0.1°	0.7649°	0.9336°	1.16%

Table 6.1 Pitch control results

6.1.2. 0.075° Error in roll and -0.075° Error in yaw

In this section, a detailed analysis is conducted on the roll and yaw control systems operating under normal conditions. Typically, the Attitude Determination and Control Electronics (ADCE) responds to deviations from the desired attitude by referencing the Inertial Reference System (IRES). A deviation of approximately $\pm 0.05°$ in the roll attitude triggers the ADCE to initiate corrective measures to realign the satellite.

To thoroughly evaluate the performance and robustness of the control systems, a scenario has been selected that pushes the controllers beyond standard operational requirements. Specifically, the first case involves an induced error of 0.075° in roll and -0.075° in yaw. This scenario provides a rigorous test environment to assess the controllers' effectiveness under slightly exaggerated deviations, offering valuable insights into their dynamic response and stability under stress.

Two advanced control methods, Integral Plus State Variable Feedback Control and Integral Sliding Mode Control, are examined in this context. Each method is analyzed independently to understand their unique control dynamics and efficacy in handling deviations. A

comprehensive comparison of both control methods, focusing on their performance metrics and operational efficiencies, is subsequently detailed in Section 6.4..

6.1.2.1. Integral Plus State Variable Feedback Control Results

The results of the Integral Plus State Variable Feedback Control, with an initial error of 0.075° in roll and -0.075° in yaw, are comprehensively illustrated in Figure 6.3.

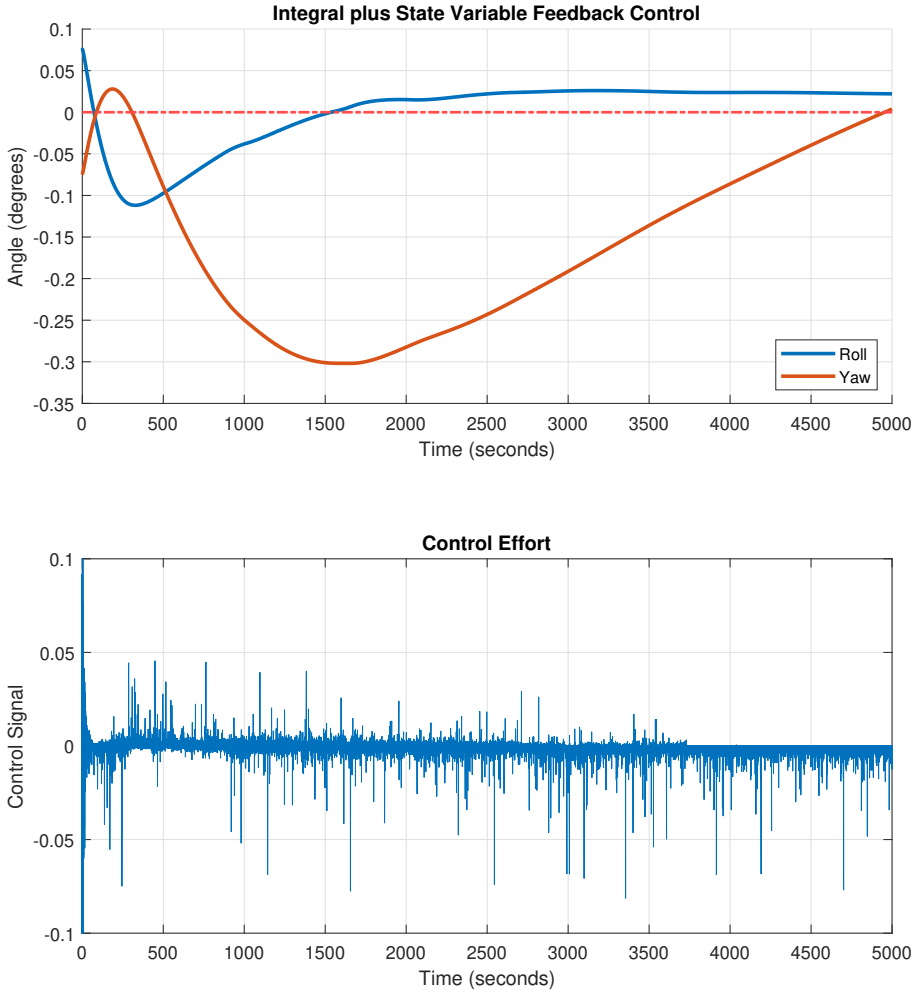

Figure 6.3 Integral plus state variable feedback control with 0.075° error in roll and -0.075° error in yaw

The roll axis exhibits a swift and effective corrective action, achieving a zero-degree orientation by 1540 seconds. The system maintains a steady-state error of 0.025 degrees on the roll axis, which is well within acceptable performance limits. The maximum deviation recorded on the roll axis is -0.11 degrees. On the yaw axis, the initial oscillation reaches a peak of -0.30 degrees, demonstrating the system's capability to respond dynamically. The total control effort, measured at 322.78, underscores the effectiveness of the system in stabilizing the satellite under various conditions while also highlighting the substantial energy required for these adjustments. This consideration is crucial for assessing the system's operational efficiency and long-term sustainability.

6.1.2.2. Integral Sliding Mode Control Results

The results for the Integral Sliding Mode Control are illustrated in Figure 6.4. This control system carries out a decisive corrective action on the roll axis, realigning to a zero-degree orientation by 2000 seconds. This prompt and effective adjustment demonstrates the system's robust efficiency in managing deviations. Furthermore, the system maintains an exceptionally low steady-state error of just 0.002 degrees on the roll axis, highlighting its unparalleled precision and consistent ability to maintain near-perfect alignment over time. The maximum deviation observed on the roll axis is -0.08 degrees, which underscores the system's superior capability in minimizing overshoots and ensuring satellite stability with minimal variance from the targeted orientation. For the yaw axis, the initial oscillation peaks at -0.13 degrees, showcasing the system's ability to swiftly address and mitigate perturbations, thus enabling rapid stabilization. While the total control effort, measured at 644.31, represents a significant energy commitment, it reflects the system's robust and effective control in maintaining the satellite's attitude under dynamic conditions.

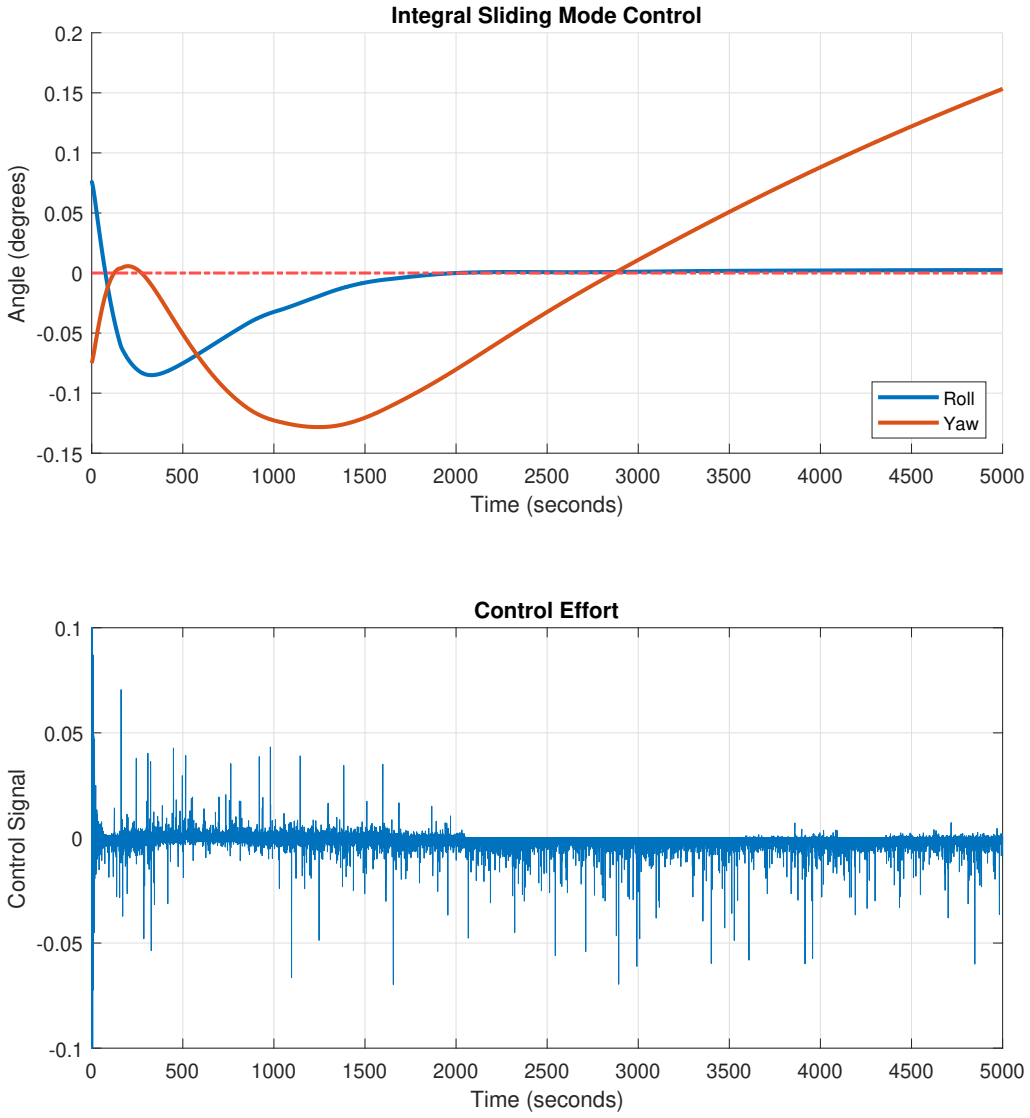

Figure 6.4 Integral sliding mode control with 0.075° error in roll and -0.075° error in yaw

6.1.3. -0.075° Error in roll and 0.075° Error in yaw

In the second scenario, errors of -0.075° in roll and 0.075° in yaw were examined.

6.1.3.1. Integral Plus State Variable Feedback Control Results

The findings for the Integral Plus State Variable Feedback Control are displayed in Figure 6.5.

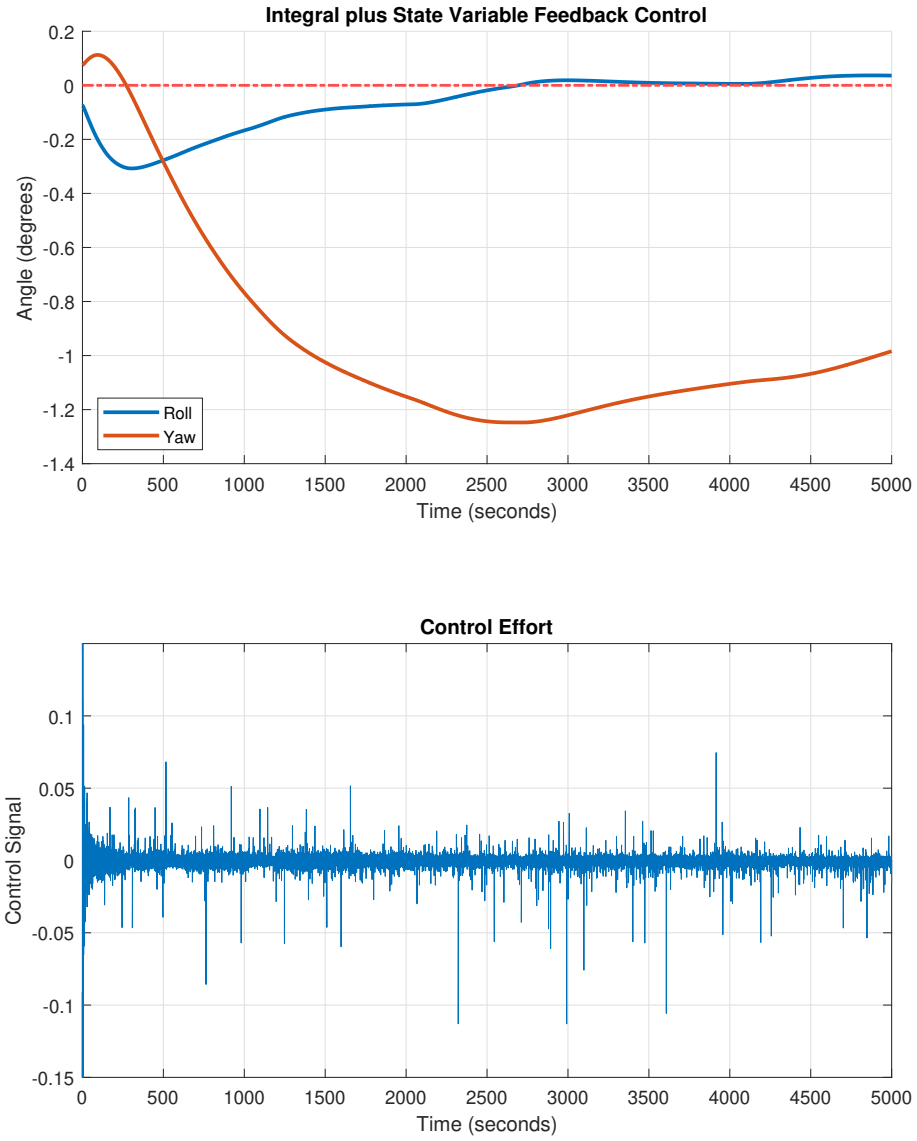

Figure 6.5 Integral plus state variable feedback control with -0.075° error in roll and 0.075° error in yaw

The roll angle demonstrates a peak deviation of -0.307 degrees before it stabilizes at 0 degrees, achieved at approximately 2692 seconds. On the yaw axis, a maximum deviation of -1.25 degrees is noted, suggesting a larger displacement compared to the roll axis. Despite this considerable deviation, the yaw performance remains within acceptable limits. The maximum steady-state error recorded for the system is 0.036 degrees. Furthermore, the total control effort necessary to manage these angles is quantified at 227.99.

6.1.3.2. Integral Sliding Mode Control Results

The results for the Integral Sliding Mode Control are shown in Figure 6.6. The maximum deviation on the roll axis is -0.299 degrees, and it nears zero by approximately 3140 seconds. The system maintains a notably low steady-state error of 0.016 degrees. For the yaw axis, the initial oscillation peaks at -1.08 degrees. The control effort required for these adjustments is quantified at 169.92. This relatively lower control effort demonstrates a more efficient utilization of resources by the Integral Sliding Mode Control, thereby enhancing satellite stability while optimizing energy consumption.

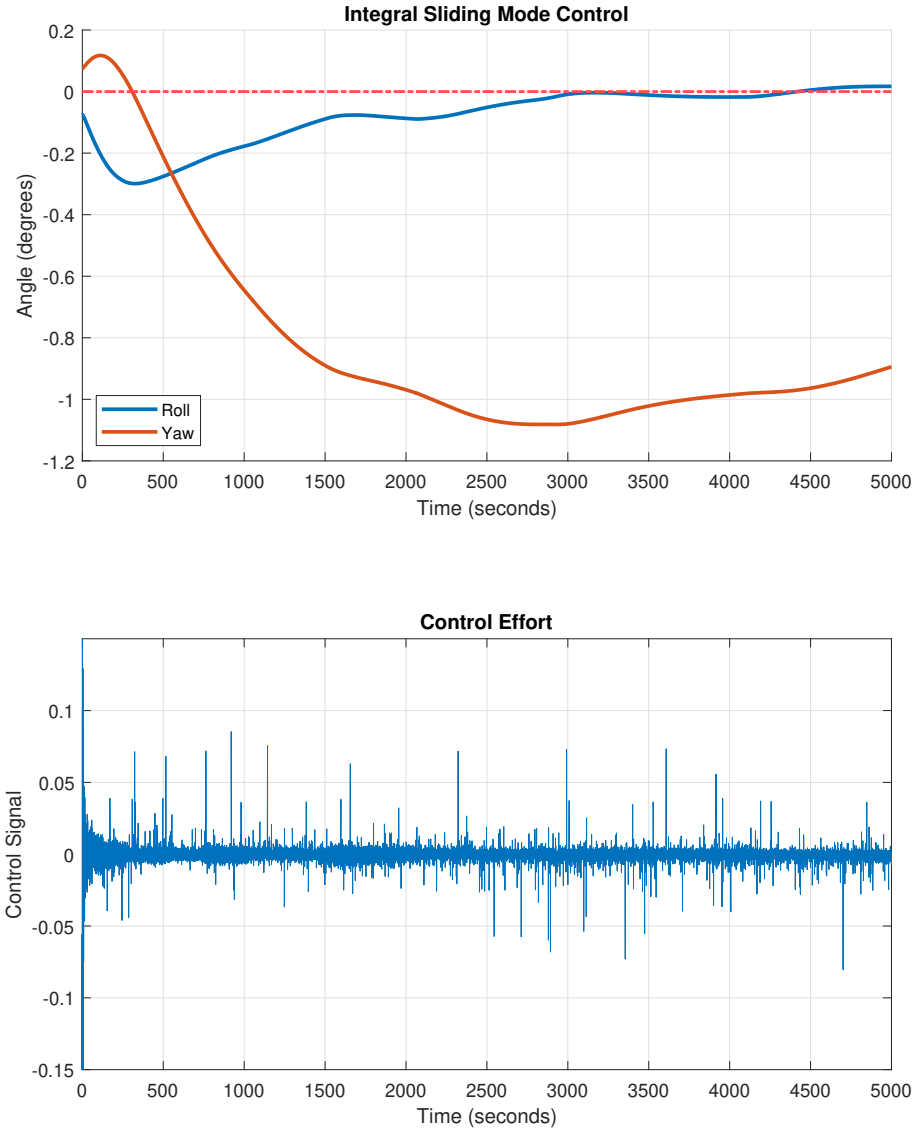

Figure 6.6 Integral sliding mode control with -0.075° error in roll and 0.075° error in yaw

6.1.4. 0.1° Error in roll and yaw

In the final case, errors of 1° in both roll and yaw were examined. This scenario represents a deviation double the amount typically allowed, but the analysis was conducted to assess the system's response in extreme cases.

6.1.4.1. Integral Plus State Variable Feedback Control Results

The results of the Integral Plus State Variable Feedback Control are showcased in Figure 6.7. This control approach enables the roll axis to exhibit a strong and effective response, achieving a zero-degree orientation by 2230 seconds. The system maintains a steady-state error of 0.034 degrees on the roll axis, illustrating its precision in maintaining alignment. The maximum deviation noted on the roll axis is -0.25 degrees. For the yaw axis, the initial oscillation peaks at -0.73 degrees, effectively demonstrating the system's ability to dampen perturbations. The total control effort required to manage these angles, measured at 327.52, underscores the system's substantial energy commitment to ensuring stability and precise control.

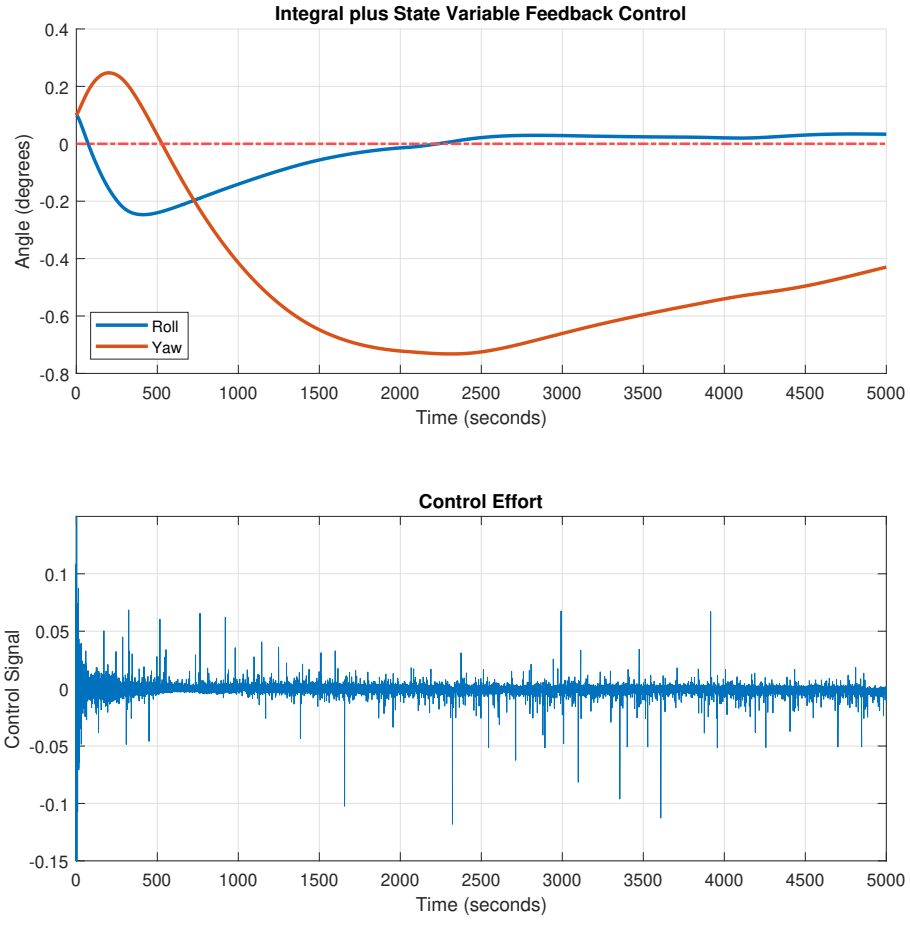

Figure 6.7 Integral plus state variable feedback control with 0.1° error in roll and yaw

6.1.4.2. Integral Sliding Mode Control Results

The performance of the Integral Sliding Mode Control is effectively captured in Figure 6.8. For the roll axis, the system realigns to a zero-degree orientation by 2288 seconds, while maintaining a steady-state error of just 0.017 degrees. This showcases its exceptional precision in maintaining the desired orientation consistently. The maximum deviation on the roll axis is noted at -0.22 degrees, demonstrating the control system's capability to minimize overshoots and stabilize the satellite efficiently. On the yaw axis, the initial oscillation peaks at -0.56 degrees, illustrating the system's ability to rapidly dampen perturbations and achieve stabilization. The total control effort required for managing these angles is recorded at 528.18.

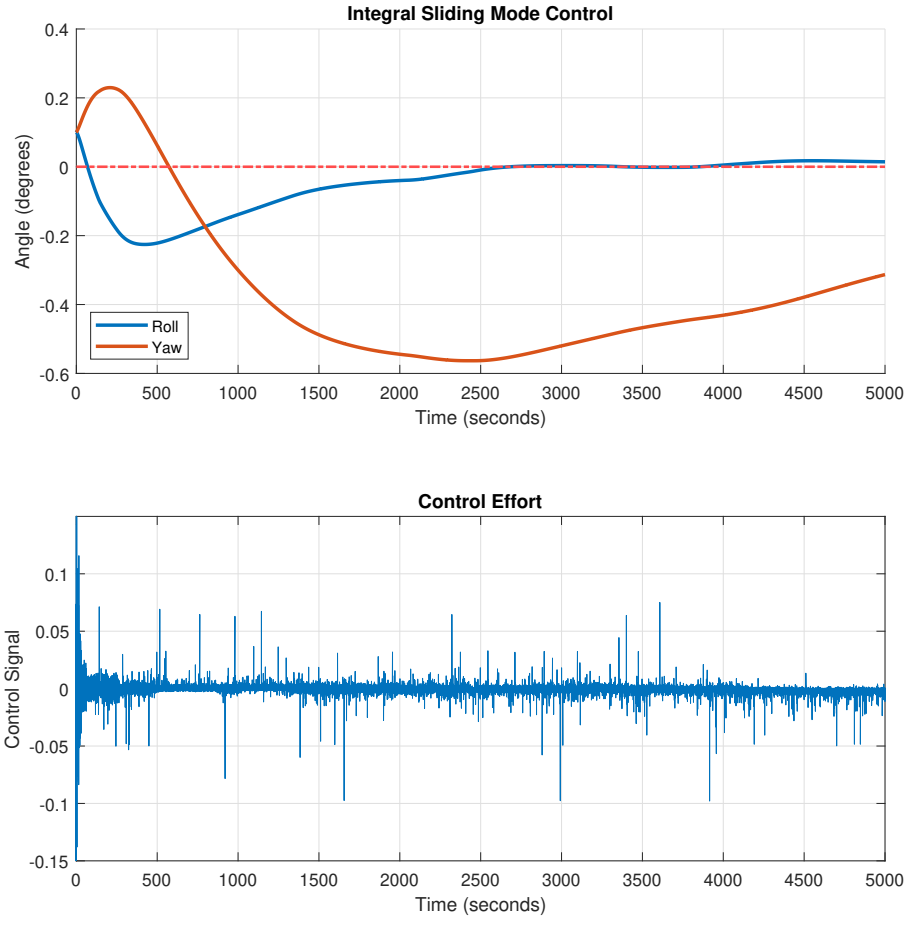

Figure 6.8 Integral sliding mode control with 0.1° error in roll and yaw

6.1.5. Long Term Stability Analysis

Long-term stability analysis is a crucial aspect of evaluating the performance of control systems in communication satellites. The ability to maintain a stable attitude over an extended period, without compromising on the quality of the transmitted signal, is essential for ensuring reliable and efficient satellite operations. In this study, the long-term stability of the proposed control system is investigated by simulating its behavior over a 24-hour period. This allows us to assess how well the controller performs under normal operating conditions, as well as its ability to adapt to changing environmental factors such as solar radiation and atmospheric drag.

The simulation begins with an initial condition where the satellite's roll angle is 0.075° off-nominal and its yaw angle is -0.075° off-nominal. The goal of the control system is to rapidly correct these errors and maintain a stable attitude over an extended period.

By analyzing the satellite's attitude over an extended period, insights into the controller's performance in terms of settling time, steady-state error, and control effort can be gained. This information is critical for evaluating the overall effectiveness of the control system design and identifying potential areas for improvement. In this section, the results of the long-term stability analysis are presented, highlighting the behavior of the Integral Plus State Variable Feedback Control and Integral Sliding Mode Control under normal operating conditions over a 24-hour period with an initial condition of 0.075° error in roll and -0.075° error in yaw.

6.1.5.1. Integral Plus State Variable Feedback Control Results

The long-term stability analysis of the Integral Plus State Variable Feedback Control system is presented in Figure 6.9. The simulation results demonstrate that the controller is able to maintain a stable roll angle within the desired range of $\pm 0.05°$ over a 24-hour period, despite the presence of disturbances. While some oscillations are observed, they remain relatively small and do not exceed the acceptable limits.

Similarly, the yaw angle also exhibits some oscillatory behavior, but its amplitude remains less than 1°, which is well within the maximum allowed tolerance of 5°. Overall, the Integral Plus State Variable Feedback Control system is shown to be effective in maintaining a stable attitude over an extended period, meeting the requirements for reliable and efficient satellite operations.

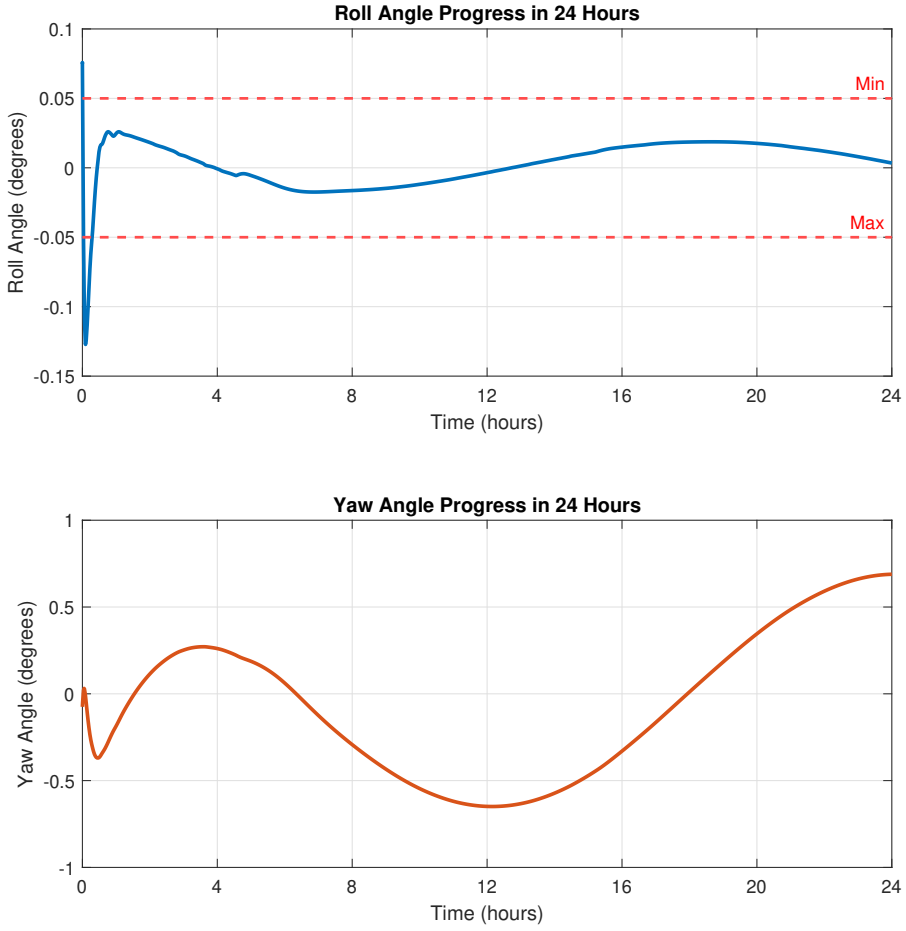

Figure 6.9 24-hour simulation of integral plus state variable feedback control with 0.075° error in roll and -0.075° error in yaw

6.1.5.2. Integral Sliding Mode Control Results

The long-term stability analysis of the Integral Sliding Mode Control system is presented in Figure 6.10. The simulation results demonstrate that the controller is able to maintain a stable

roll angle within the desired range of ±0.05° over a 24-hour period, despite the presence of disturbances.

Initially, the controller exhibits a similar response to the Integral Plus State Variable Feedback Control system, with some oscillations observed in both the roll and yaw angles. However, after reaching zero steady-state error, the Integral Sliding Mode Control system shows improved performance, with a reduced overshoot and a more accurate tracking of the desired attitude.

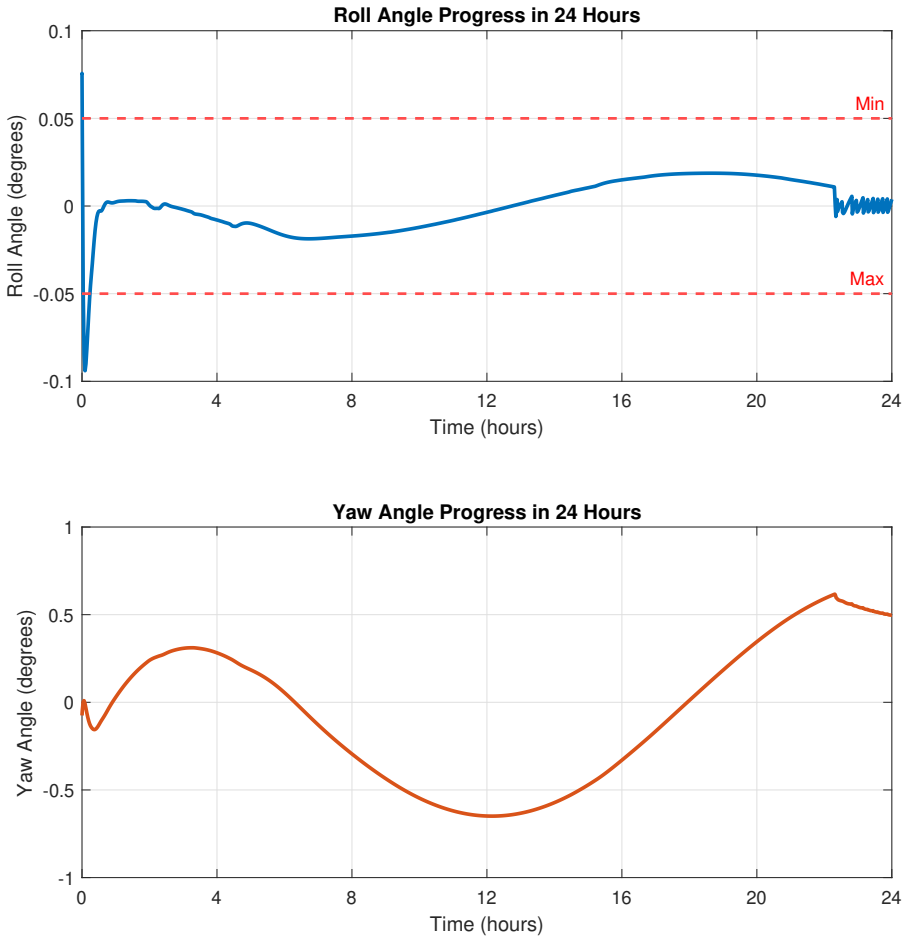

Figure 6.10 24-hour simulation of integral sliding mode control with 0.075° error in roll and -0.075° error in yaw

A closer examination of the sliding surface, presented in Figure 6.11, reveals that it converges to zero around hour 22. However, after this point, the system exhibits chattering behavior, where the control signal oscillates rapidly around the nominal value. The reason for this chattering response is due to the inherent nature of sliding mode controllers, which use a switching function to determine when to switch between different control modes.

The ability to modify and fine-tune the sliding surface (Figure 6.11) offers a significant advantage for future satellite missions requiring different payload and pointing accuracy requirements. By adjusting the parameters of the sliding surface, the controller can be optimized for specific mission scenarios, ensuring that the desired level of stability and accuracy is achieved.

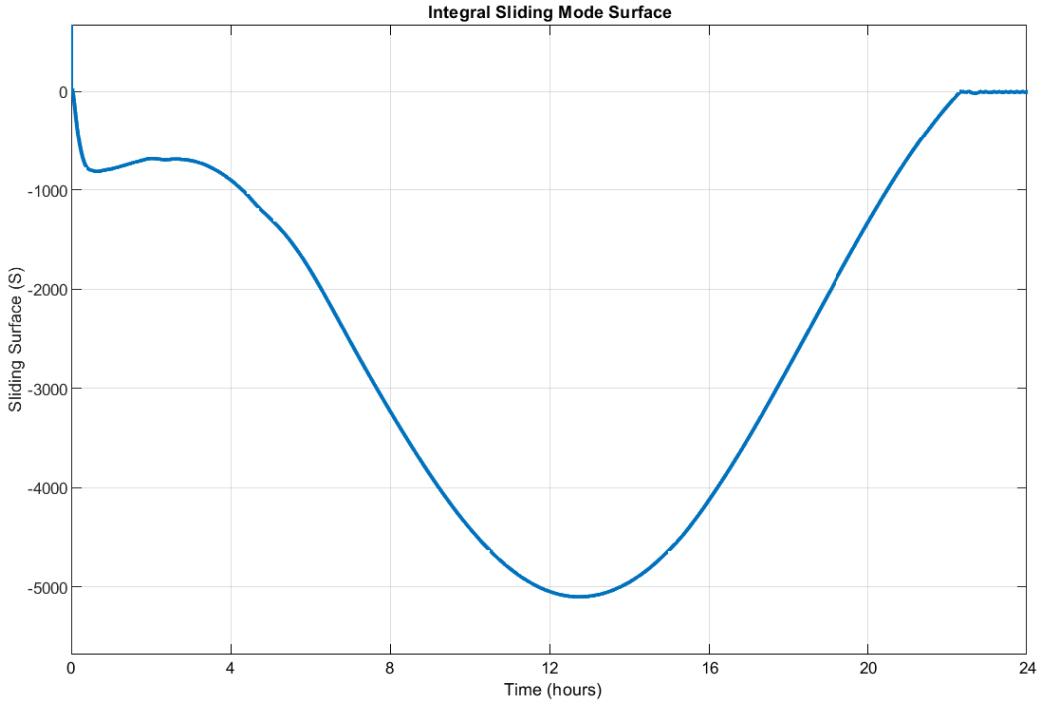

Figure 6.11 Integral sliding mode control surface

6.1.6. Discussion of Results

6.1.6.1. Pitch Control

The simulation results for pitch control under normal operating conditions demonstrate the effectiveness and robustness of the chosen PD controller. In all tested scenarios, the controller successfully stabilized the satellite's pitch attitude within the desired range of ±0.1°, even in the presence of cyclic disturbances and random measurement errors. The settling time was consistently within the expected range, and overshoot was minimal. Additionally, the steady-state error remained negligible, indicating accurate pitch control.

The control effort required to achieve the desired pitch attitude was also analyzed. The initial spike in control effort observed in all scenarios is expected as the controller corrects the initial pitch error. However, the control effort quickly settles to a relatively low level, indicating efficient control action and minimizing unnecessary energy expenditure.

Overall, the pitch control system demonstrates excellent performance and robustness under normal operating conditions. The chosen PD controller effectively mitigates disturbances and measurement errors, ensuring accurate and efficient pitch control for the communication satellite.

6.1.6.2. Roll/Yaw Control

The efficacy of Integral Sliding Mode Control and Integral Plus State Variable Feedback Control under nominal conditions are assessed, focusing on their performance in challenging operational scenarios. These scenarios were designed to test the controllers' ability to maintain roll and yaw angles within the stringent tolerance of ±0.05°.

The simulation results are methodically summarized in Table 6.2 for Integral Plus State Variable Feedback Control and Table 6.3 for Integral Sliding Mode Control. The outcomes from these simulations indicate that both control strategies successfully managed the

satellite's roll and yaw orientations, ensuring that deviations remained within the targeted range.

Roll / Yaw Initial Error	Duration of Roll Reaching 0°	Roll Maximum	Roll Max Deviation	Yaw Maximum
0.075° / -0.075°	1540 s	-0.11°	0.025°	-0.30°
-0.075° / 0.075°	2692 s	-0.307°	0.036°	-1.25°
0.1° / 0.1°	2230 s	-0.25°	0.034°	-0.73°

Table 6.2 Integral plus state variable feedback control results in nominal condition

Roll / Yaw Initial Error	Duration of Roll Reaching 0°	Roll Maximum	Roll Max Deviation	Yaw Maximum
0.075° / -0.075°	2000 s	-0.08°	0.002°	-0.13°
-0.075° / 0.075°	3140 s	-0.299°	0.016°	-1.08°
0.1° / 0.1°	2288 s	-0.22°	0.017°	-0.56°

Table 6.3 Integral sliding mode control results in nominal condition

Furthermore, the required control effort is summarized in Table 6.4. This highlights the trade-off between performance and control effort, as ISMC requires significantly higher control efforts than traditional Integral Plus State Variable Feedback Control. The results demonstrate the robustness and effectiveness of both controllers under nominal conditions.

Roll / Yaw Initial Error	State Feedback Control Effort	Integral Sliding Mode Control Effort
0.075° / -0.075°	322.78	644.31
-0.075° / 0.075°	227.99	169.92
0.1° / 0.1°	327.52	528.18

Table 6.4 Control effort results in nominal condition

6.2. Performance Loss in Thrusters

This section examines the implications of performance loss in thrusters, specifically focusing on the operational challenges posed by degraded thruster efficiency. The study considers initial conditions with a 0.075° error in roll and a -0.075° error in yaw to evaluate both controllers under these specific misalignments. Over time and with continuous use, thrusters 5A and 5B are hypothesized to experience a performance degradation of approximately 15%. This scenario is critical for understanding the resilience and adaptability of the control systems when faced with realistic operational impairments in thruster efficiency. The analysis aims to illustrate how such performance losses affect the overall stability and control precision of the satellite's orientation.

6.2.1. Integral Plus State Variable Feedback Control Results

The performance of the Integral Plus State Variable Feedback Control is presented in Figure 6.12. This method allows the roll axis to respond robustly and effectively, reaching a stable orientation at zero degrees within 1142 seconds. The roll axis demonstrates high precision by maintaining a steady-state error of 0.029 degrees, with the largest observed deviation being -0.068 degrees. In terms of the yaw axis, an initial peak oscillation of -0.15 degrees effectively showcases the system's capability to attenuate disturbances. The energy expended in controlling these angles, quantified at 404.30, highlights the significant effort required by the system to ensure both stability and precise alignment.

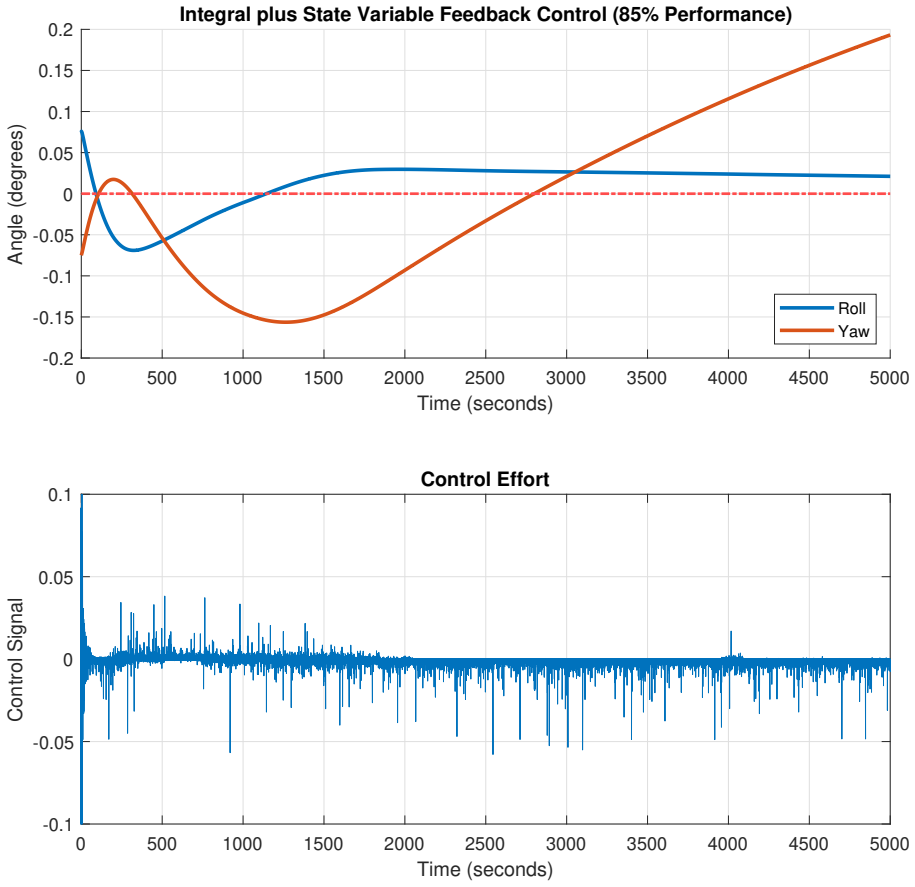

Figure 6.12 Integral plus state variable feedback control with 15% performance loss in thrusters

6.2.2. Integral Sliding Mode Control Results

Figure 6.13 effectively illustrates the performance of the Integral Sliding Mode Control. The system aligns the roll axis back to a zero-degree orientation within 980 seconds, while maintaining an exceedingly low steady-state error of only 0.0001 degrees, underscoring its exceptional accuracy in sustaining the targeted orientation. The greatest observed deviation on the roll axis is a minimal -0.041 degrees, highlighting the control system's proficiency in limiting overshoots and efficiently stabilizing the satellite. For the yaw axis, the initial peak oscillation at -0.03 degrees demonstrates the system's rapid response to dampen disturbances

and secure stabilization. The total effort exerted in controlling these angles, quantified at 916.48, reflects the system's substantial commitment to precision and stability management.

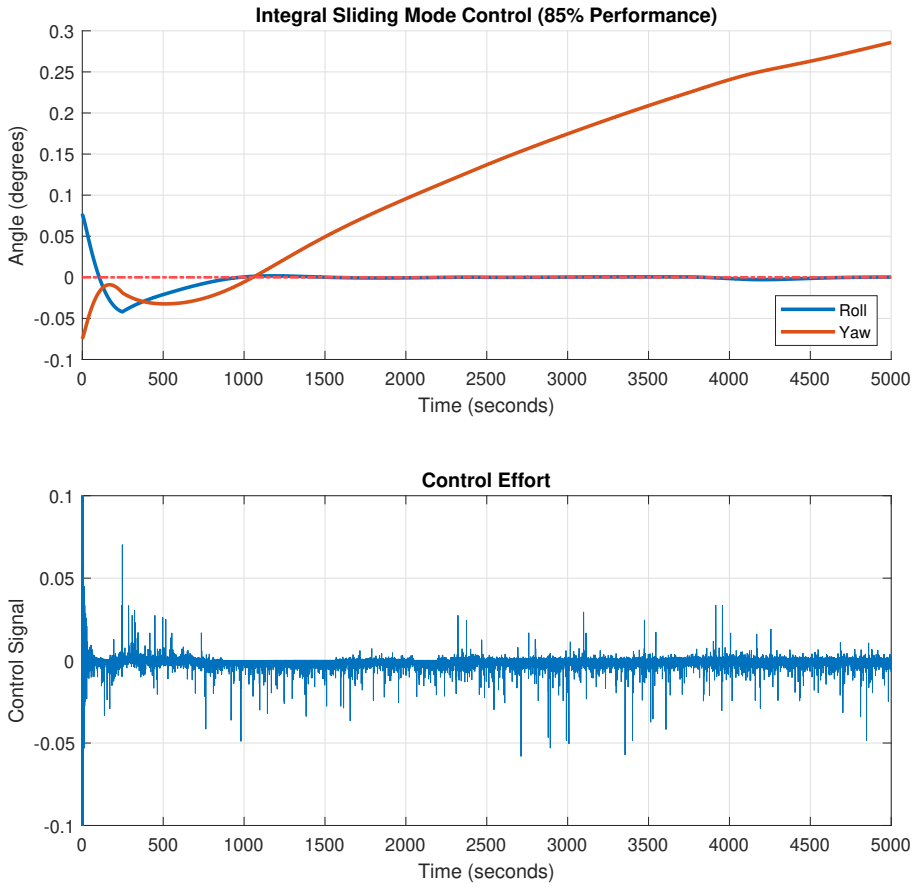

Figure 6.13 Integral sliding mode control with 15% performance loss in thrusters

6.2.3. Discussion of Results

Table 6.5 elucidates the comparative performance of the Integral Plus State Variable Feedback Control and the Integral Sliding Mode Control under both nominal and reduced thruster efficiency conditions. This analysis highlights the relative changes in performance metrics due to a 15% loss in thruster efficiency and compares the resilience of each control method.

Control Method	Duration of Roll Reaching 0°	Roll Maximum	Roll Max Deviation	Yaw Maximum
State Feedback (85%)	1142 s	-0.068°	0.029°	-0.15°
State Feedback (100%)	1540 s	-0.11°	0.025°	-0.30°
Integral Sliding Mode (85%)	980 s	-0.041°	0.0001°	-0.03°
Integral Sliding Mode (100%)	2000 s	-0.08°	0.002°	-0.13°

Table 6.5 15% performance loss effect on controller comparison

With a 15% performance loss, the Integral Plus State Variable Feedback Control demonstrates a notable improvement in response time for aligning the roll axis to 0°, achieving this approximately 26% faster than under full performance conditions. This suggests that the controller might be compensating more dynamically when faced with reduced thruster efficiency. Conversely, the maximum roll deviation increases by approximately 16%, but the maximum yaw deviation improved by 100%.

Conversely, under conditions of reduced thruster performance, the Integral Sliding Mode Control shows a substantial increase in response efficiency. It aligns the roll axis to 0° more than twice as fast, with a decrease in response time by approximately 68.4%. This responsiveness indicates a heightened sensitivity to thruster performance, accompanied by a significant reduction in roll deviation by 180.9%. Additionally, the yaw deviation is reduced by 125%, demonstrating ISMC's enhanced control capabilities under compromised conditions.

Comparing both controllers under performance loss conditions, the Integral Plus State Variable Feedback Control adjusts more quickly to changes, albeit at the expense of increased deviations which may impact operational stability. The Integral Sliding Mode Control, while slower in adverse conditions, maintains a closer adherence to its target deviations, suggesting better overall control stability but with significantly increased response times.

The comparative evaluation of control effort required by each method under both nominal and reduced performance conditions is detailed in Table 6.6. This analysis offers insights

into the operational efficiency of the controllers in terms of energy expenditure.

Control Method	Control Effort
State Feedback (85%)	404.30
State Feedback (100%)	322.78
Integral Sliding Mode (85%)	916.48
Integral Sliding Mode (100%)	644.31

Table 6.6 15% performance loss effect on control effort comparison

For the Integral Plus State Variable Feedback Control, a 15% reduction in thruster performance leads to a 25% increase in control effort, rising from 322.78 under full performance to 404.30. This increase suggests that compensating for the reduced performance of the thrusters demands significantly more energy, likely due to the controller needing to work harder to achieve similar control outcomes.

Conversely, the Integral Sliding Mode Control shows a 42% increase in control effort under reduced performance conditions, escalating from 644.31 to 916.48. This substantial rise in control effort highlights the controller's higher sensitivity to thruster performance, as it utilizes more energy to maintain control precision and stability despite reduced thruster efficacy.

6.3. Total Loss of a Thruster

In satellite operations, the complete failure of a thruster represents a critical test of the system's resilience and fault tolerance. This section delves into the implications and management of such a scenario, focusing on the total loss of Thruster 5A, a key component in the satellite's attitude control system. This failure is particularly challenging, as it requires immediate and effective intervention by the Fault Detection, Isolation, and Recovery (FDIR) system to ensure continued operational stability and safety.

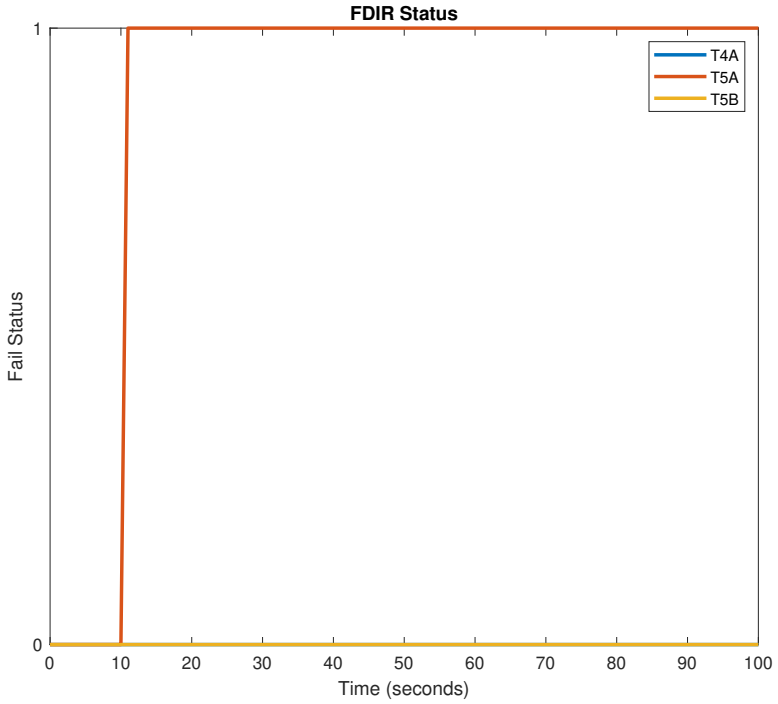

Figure 6.14 FDIR status for the total loss of thruster case

Upon detecting the malfunction of Thruster 5A, the FDIR system promptly takes corrective action. It deactivates the failed thruster and activates Thruster 4A to compensate for the loss, effectively reconfiguring the control strategy to maintain control authority. The operational dynamics and efficacy of this adaptive response can be visualized in Figure 6.14, which illustrates the FDIR system's real-time response to the thruster failure.

The scenario is evaluated under an initial condition of a 0.1° error in both roll and yaw, chosen to simulate a severe yet plausible worst-case situation. This setup tests the system's ability to handle significant disturbances and assesses the robustness of the alternative control measures implemented by the FDIR system. The analysis aims to highlight the critical capabilities of satellite control systems in maintaining functionality and stability, even under extreme conditions where a primary control element fails completely.

6.3.1. Integral Plus State Variable Feedback Control Results

In the scenario of a total loss of Thruster 5A, the performance of the Integral Plus State Variable Feedback Control is critically analyzed. The system's response, depicted in Figure 6.15, illustrates the effectiveness and adaptability of this control strategy under severe constraints.

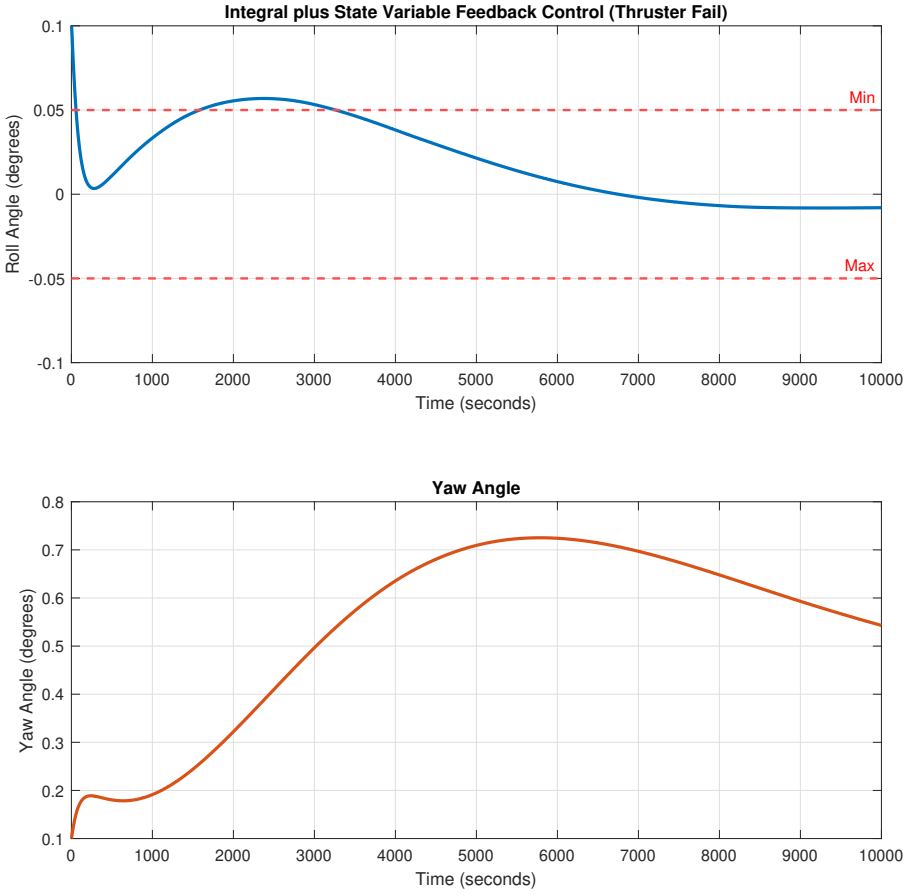

Figure 6.15 Integral plus state variable feedback control with total loss of thruster 5A

Upon the complete failure of Thruster 5A, the FDIR system's activation of Thruster 4A challenged the Integral Plus State Variable Feedback Control to maintain satellite orientation. The system took approximately 6745 seconds to realign the roll axis to a zero-degree

orientation, reflecting a significant delay compared to normal operational scenarios. This delay is indicative of the system's strain under the loss of a primary control element but also demonstrates its capability to eventually achieve stabilization.

The maximum deviation recorded in the roll axis was a modest 0.056 degrees, with a steady-state error of just 0.008 degrees. This level of precision under such adverse conditions underscores the control system's robust design and tuning. In the yaw axis, the maximum deviation reached 0.72 degrees, a relatively higher deviation which highlights the increased difficulty in controlling yaw without Thruster 5A.

The control effort required to manage these angles under total thruster loss was quantified at 487.90. This figure represents an increase in the usual operational demand placed on the system, reflecting the additional energy and resources needed to compensate for the failed thruster.

6.3.2. Integral Sliding Mode Control Results

Following the total loss of Thruster 5A, the performance of the Integral Sliding Mode Control is rigorously evaluated to assess its efficacy in managing the satellite's stability and orientation under extreme conditions. The findings, illustrated in Figure 6.16, offer a detailed insight into the robustness of this control method when faced with the worst-case scenario of a critical thruster failure.

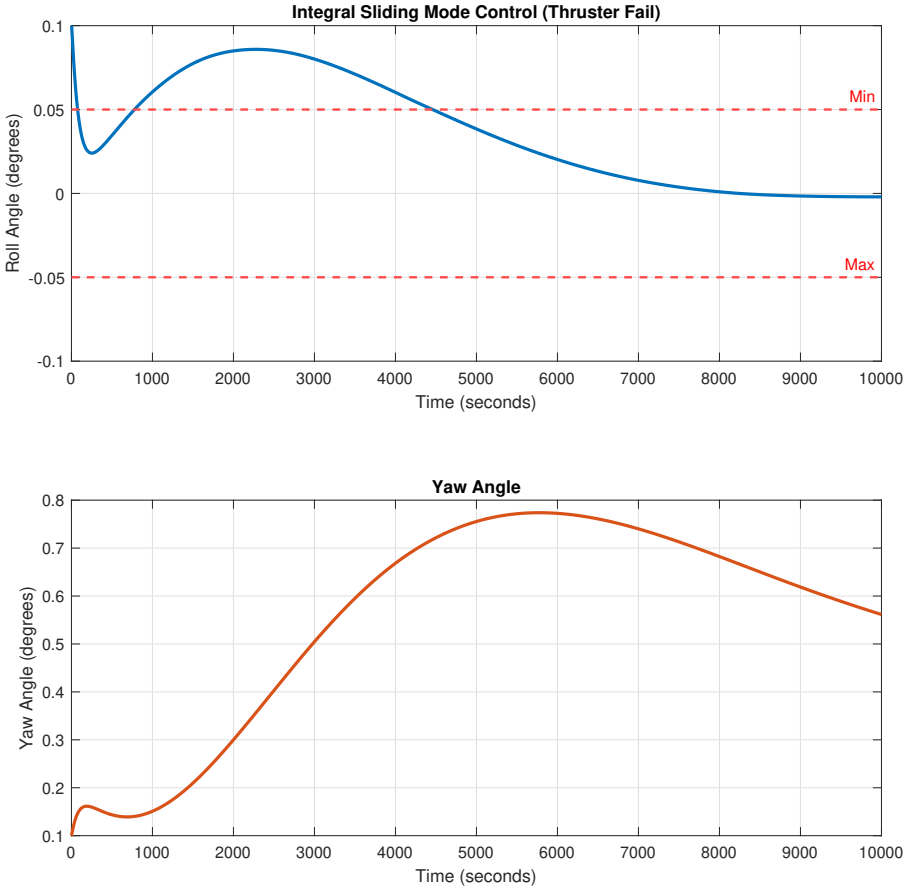

Figure 6.16 Integral sliding mode control with total loss of thruster 5A

In response to the complete failure and subsequent deactivation of Thruster 5A, and the activation of Thruster 4A by the FDIR system, the Integral Sliding Mode Control required a prolonged duration of 8205 seconds to adjust the roll axis back to a zero-degree orientation. This duration, considerably longer than typical operations, highlights the challenges posed by the absence of a key thruster, testing the control system's limits in maintaining effective satellite control.

Despite these challenges, the control strategy managed to maintain a commendably low maximum deviation in roll at only 0.085 degrees and an even lower steady-state error of 0.002 degrees. These values demonstrate the control's precision in achieving and maintaining the desired orientation, reflecting its inherent robustness and precision.

In the yaw axis, the maximum deviation slightly increased to 0.77 degrees, illustrating a modest struggle in managing yaw movements without the support of Thruster 5A. This deviation, although small, suggests that controlling yaw is inherently more challenging under thruster loss conditions.

The control effort expended to manage these angles post-thruster loss was recorded at 525.72. This increased control effort compared to typical conditions signifies the additional resources required to stabilize the satellite in the absence of Thruster 5A.

6.3.3. Discussion of Results

In this section, the results from the Integral Plus State Variable Feedback Control and the Integral Sliding Mode Control are compared under the challenging conditions of total thruster loss, as detailed in Table 6.7. This comparison aims to highlight the differences in their performance efficiencies and robustness in severe scenarios.

Control Method	Duration of Roll Reaching 0°	Roll Maximum	Roll Max Deviation	Yaw Maximum
State Feedback (Total Loss)	6745 s	0.056°	0.008°	0.72°
Integral Sliding Mode (Total Loss)	8205 s	0.085°	0.002°	0.77°

Table 6.7 Integral plus state variable feedback control results in worst-case condition

The Integral Sliding Mode Control took longer to stabilize the roll axis to zero degrees compared to the State Variable Feedback Control, with a relative increase of approximately 22%. This indicates that while the Integral Sliding Mode Control is precise, it may require more time to adjust in scenarios of extreme hardware failure.

In terms of deviation, the Integral Sliding Mode Control demonstrated a substantially lower steady-state error in roll, reducing it by 75%, which showcases its superior precision in maintaining the desired orientation despite a slower response time. Additionally, the maximum roll deviation was 120% lower, highlighting its robust control capabilities.

However, the maximum yaw deviation under ISMC was slightly higher, increasing by about 7%, indicating a trade-off in the control dynamics between the roll and yaw axes.

Control Method	Control Effort
State Feedback (Total Loss)	487.90
Integral Sliding Mode (Total Loss)	525.72

Table 6.8 Control effort results in worst-case condition

Examining the control effort in Table 6.8, the Integral Sliding Mode Control required approximately 7.7% more effort than the State Variable Feedback Control. This increase reflects the additional resources needed by the Integral Sliding Mode Control to maintain precision under the constraints of a failed thruster.

6.4. Comparison of Results

The research primarily focuses on the roll/yaw control system of the satellite, particularly emphasizing the roll control dynamics. Given that the yaw angle is passively controlled, the detailed comparative analysis concentrates on the roll axis, examining various initial error cases ranging from 0.075 degrees to 0.1 degrees. This spectrum of scenarios allows us to thoroughly evaluate the resilience and efficacy of two control systems—Integral Plus State Variable Feedback Control and Integral Sliding Mode Control—under different stress conditions including normal operational conditions, scenarios with induced performance degradation in thrusters, and critical conditions involving the total loss of a thruster. Each test provides invaluable insights into the robustness, adaptability, and efficiency of the respective control strategies, offering a clear perspective on their suitability for real-world satellite operations.

Figure 6.17 for the case with a 0.075° error in roll demonstrates that the Integral Sliding Mode Control achieves a 27.3% reduction in maximum roll and exhibits 92% improvement in maximum deviations compared to Integral Plus State Variable Feedback Control. However,

this performance advantage comes at a cost, with ISMC requiring nearly double the control effort. Detailed results regarding the performance metrics are provided in Table 6.2 and Table 6.3, illustrating the specific numerical comparisons between Integral Sliding Mode Control and Integral Plus State Variable Feedback Control across various parameters.

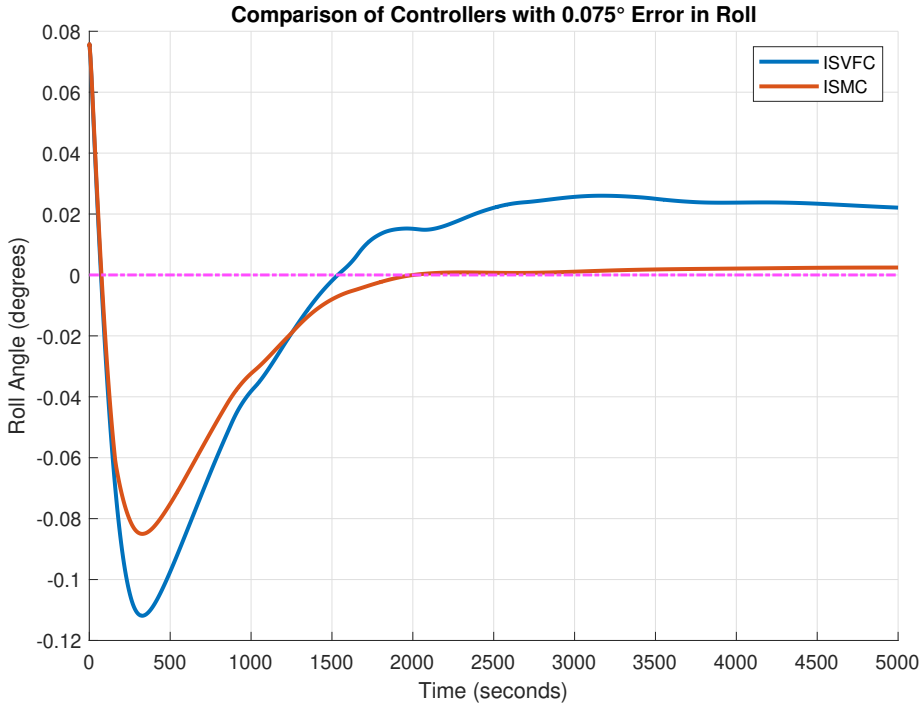

Figure 6.17 Comparison of controllers in roll axis with 0.075° error in roll

Examining Figure 6.18 for the case with a -0.075° error in roll, it is observed that the Integral Sliding Mode Control not only reduces the maximum roll by 2.6% but also enhances the maximum deviations by 55.5% compared to Integral Plus State Variable Feedback Control. Additionally, ISMC achieves these improvements with 25.5% less control effort.

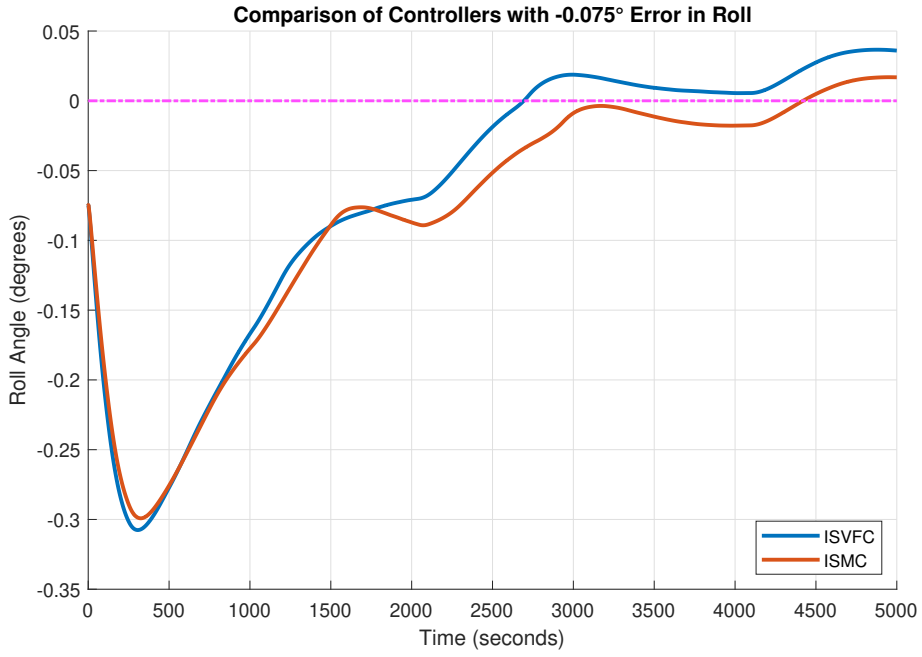

Figure 6.18 Comparison of controllers in roll axis with -0.075° error in roll

Overall, the Integral Sliding Mode Control consistently reduces the maximum roll angle and deviations from the reference across all tested cases. In several instances, ISMC also requires less control effort, further enhancing its appeal as an efficient control solution.

Upon examining Figure 6.19, depicting the stability evaluation over a 24-hour period, it becomes evident that Integral Sliding Mode Control adeptly manages initial deviations. Moreover, upon reaching the desired position, it smoothly transitions to an optimal controller. In this instance, the optimal controller utilized is the same as that used in Integral Plus State Variable Feedback Control, resulting in comparable long-term performance. This setup allows for a direct assessment of the benefits attributable solely to the Integral Sliding Mode Control. Notably, the issue of chattering begins to manifest after 22 hours, highlighting a potential area for further optimization in the ISMC approach.

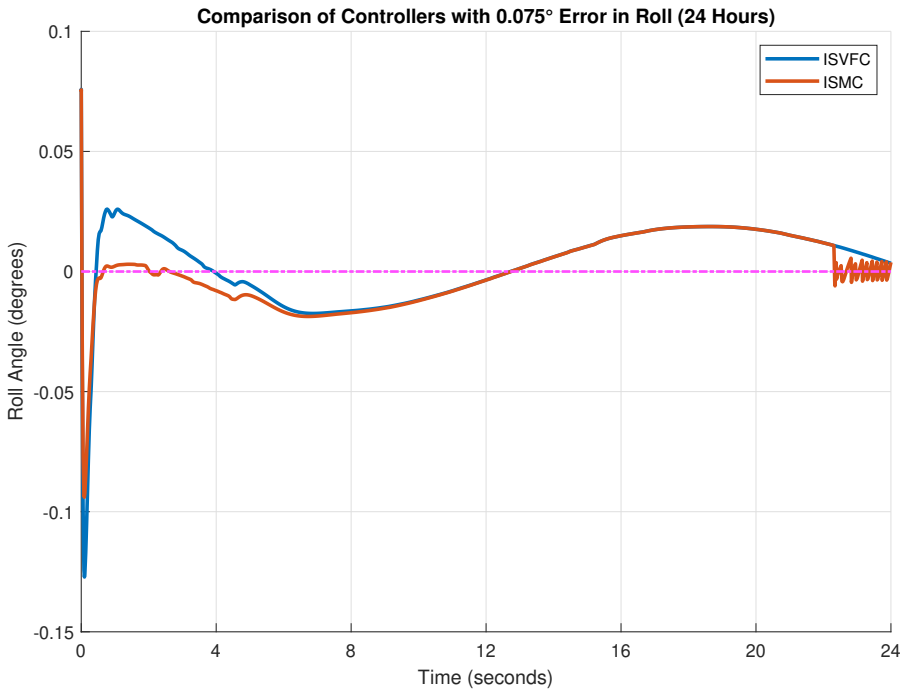

Figure 6.19 Comparison of controllers in roll axis with 0.075° error in roll (24 hours)

The impact of various control methods on the yaw angle is illustrated in Figure 6.20. Initially, there are fewer deviations during the first oscillations, although a higher peak value follows. Subsequent behavior remains consistent, attributed to the controller design as previously explained. This demonstrates the tailored response dynamics engineered into the control strategy.

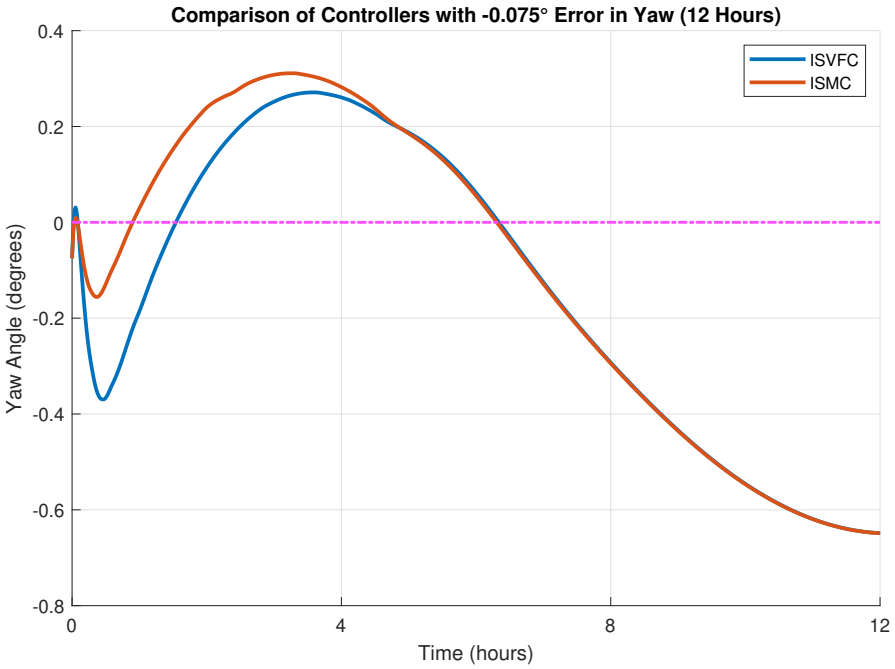

Figure 6.20 Comparison of controllers in roll axis with -0.075° error in yaw (12 hours)

To evaluate the stability of the controllers under stress, a 15% performance degradation was simulated in the thrusters, with the outcomes depicted in Figure 6.21. The Integral Plus State Variable Feedback Control exhibited 198.6% higher maximum deviations and a 49.5% increased maximum roll angle compared to ISMC. However, it was able to align to 0° 15.3% more quickly. Additionally, ISVFC required 77.5% less control effort, reflecting a looser control strategy under these conditions. Detailed results are provided in Table 6.5 and Table 6.6.

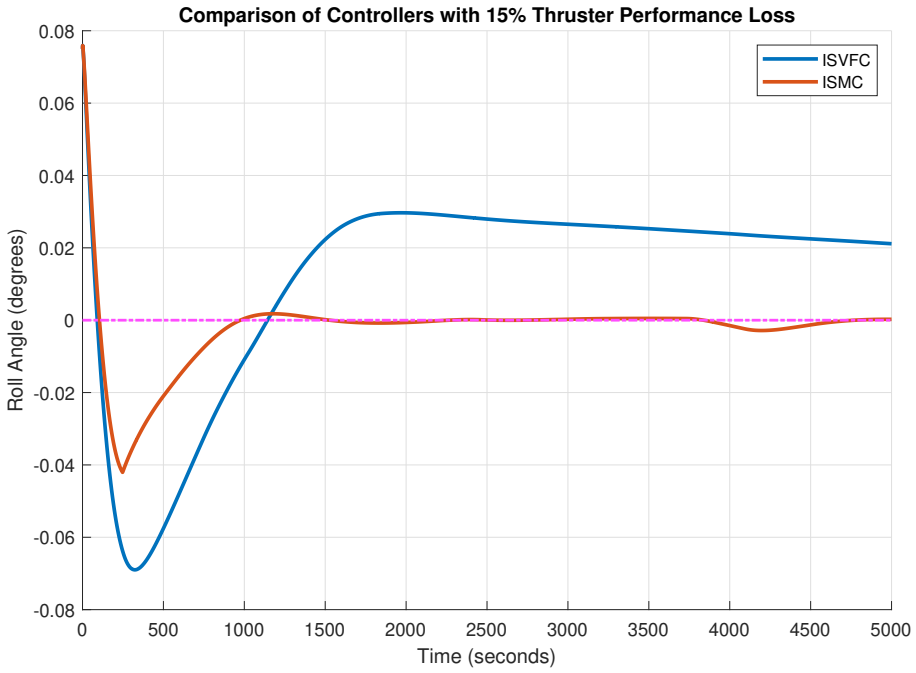

Figure 6.21 Comparison of controllers in roll axis with 15% thruster performance loss

For the ultimate endurance test, the total loss of Thruster 5A was simulated, accompanied by an extreme error of 0.1°. The results, displayed in Figure 6.22, reveal that the Integral Sliding Mode Control took 22% longer to reach a 0° alignment but achieved a remarkable 75% reduction in overall deviation. Additionally, the maximum deviation in roll was 120% lower, significantly underscoring ISMC's superior precision and stability in handling severe disruptions. In terms of deviation, ISMC demonstrated a substantially lower steady-state error in roll, reduced by 75%, which showcases its exceptional precision in maintaining the desired orientation despite a slower response time. Furthermore, the maximum roll deviation was 120% lower, highlighting its robust control capabilities. However, achieving these enhanced performance metrics requires 7.7% more control effort, reflecting the increased resources necessary to manage such critical situations effectively. Detailed results are provided in Table 6.7 and Table 6.8.

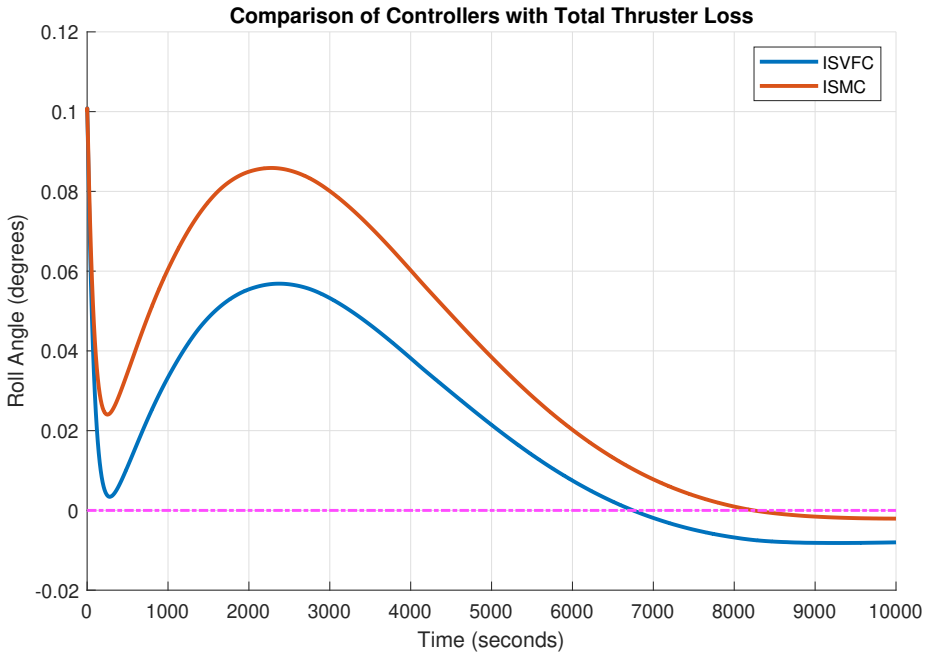

Figure 6.22 Comparison of controllers in roll axis with total loss of thruster 5A

6.5. Conclusion

The comprehensive evaluation of satellite control systems through nonlinear simulation across multiple scenarios has revealed critical insights into the robustness, adaptability, and efficiency of the Integral Plus State Variable Feedback Control and Integral Sliding Mode Control systems. The study systematically examined these controls under nominal conditions, with induced performance degradations, and in extreme cases involving total thruster loss.

Under nominal conditions, both control systems effectively managed the roll and yaw axes within stringent tolerances. The Integral Sliding Mode Control exhibited superior precision in maintaining close to zero steady-state errors and minimized maximum deviations, indicating its robustness in dynamic response and stability management. In scenarios involving performance degradation and total thruster loss, the Integral Sliding Mode Control demonstrated notable adaptability by maintaining performance with minimal deviation and

consistent control effort, thereby underscoring its suitability for critical mission scenarios where reliability is paramount.

The Integral Plus State Variable Feedback Control, while generally requiring less control effort under nominal conditions, showed increased sensitivity under stress scenarios, particularly in the presence of performance degradation. This sensitivity was evident from its quicker response times but at the cost of larger deviations, suggesting a potential trade-off between speed and precision. Conversely, the Integral Sliding Mode Control maintained tighter control over deviations and exhibited a robust response even when thruster performance was compromised, highlighting its potential for applications requiring high reliability and precision under varying operational conditions.

The analysis of control effort revealed that while the Integral Sliding Mode Control often required more energy and resources, particularly in scenarios of extreme conditions, its ability to maintain precision and stability justifies the additional expenditure, particularly for missions where failure costs are high. The increased control effort in scenarios of thruster degradation and total loss within the Integral Sliding Mode Control emphasizes the importance of optimizing control strategies to balance performance with energy efficiency, especially for long-duration missions.

These findings highlight the importance of selecting a control system that not only meets the basic operational requirements but also aligns with the specific mission profiles and expected environmental conditions. The resilience of the Integral Sliding Mode Control system makes it a suitable candidate for missions that might encounter unpredictable conditions or require exceptionally high reliability. The ability of the Integral Plus State Variable Feedback Control to quickly adapt to reduced thruster performance with minimal impact on control precision suggests its utility in environments where thruster wear could be anticipated, allowing for efficient mission management.

7. CONCLUSION

This thesis introduced a novel fault-tolerant sliding mode control designed specifically for a geostationary communication satellite utilizing chemical propulsion. The methodology proposed in this study was tailored to enhance the operational robustness and fault resilience of the satellite. The dynamical model of the satellite and the actuator models employed in this research closely mirrored those utilized in the TÜRKSAT 1B satellite, ensuring a realistic and applicable foundation for the investigation. By aligning with the dynamics of an existing satellite, the study not only leveraged real-world relevance but also facilitated a more accurate evaluation of the fault-tolerant Integral Sliding Mode Control's performance in practical scenarios. This tailored approach laid the groundwork for a comprehensive exploration of control strategies within the specific context of geostationary communication satellites with chemical propulsion.

The study began with a thorough review of sliding-mode approaches in satellite control, exploring various applications with different actuators. This set the stage for introducing innovative fault-tolerant strategies. Following this, the satellite model based on TÜRKSAT 1B parameters was outlined, providing a practical foundation for the proposed sliding mode control methodology. This approach ensured a comprehensive exploration, seamlessly integrating theoretical foundations with practical considerations in the discourse on satellite control methodologies.

The effects of solar radiation pressure and gravity gradient perturbations were accounted for in the Simulink model. Pitch control was achieved with a strap-down momentum wheel, while roll and yaw control were accomplished with thrusters. Yaw motion was not actively managed, allowing for a higher bias in regulation as long as the total yaw attitude did not exceed 10 degrees to maintain valid linearization. For thruster sampling and activation period selection, different proposed values in the literature were evaluated and selected. The thruster model and the momentum wheel model were integrated into the satellite model, along with uncertainties and additional perturbations.

The design of Integral Sliding Mode Control involved a systematic process aimed at ensuring robust performance despite system uncertainties and faults. Initially, the system was modeled and potential faults were identified through a comprehensive analysis of the system's dynamics and potential failure modes. Subsequently, an Integral Sliding Mode Control strategy was developed to ensure stability and robustness. This strategy encompassed the definition of sliding surfaces and the design of control laws. To enhance fault tolerance, fault detection and isolation mechanisms were augmented within the controller. These mechanisms enabled the system to identify and compensate for faults in real-time.

For the comparison of the proposed Integral Sliding Mode Control, an Integral Plus State Variable Feedback Control system was specifically designed for roll and yaw control, while pitch control was regulated using a PD controller to maintain consistency. This deliberate approach facilitated an effective comparison of different control methods. By isolating roll and yaw control and keeping pitch control constant, the study was structured to reveal specific strengths and weaknesses of the Integral Sliding Mode Control in contrast to other strategies.

Both controllers were rigorously tested across three scenarios: normal operating conditions, thrust performance degradation, and total loss of a single thruster. This thorough analysis aided in evaluating their effectiveness and robustness under varied conditions. Notably, the Integral Sliding Mode Control exhibited superior pointing accuracy on the roll axis with very low deviations. In scenarios of performance degradation and total thruster loss, it demonstrated remarkable adaptability, maintaining performance with minimal deviation and consistent control effort, albeit at the cost of increased control effort in several instances. Although pointing accuracy requirements had not been challenging to date, emerging technologies such as inter-satellite links and higher frequency bands with smaller beam footprints on Earth are set to increase these demands annually. Therefore, exploring newer control methods and performing trade-offs before these more stringent requirements become prevalent was crucial.

Given the harsh space conditions and long operational life without maintenance, high reliability and robustness in satellite design are crucial. Satellites must withstand extreme environments to ensure continuous service and protect substantial investments. High-reliability control methods, such as Integral Sliding Mode Control, are essential for maintaining performance. Extending a satellite's operational life enhances financial viability, maximizing revenue and enabling profits beyond cost recovery. This additional income can be reinvested in new projects, fostering innovation. Thus, reliability and robustness are key to reducing risks and ensuring long-term financial and operational success.

For future work, the optimization of the sliding surface is planned to further enhance control performance. Addressing the chattering problem inherent in sliding mode controls remains a priority, with ongoing research aimed at mitigating this issue. Additionally, exploring different control methods will be crucial for improving overall system robustness and efficiency. Future research will involve assessing various strategies to refine the control approach and achieve superior performance metrics.

8. REFERENCES

[1] *SCC/SCC-BU Operations Handbook*. Aerospatiale Espace and Defence, **1993**.

[2] Hakkı Özgür Derman. *3-Axis Attitude Control of a Geostationary Satellite*. M.S Thesis in Aeronautical Engineering, Middle East Technical University, Ankara, **1999**.

[3] Thomas G. Roberts. Popular orbits 101. https://aerospace.csis.org/aerospace101/earth-orbit-101, **2022**. Accessed: 25.03.2024.

[4] Jeff Foust. Kepler space telescope reaction wheel remains a concern. https://spacenews.com/34692kepler-space-telescope-reaction-wheel-remains/-a-concern/, **2013**. Accessed: 25.03.2024.

[5] Joseph Banks. Chemical propulsion systems. https://www1.grc.nasa.gov/research-and-engineering/chemical-propulsion-systems/, **2023**. Accessed: 25.03.2024.

[6] Opinion Writers. Testing ion thrusters for space exploration. https://www.aerospacetestinginternational.com/features/testing-ion-thrusters-for-space-exploration.html#prettyPhoto, **2019**. Accessed: 25.03.2024.

[7] Hywel. Magnetorquers available on the global marketplace. https://blog.satsearch.co/2019-08-21-magnetorquers-an-overview-of-magnetic/-torquer-products-available-on-the-global-marketplace/-for-space, **2024**. Accessed: 25.03.2024.

[8] Brent Prokosh. Fss capacity pricing and supply dynamics in mobility markets. https://www.msua.org/single-post/2020/01/20/

FSS-Capacity-Pricing-and-Supply-Dynamics-in-Mobility-Markets, **2020**. Accessed: 02.05.2024.

[9] Qinglei Hu. Robust adaptive sliding-mode fault-tolerant control with l2-gain performance for flexible spacecraft using redundant reaction wheels. *IET Control Theory and Applications*, 4:1055–1070, **2010**. ISSN 17518644. doi:10.1049/IET-CTA.2009.0140/CITE/REFWORKS.

[10] Teng Cao, Huajun Gong, and Bing Han. Sliding mode fault tolerant attitude control scheme for spacecraft with actuator faults. *Transactions of Nanjing University of Aeronautics & Astronautics*, 36:124–132, **2019**. ISSN 1005-1120. doi:10.16356/J.1005-1120.2019.01.011.

[11] Özge Uslu. *Orbit Dynamics, Attitude Dynamics and Control Investigation into Possible Applications to TÜRKSAT*. M.S Thesis in Aeronautical Engineering, Middle East Technical University, Ankara, **1997**.

[12] Karla Raigoza and Timothy Sands. Autonomous trajectory generation comparison for de-orbiting with multiple collision avoidance. *Sensors*, 22:7066, **2022**. doi:10.3390/s22187066.

[13] Katsuhiko Ogata. *Modern Control Engineering*. Prentice Hall, **2010**.

[14] George Kopsakis. Feedback control systems loop shaping design with practical considerations. http://www.sti.nasa.gov, **2007**. Accessed: 02.05.2024.

[15] Mike Ruth, Ken Lebsock, and Cornelius Dennehy. What's new is what's old: Use of bode's integral theorem (circa 1945) to provide insight for 21st century spacecraft attitude control system design tuning. *AIAA Guidance, Navigation, and Control Conference*, **2010**. doi:10.2514/6.2010-8428.

[16] Yoshiro Hamada, Takashi Ohtani, Takashi Kida, and Tomoyuki Nagashio. Gain scheduling controller design for engineering test satellite-viii. *IFAC Proceedings Volumes*, 40:591–596, **2007**. ISSN 1474-6670. doi:10.3182/20070625-5-FR-2916.00101.

[17] Alexandre Falcoz, Christelle Pittet, Samir Bennani, Anne Guignard, Cedric Bayart, and Benoit Frapard. Systematic design methods of robust and structured controllers for satellites: Application to the refinement of rosetta's orbit controller. *CEAS Space Journal*, 7:319–334, **2015**. ISSN 18682510. doi:10.1007/S12567-015-0099-8/FIGURES/29.

[18] Liming Fan, Yanjun Xing, Zongbo He, Qiang Zhang, and Zeming Chen. Robust attitude control of a flexible satellite assembled with a partially expanded coilable mast. *Aerospace Science and Technology*, 148:109093, **2024**. ISSN 1270-9638. doi:10.1016/J.AST.2024.109093.

[19] Himanshu Prabhat, Bijoy K. Mukherjee, Dipak Kumar Giri, and Manoranjan Sinha. Fault-tolerant sliding mode satellite attitude stabilization using magneto-coulombic torquers. *Aerospace Science and Technology*, 121:107316, **2022**. ISSN 1270-9638. doi:10.1016/J.AST.2021.107316.

[20] Jaehyun Jin, Sangho Ko, and Chang Kyung Ryoo. Fault tolerant control for satellites with four reaction wheels. *Control Engineering Practice*, 16:1250–1258, **2008**. ISSN 09670661. doi:10.1016/J.CONENGPRAC.2008.02.001.

[21] Jovan D. Boskovic, Sai Ming Li, and Raman K. Mehra. Fault tolerant control of spacecraft in the presence of sensor bias. *Proceedings of the American Control Conference*, 2:1205–1209, **2000**. ISSN 07431619. doi:10.1109/ACC.2000.876691.

[22] Halim Alwi and Christopher Edwards. Fault tolerant control using sliding modes with on-line control allocation. *Automatica*, 44:1859–1866, **2008**. ISSN 0005-1098. doi:10.1016/J.AUTOMATICA.2007.10.034.

[23] Qiang Shen, Danwei Wang, Senqiang Zhu, and Eng Kee Poh. Integral-type sliding mode fault-tolerant control for attitude stabilization of spacecraft. *IEEE*

Transactions on Control Systems Technology, 23, **2015**. doi:10.1109/TCST.2014.2354260.

[24] Bing Xiao, Qinglei Hu, and Youmin Zhang. Fault-tolerant attitude control for flexible spacecraft without angular velocity magnitude measurement. *Journal of Guidance, Control, and Dynamics*, 34:1556–1561, **2012**. ISSN 15333884. doi:10.2514/1.51148.

[25] Duan Wenjie, Wang Dayi, and Liu Chengrui. Integral sliding mode fault-tolerant control for spacecraft with uncertainties and saturation. *Asian Journal of Control*, 19:372–381, **2017**. doi:10.1002/asjc.1365.

[26] Bing Xiao, Qinglei Hu, and Youmin Zhang. Adaptive sliding mode fault tolerant attitude tracking control for flexible spacecraft under actuator saturation. *IEEE Transactions on Control Systems Technology*, 20:1605, **2012**. doi:10.1109/TCST.2011.2169796.

[27] Bing Xiao, Qinglei Hu, and Michael I. Friswell. Active fault-tolerant attitude control for flexible spacecraft with loss of actuator effectiveness. *International Journal of Adaptive Control and Signal Processing*, 27:925–943, **2013**. ISSN 08906327. doi:10.1002/ACS.2363.

[28] Wen Chen and Mehrdad Saif. Observer-based fault diagnosis of satellite systems subject to time-varying thruster faults. *Journal of Dynamic Systems, Measurement, and Control*, 129:352–356, **2007**. ISSN 0022-0434. doi:10.1115/1.2719773.

[29] Ganesh B. Maganti and Sahjendra N. Singh. Simplified adaptive control of an orbiting flexible spacecraft. *Acta Astronautica*, 61:575–589, **2007**. ISSN 0094-5765. doi:10.1016/J.ACTAASTRO.2007.02.004.

[30] Vladimir A. Chobotov. *Spacecraft Attitude Dynamics and Control*. Krieger Publishing Co., Florida, **1991**.

[31] *Türksat Engineering Training Documents*. Aerospatiale Espace and Defence, **1993**.

[32] JR. A. E. Bryson. *Control of Spacecraft and Aircraft*. Princeton University Press, Princeton, New Jersey, USA, **1994**.

[33] J. R. Wertz. *Spacecraft Attitude Dynamics and Control*. D. Reidel Publishing Co., **1985**.

[34] Mirza Tariq Hamayun, Christopher Edwards, and Halim Alwi. *Fault Tolerant Control Schemes Using Integral Sliding Modes*, volume 61. Springer International Publishing, **2016**. ISBN 978-3-319-32236-0. doi:10.1007/978-3-319-32238-4.

[35] Vadim I. Utkin. *Sliding Modes in Control and Optimization*. Springer Berlin Heidelberg, **1992**. doi:10.1007/978-3-642-84379-2.

9. APPENDICES

9.1. Appendix 1 - Satellite Parameters

Phase	Event	Mass [kg]
Launch	All appendages stowed	1783.678
B.O.T	Solar array partially & Reflector deployed	1783.678
E.O.T	Solar array partially & Reflector deployed	1082.578
B.O.L	Solar array & Reflector deployed	1082.578
E.O.L	Solar array & Reflector deployed	835.898

Table 9.1 Mass evolution during different phases [1]

Thruster	X	Y	Z
4A	11.3193	-4.5E-05	1.3367
4B	-10.0034	-2.7E-05	3.9644
5A	10.2156	4.12E-05	6.1057
5B	-11.0438	-1.9E-05	-1.0992

Table 9.2 Roll Thruster Net Torque Components (Nm) [2]

The physical parameters of the momentum wheel are [2]:

- **Armature inductance (L_a):** 0.005 H
- **Torque constant (K_i):** 0.3 Nm/A
- **Back EMF constant (K_b):** 0.3 V/rad/s
- **Viscous-friction coefficient (B_m):** 0.002
- **Total inertia of motor (J_w):** 0.12456 kg m^2 (including rotor and wheel)
- **Armature resistance (R_a):** 5 Ω

9.2. Appendix 2 - Simulink Blocks

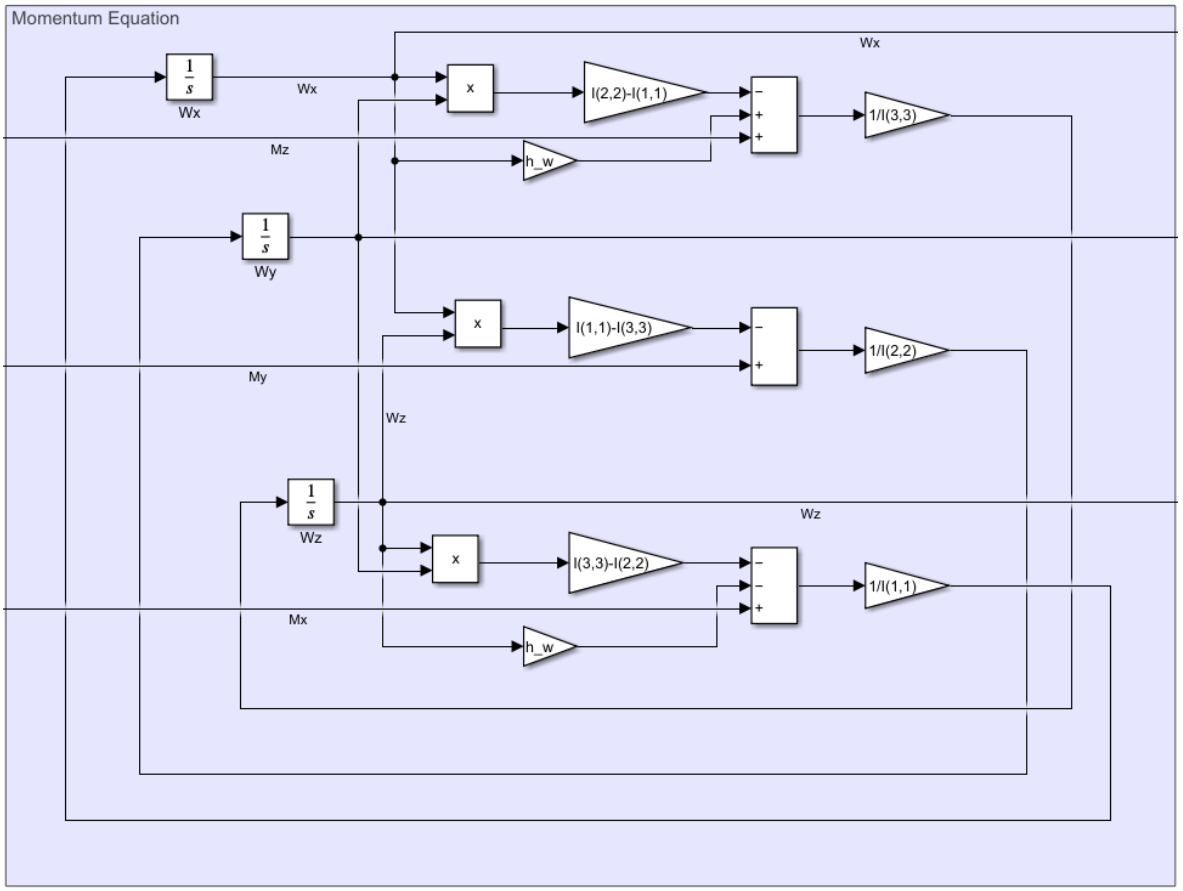

Figure 9.1 Moment equations modeled in Simulink

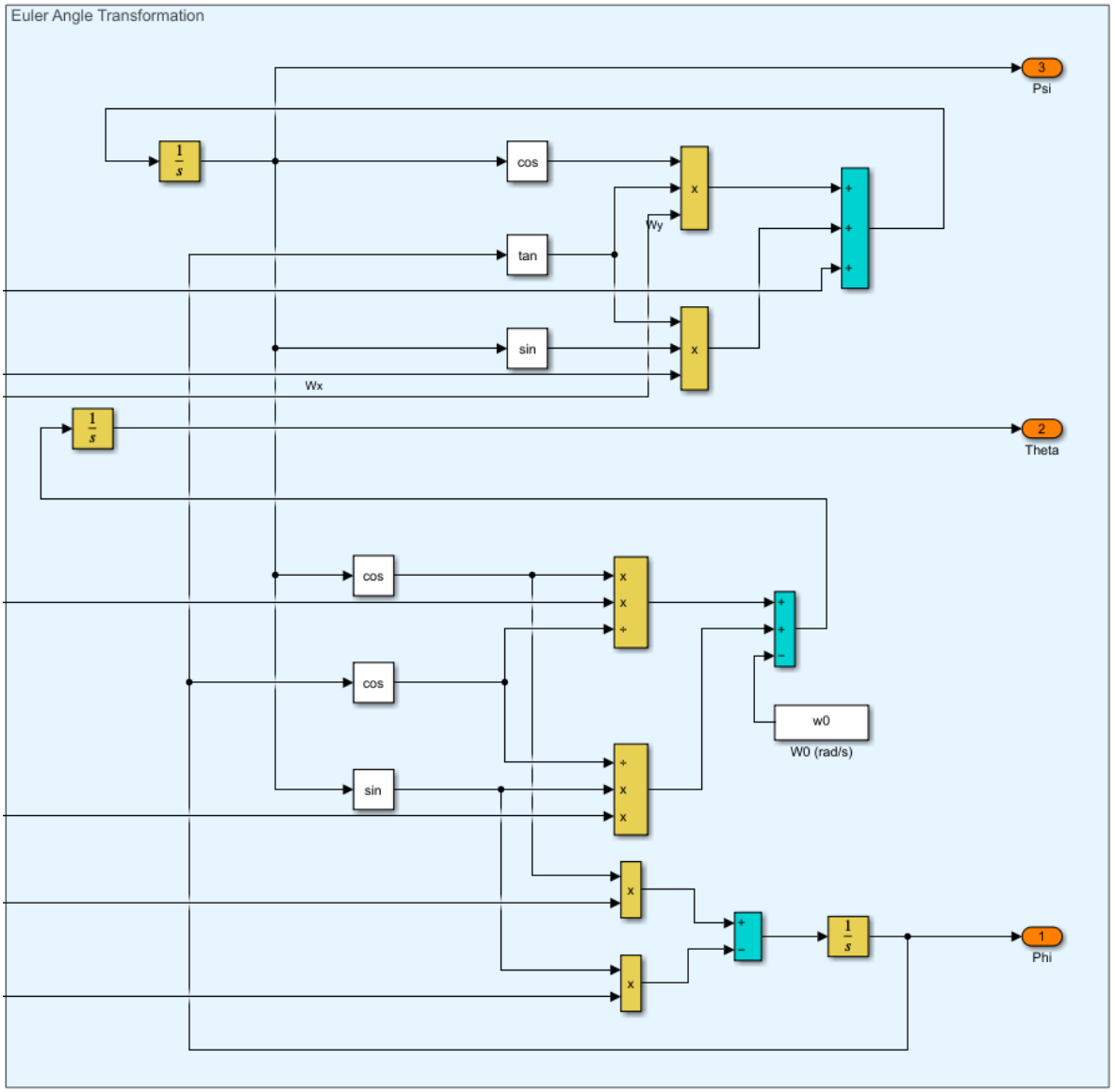

Figure 9.2 Euler angle transformation in Simulink

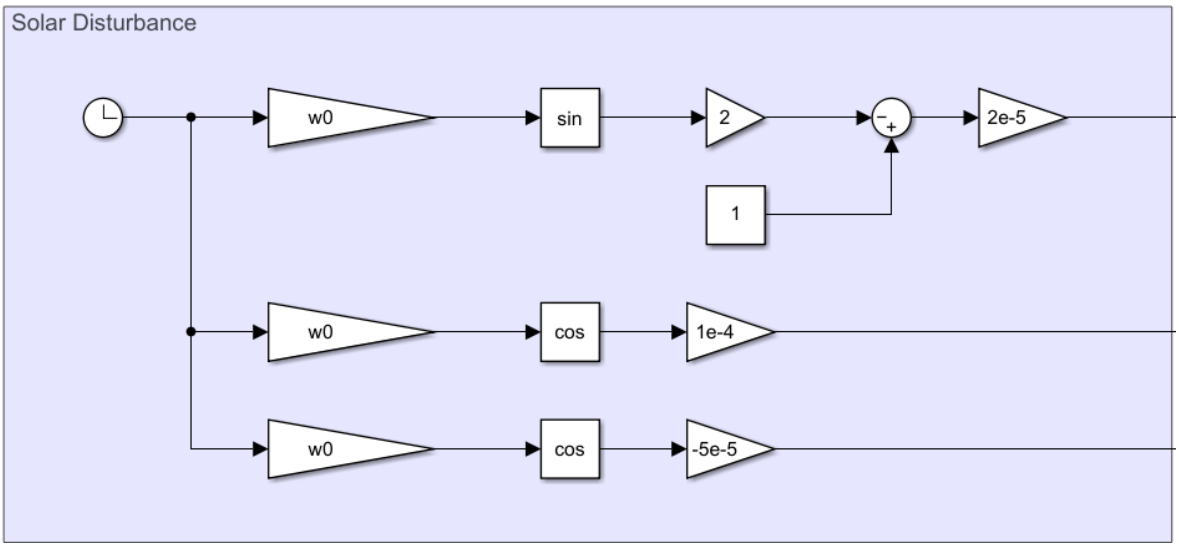

Figure 9.3 Solar radiation pressure model in Simulink

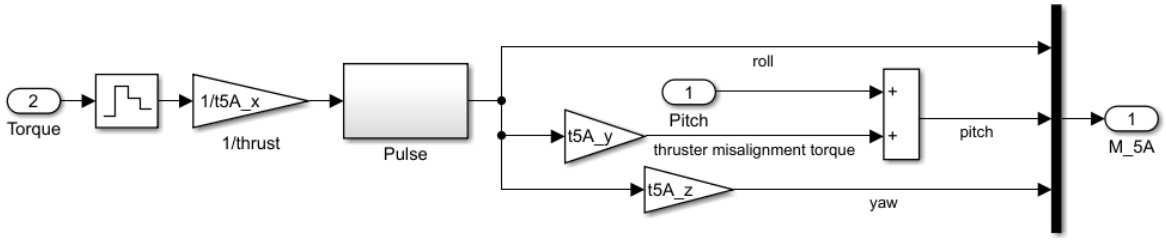

Figure 9.4 Thruster 5A model in Simulink

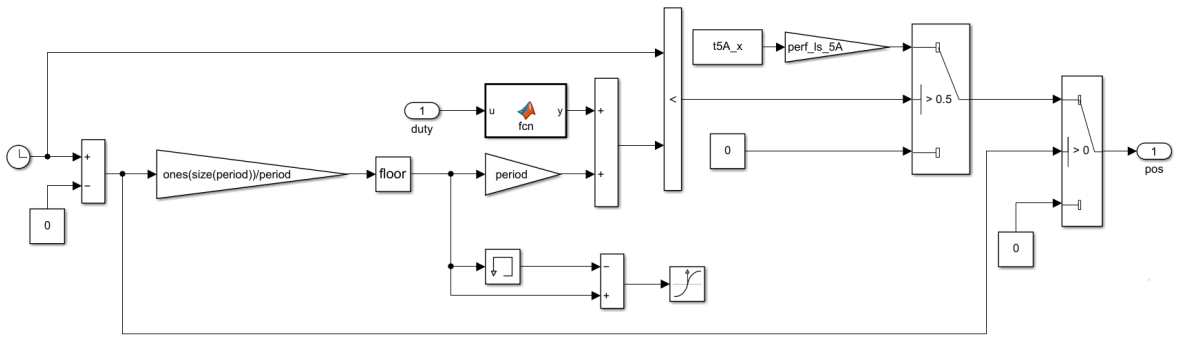

Figure 9.5 Pulse block in Simulink

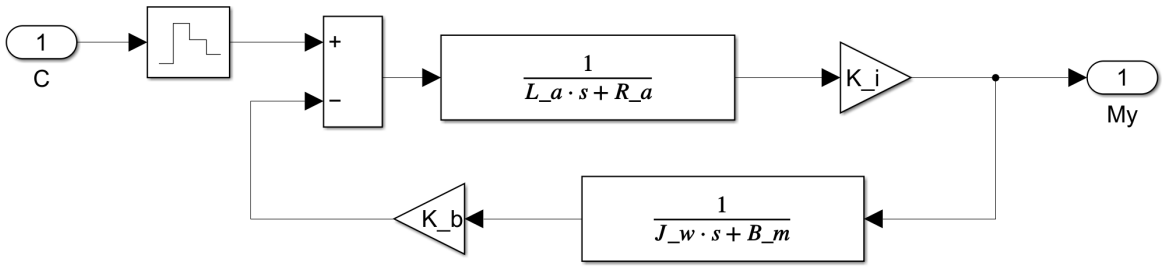

Figure 9.6 Actuator Model in Simulink

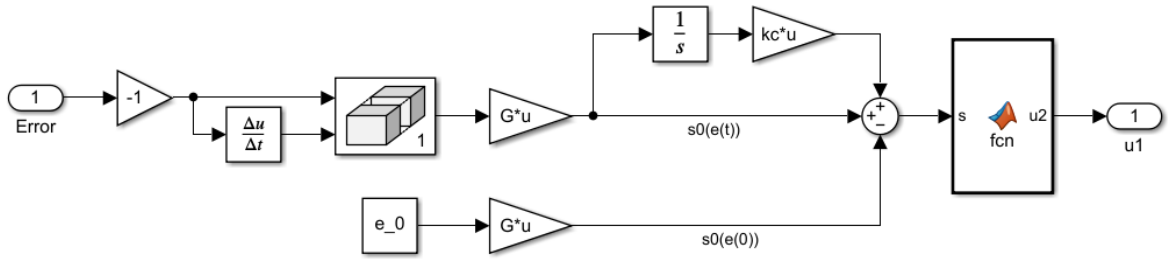

Figure 9.7 Discontinuous control in Simulink

9.3. Appendix 3 - MATLAB Code

```
clear, clc

% Motor Parameters
L_a = 0.005; % (H) Armature inductance
K_i = 0.3; % (N.m/A) Torque constant
K_b = 0.3; %(V/rad/s) Back EMF constant
B_m = 0.002; % viscous-friction coefficient
J_w = 0.12456; % (kg.m2) total (rotor+wheel) inertia of motor
R_a = 5; % (ohm) Armature resistance

%Satellite Parameters
w0 = 7.2722e-5; % orbit rate of one revolution per day
h_w = 60; % (N.m) torque of the momentum wheel
I = [3770 0 0; 0 730 0; 0 0 4020]; % (kg.m2)

%Disturbance
perf_loss_limit = 0.3;
perf_ls_4A = 1;
perf_ls_5A = 1;
perf_ls_5B = 1;

%Measurement Noise
rangle_power = 0.00005 *pi/180; % (rad)
rrate_power = 0.00001 *pi/180; % (rad/s)

%Perturbations
grav_disturbance = [5.21975e-5; 3.96637e-6; 0];

```

```
% Initial Bias
wx_in = w0 / 5;
wy_in = w0 / 8;
wz_in = w0 / 13;

pitch_ref = 0.8336 *pi/180; % (rad)
roll_ref = 0 *pi/180; % (rad)
yaw_ref = 0 *pi/180; % (rad)

theta_in = pitch_ref - 0.1 *pi/180;
phi_in = roll_ref + 0.075 *pi/180;
psi_in = yaw_ref - 0.075 *pi/180;

%Thruster Parameters
period = 0.1;

t4A_x = 11.3193;
t4A_y = -4.5e-5 / t4A_x;
t4A_z = 1.3367 / t4A_x;

t5A_x = 10.2156;
t5A_y = 4.12e-5 / t5A_x;
t5A_z = 6.1057 / t5A_x;

t5B_x = -11.0438;
t5B_y = -1.9e-5 / t5B_x;
t5B_z = -1.0992 / t5B_x;

%Controller Parameters
```

```
Kp = 50;
Kd = 2.5;

kc = 25;
G = [kc 1];
x_0 = [phi_in; wx_in];

%Roll/Yaw System Matrices
a = [0 0 1 0; 0 0 0 1; 3.6342e-7 0 0 -1.595767e-2;...
    0 3.39113e-7 1.492764e-2 0];
b = [0 ; 0; 2.6525e-4; 0.3*2.4876e-4];
c = [1 0 0 0];
d = 0;

%SS for output feedback
A1=[a zeros(4,1); -c 0];
B1=[b;0];

%Controllability
M=[B1 A1*B1 A1^2*B1 A1^3*B1 A1^4*B1];
rank(M); % if rank is 5 then the system is controllable

%Ackermann
p_cl = [-0.004-0.0015*1i -0.004+0.0015*1i...
    -0.0001-(1e-5)*1i -0.0001+(1e-5)*1i -4.5];
k_cl = place(A1,B1,p_cl);
K1 = k_cl(1), K2 = k_cl(2), K3 = k_cl(3), K4 = k_cl(4)
Ki = k_cl(5)
```